LBL-14875 c.2
SAC-52
UC-70

SWEDISH-AMERICAN COOPERATIVE PROGRAM ON RADIOACTIVE WASTE STORAGE IN MINED CAVERNS IN CRYSTALLINE ROCK

RECEIVED
LAWRENCE
BERKELEY LABORATORY
DEC 1985
LIBRARY AND
DOCUMENTS SECTION

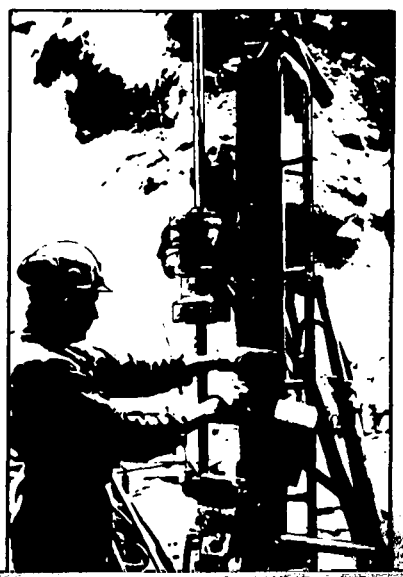

Technical Information Report No. 52

CHARACTERIZATION OF THE FRACTURE SYSTEM AT STRIPA WITH EMPHASIS ON THE VENTILATION DRIFT

A. Rouleau
University of Waterloo
Waterloo, Ontario, Canada

J.E. Gale
Memorial University of Newfoundland
St. John's, NFLD, Canada

October 1985

TWO-WEEK LOAN COPY
This is a Library Circulating Copy
which may be borrowed for two weeks.

A Joint Project of

Swedish Nuclear Fuel Supply Co.
Fack 10240 Stockholm, Sweden

Operated for the Swedish
Nuclear Power Utility Industry

Lawrence Berkeley Laboratory
Earth Sciences Division
University of California
Berkeley, California 94720, USA

Operated for the U.S. Department of
Energy under Contract DE-AC03-76SF00098

LBL-14875 c.2

DISCLAIMER

This document was prepared as an account of work sponsored by the United States Government. While this document is believed to contain correct information, neither the United States Government nor any agency thereof, nor the Regents of the University of California, nor any of their employees, makes any warranty, express or implied, or assumes any legal responsibility for the accuracy, completeness, or usefulness of any information, apparatus, product, or process disclosed, or represents that its use would not infringe privately owned rights. Reference herein to any specific commercial product, process, or service by its trade name, trademark, manufacturer, or otherwise, does not necessarily constitute or imply its endorsement, recommendation, or favoring by the United States Government or any agency thereof, or the Regents of the University of California. The views and opinions of authors expressed herein do not necessarily state or reflect those of the United States Government or any agency thereof or the Regents of the University of California.

LBL-14875

SAC-52

UC-70

CHARACTERIZATION OF THE FRACTURE SYSTEM AT STRIPA WITH EMPHASIS ON THE VENTILATION DRIFT

A. Rouleau*
Department of Earth Sciences
University of Waterloo
Waterloo, Ontario, CANADA, N2L 3G1

John E. Gale
Department of Earth Sciences
Memorial University of Newfoundland
St. John's, NFLD., CANADA, A1B 3X5

Prepared for
Lawrence Berkeley Laboratory
University of California
Berkeley, California 94720

October 1985

This work was supported by the Assistant Secretary for Nuclear Energy, Office of Civilian Waste Management of the Department of Energy under Contract No. DE-AC03-76SF00098. Funding for this project is administered by the Office of Crystalline Repository Development at Battelle Memorial Institute.

*Present Address: National Hydrology Research Institute
Environment Canada
562 Booth St., Ottawa, Canada, K1A 0E7

PREFACE

This report is one of a series documenting the results of the Swedish-American cooperative research program in which the cooperating scientists explore the geological, geophysical, hydrological, geochemical, and structural effects anticipated from the use of a large crystalline rock mass as a geologic repository for nuclear waste. This program has been sponsored by the Swedish Nuclear Power Utilities through the Swedish Nuclear Fuel Supply Company (SKBF), and the U.S. Department of Energy (DOE) through the Lawrence Berkeley Laboratory.

The principal investigators are L.B. Nilsson and O. Degerman for SKBF, and N.G.W. Cook, P.A. Witherspoon, and J.E. Gale for LBL. Other participants will appear as authors of the individual reports.

Previous technical reports in this series are listed below.

1. Swedish-American Cooperative Program on Radioactive Waste Storage in Mined Caverns by P.A. Witherspoon and O. Degerman. (LBL-7049, SAC-01).

2. Large Scale Permeability Test of the Granite in the Stripa Mine and Thermal Conductivity Test by Lars Lundstrom and Haken Stille. (LBL-7052, SAC-02).

3. The Mechanical Properties of the Stripa Granite by Graham Swan. (LBL-7074, SAC-03).

4. Stress Measurements in the Stripa Granite by Hans Carlsson. (LBL-7078, SAC-04).

5. Borehole Drilling and Related Activities at the Stripa Mine by P.J. Kurfurst, T. Hugo-Persson, and G. Rudolph. (LBL-7080, SAC-05).

6. A Pilot Heater Test in the Stripa Granite by Hans Carlsson. (LBL-7086, SAC-06).

7. An Analysis of Measured Values for the State of Stress in the Earth's Crust by Dennis B. Jamison and Neville G.W. Cook. (LBL-7071, SAC-07).

8. Mining Methods Used in the Underground Tunnels and Test Rooms at Stripa by B. Andersson and P.A. Halen. (LBL-7081, SAC-08).

9. Theoretical Temperature Fields for the Stripa Heater Project by T. Chan, Neville G.W. Cook, and C.F. Tsang. (LBL-7082, SAC-09).

10. Mechanical and Thermal Design Considerations for Radioactive Waste Repositories in Hard Rock. Part I: An Appraisal of Hard Rock for Potential Underground Repositories of Radioactive Waste by N.G.W. Cook; Part II: In Situ Heating Experiments in Hard Rock: Their Objectives and Design by N.G.W. Cook and P.A. Witherspoon. (LBL-7073, SAC-10).

11. Full-Scale and Time-Scale Heating Experiments at Stripa: Preliminary Results by N.G.W. Cook and M. Hood. (LBL-7072, SAC-11).

12. Geochemistry and Isotope Hydrology of Groundwaters in the Stripa Granite: Results and Preliminary Interpretation by P. Fritz, J.F. Barker, and J.E. Gale. (LBL-8285, SAC-12).

13. Electrical Heaters for Thermo-Mechanical Tests at the Stripa Mine by R.H. Burleigh, E.P. Binnall, A.O. DuBois, D.O. Norgren, and A.R. Ortiz. (LBL-7063, SAC-13).

14. Data Acquisition, Handling, and Display for the Heater Experiments at Stripa by Maurice B. McEvoy. (LBL-7063, SAC-14).

15. An Approach to the Fracture Hydrology at Stripa: Preliminary Results by J.E. Gale and P.A. Witherspoon. (LBL-7079, SAC-15).

16. Preliminary Report on Ge physical and Mechanical Borehole Measurements at Stripa by P. Nelson, B. Paulsson, R. Rachiele, L. Andersson, T. Schrauf, W. Hustrulid, O. Duran, and K.A. Magnussen. (LBL-8280, SAC-16).

17. Observations of a Potential Size-Effect in Experimental Determination of the Hydraulic Properties of Fractures by P.A. Witherspoon, C.H. Amick, J.E. Gale, and K. Iwai. (LBL-8571, SAC-17).

18. Rock Mass Characterization for Storage in Nucler Waste in Granite by P.A. Witherspoon, P. Nelson, T. Doe, R. Thorpe, B. Paulsson, J.E. Gale, and C. Forster. (LBL-8570, SAC-18).

19. Fracture Detection in Crystalline Rock Using Ultrasonic Shear Waves by K.H. Waters, S.P. Palmer, and W.F. Farrell. (LBL-7051, SAC-19).

20. Characterization of Discontinuities in the Stripa Granite--Time Scale Heater Experiment by R. Thorpe. (LBL-7083, SAC-20).

21. Geology and Fracture System at Stripa by A. Okliewicz, J.E. Gale, R. Thorpe, and B. Paulsson. (LBL-8907, SAC-21).

22. Calculated Thermally Induced Displacements and Stresses for Heater Experiements at Stripa by T. Chan and N.G.W. Cook. (LBL-7061, SAC-22).

23. Validity of Cubic Law for Fluid Flow in a Deformable Rock Fracture by P.A. Witherspoon, J. Wang, K. Iwai, and J.E. Gale. (LBL-9557, SAC-23).

24. Determination of In-Situ Thermal Properties of Stripa Granite from Temperature Measurements in the Full-Scale Heater Experiments: Methods and Primary Results by J. Jeffry, T. Chan, N.G.W. Cook and P.A. Witherspoon. (LBL-8424, SAC-24).

25. Instrumentation Evaluation, Calibration, and Installation for Heater Tests Simulating Nuclear Waste in Crystalline Rock, Sweden by T. Schrauf, H. Pratt, E. Simonson, W. Hustrulid, P. Nelson, A. DuBois, E. Binnall, and R. Haught. (LBL-8313, SAC-25)

26. Part I: Some Results From a Field Investigation of Thermo-Mechanical Loading of a Rock Mass When Heater Canisters are Emplaced in the Rock by M. Hood. Part II: The Application of Field Data from Heater Experiments Conducted at Stripa, Sweden for Repository Design by M. Hood, H. Carlsson, and P.H. Nelson. (LBL-9392, SAC-26).

27. Progress with Field Investigations at Stripa by P.A. Witherspoon, N.G.W. Cook, and J.E. Gale (LBL-10559, SAC-27).

28. A Laboratory Assessment of the Use of Borehole Pressure Transients to Measure the Permeability of Fractured Rock Masses by C.B. Forster and J.E. Gale. (LBL-8674, SAC-28).

29. Thermal and Thermomechanical Data for In Situ Heater Experiments at Stripa, Sweden by T. Chan, E. Binnall, P. Nelson, O. Wan, C. Weaver, K. Ang, J. Braley, and M. McEvoy. (LBL-11477, SAC-29).

30. The Effect of Radon Transport in Groundwater Upon Gamma Ray Borehole Logs by P.H. Nelson, R. Rachiele, and A. Smith. (LBL-11180, SAC-30).

31. Strength and Permeability Tests on Ultra-Large Stripa Granite Core by R. Thorpe, D.J. Watkins, W.E. Ralph, R. Hsu, and S. Flexser. (LBL-11203, SAC-31).

32. Ultrasonic and Acoustic Emission Results from the Stripa Heater Experiments. Part I: A Cross-Hole Investigation of a Rock Mass Subjected to Heating by B.N.P. Paulsson and M.S. King. Part II: Acoustic Emission Monitoring During Cool-Down of the Stripa Heater Experiment by R. Rachiele. (LBL-10975, SAC-32).

33. Numerical Modeling to Assess Possible Influence of the Mine Openings on Far-Field In Situ Stress Measurements at Stripa by T. Chan, V. Guvanasen, and N. Littlestone (LBL-12469, SAC-33).

34. A Field Assessment of the Use of Borehole Pressure Transients to Measure the Permeability of Fractured Rock Masses by C.B. Forster and J.E. Gale. (LBL-11829, SAC-34).

35. Water Inflow into Boreholes During the Stripa Experiments by P.H. Nelson, R. Rachiele, J.S. Remer and H.S. Carlsson. (LBL-12574, SAC-35).

36. Petrology and Radiogeology of the Stripa Pluton by H. Wollenberg, S. Flexser, and L. Andersson. (LBL-11654, SAC-36).

37. Geohydrological Data from the Macopermeability Experiment at Stripa, Sweden by C.R. Wilson, J.C.S. Long, R.M. Galbraith, K. Karasaki, H.K. Endo, A.O. DuBois, M.J. McPherson, and G. Ramqvist. (LBL-12520, SAC-37).

38. Characterization of Discontinuities in the Stripa Granite--Full-Scale Heater Experiments by B.N.P. Paulsson, P.H. Nelson, and P.J. Kurfurst. (LBL-9063, SAC-38).

39. Application of Borehole Geophysics at an Experimental Waste Storage Site by P.H. Nelson, K.A. Magnusson, and R. Rachiele. (LBL-11982, SAC-39).

40. Laboratory Investigations of Thermomechanical Properties of Stripa Granite by L. Myer and R. Rachiele. (LBL-13435, SAC-40)

41. Petrologic Changes and Damage in the Stripa Quartz Monzonite in Response to Heater Tests by S. Flexser, H. Wollenberg, and D.E. Wedge. (LBL-14929, SAC-41).

42. Fracture Mapping in the Ventilation Drift at Stripa: Procedures and Results by A. Rouleau, J.E. Gale, and J. Baleshta. (LBL-13071, SAC-42).

43. Thermal Analysis of the Stripa Heater Test Data from the Full Scale Drift by I. Javandel and P.A. Witherspoon. (LBL-13217, SAC-43).

44. In Situ Stress Measurements at the Stripa Mine, Sweden by T.W. Doe, K. Ingevald, L. Strindell, B. Leijon, W. Hustrulid, E. Majer, and H. Carlsson. (LBL-15009, SAC-44).

45. Fracture Detection in Crystalline Rock Using Ultrasonic Reflection Techniques by S.P. Palmer. (LBL-16347, SAC-45).

46. Fracture and Hydrology Data from Field Studies at Stripa, Sweden by J.E. Gale. (LBL-13101, SAC-46).

47. Equipment Design, Installation, and Operation for the Macropermeability Experiment at Stripa, Sweden by R.M. Galbraith, C.R. Wilson, A.O. DuBois, S.A. Lundgren, M.J. McPherson and G.W. West. (LBL-13392, SAC-47).

48. Effects of Sample Size on the Stress Permeability Relationship for Natural Fractures by J.E. Gale and K.G. Raven. (LBL-11865, SAC-48).

49. Progress with Hydrogeological Characterization of the Stripa Site by J.E. Gale, A. Rouleau, P.A. Witherspoon and C.R. Wilson. (LBL-14878, SAC-49).

50. Extensometer Performance During Heater Experiments at Stripa by A.O. DuBois, M. Hood, E.P. Binnall and L. Andersson. (LBL-13531, SAC-50).

51. Seismic Velocities and Attenuation in a Heated Underground Granitic Repository by B.N.P. Paulsson (LBL-16346 1/2, SAC-51).

TABLE OF CONTENTS

	Page
LIST OF FIGURES	ix
LIST OF TABLES	xi
ABSTRACT	xiii
SELECTED NOMENCLATURE	xv
ACKNOWLEDGEMENTS	xvii
EXECUTIVE SUMMARY	xix
PROJECT DESCRIPTION	xxv
1. INTRODUCTION	1
1.1 General Geology and Sources of Data	3
2. ROCK MASS CHARACTERIZATION - AN ENGINEERING APPROACH	13
2.1 Rock Mass Characterization - Purpose and Procedures	13
2.2 Characterization of the Rock Mass at Stripa	15
3. STATISTICAL CHARACTERIZATION OF THE FRACTURE SYSTEM	23
3.1 Fracture Orientations	25
3.1.1 SBH Boreholes	25
3.1.2 Test Excavations	29
3.1.2.1 Ventilation Drift	29
3.1.2.2 Full-scale Drift	32
3.1.2.3 Time-scale Drift	35
3.1.2.4 Other Drifts	37
3.1.3 Summary and Conclusion	38
3.2 Trace Length Analysis	42
3.2.1 Bias and Sources of Error	42
3.2.2 Analysis of Ventilation Drift Data	46
3.3 Spacing Analysis	51
3.3.1 Selecting the Data Set	51
3.3.2 Selecting the Method of Analysis	53
3.3.3 Analysis of Spacing for Individual Boreholes	55
3.3.4 Detailed Analysis of Spacing Around the Ventilation Drift	57
3.3.4.1 Spacing Variability	58
3.3.4.2 Analysis of Fracture Spacings from All the Oriented HG and R Holes Combined	70
3.4 Fracture Density	78
4. CONCLUSIONS AND RECOMMENDATIONS	83

Page

REFERENCES. 87

APPENDICES. 93
A. Orientation Diagrams. 93
B. Listing of Selected Computer Programs Used in Trace Length and Spacing Analysis. 101
C. Maximum Likelihood Estimation of the Parameters for the Weibull Model 113

LIST OF FIGURES

Page

1.1 Regional geology and structural geology maps of the Stripa area. 4

1.2 Frequency-strike diagram for major lineaments 5

1.3 Plan map of the Stripa site showing rock outcrops, inclined surface boreholes and underground experimental drifts 6

1.4 Vertical cross-section bearing N 89° E through boreholes SBH-2 and DBH V-1 7

1.5 Location and orientation of subsurface hydrology boreholes. . 9

1.6 Plan view of the experimental area at Stripa, 340 m underground. The coordinate system on the edge of the figure are references to the original mine coordinates (in meters) . . . 10

2.1 Plot of RQD, fractures per meter, and mean core length using a moving average, with an interval of 2.0 m and distance increment of 0.2 m; borehole R3. 16

2.2 Plot of RQD, fractures per meter, and mean core length using a moving average, with an interval of 2.0 m and a distance increment of 0.2 m; borehole R5. 17

2.3 Plot of RQD, fractures per meter, and mean core length using a moving average, with an interval of 2.0 m and a distance increment of 0.2 m; borehole R7. 18

2.4 Permeability versus fracture frequency data from the R and HG boreholes. The dashed lines indicate the 95 percent confidence limits for the mean values and the solid lines indicate the same confidence limits for the individual values 20

3.1 Pole diagram for the fracture planes intersecting the drill cores of the three SBH holes (data from the entire length of the boreholes). Lower-hemisphere equal-area plot. 26

3.2 Pole diagram for the fracture planes intersecting the drill cores from the bottom segment of the three SBH holes, i.e., from a depth of 175 m to 290 m. Lower-hemisphere equal-area plot 28

3.3 Pole diagram for all the fracture planes measured on the faces of the ventilation drift. Lower-hemisphere equal-area plot 31

3.4 Pole diagram for all the fracture planes intersecting the drill cores from all the HG holes and all the R holes, except R4 and R9. Lower-hemisphere equal-area plot 33

Page

3.5 Pole diagram for fracture planes intersecting the drill cores from the full-scale drift. Lower-hemisphere equal-area plot. 34

3.6 Pole diagram for the fracture planes intersecting the cores of the boreholes drilled in the floor of the time-scale drift. . 36

3.7 Composite diagrams showing the fracture orientation data from different areas of the test excavation 39

3.8 Pole diagram for all the joint planes intersecting the faces of the ventilation drift and the fracture planes intersecting the drill cores of all the HG holes and all the R holes, except R4 and R9. Lower-hemisphere equal-area plot 40

3.9 Portion of the fracture map of the ventilation drift. 43

3.10 Histograms of fracture trace lengths on the faces of the ventilation drift 47

3.11 Distribution of LSPAC for each fracture set in each borehole. 62

3.12 Distribution of LSPAC for each fracture set in each group of boreholes. 67

3.13 Frequency histograms for the spacings between consecutive fractures of the same set (SPAC) intersecting all the oriented HG and R drill cores 71

3.14 Quantile plots for the exponential, the lognormal and the Weibull models fitted to the spacing distribution of the four fracture set 74

3.15 A three-dimensional structure consisting of parallel surfaces. 79

A.1 Pole diagram of fracture planes intersecting the drill cores of vertical boreholes in the full-scale drift 94

A.2 Pole diagram for fracture planes intersecting the drill cores of sub-horizontal boreholes around the full-scale drift . . . 95

A.3 Pole diagram for the fracture planes intersecting the drill cores of the boreholes HG1 to HG5 96

A.4 Pole diagram for the fracture planes intersecting the drill cores of the boreholes R1 to R10, except R4 and R9. . . 97

A.5 Poles to veins measured on the faces of the ventilation drift 98

A.6 Pole diagram for the average plane of fracture zones measured on the faces of the ventilation drift. 99

LIST OF TABLES

Page

1.1 Hydrology boreholes coordinate and survey data. 11

2.1 Analysis of variance for the linear regression of the natural logarithm of permeability versus fracture frequency 21

3.1 Fracture sets defined by the fractures intersecting the drill cores from the bottom segment of the SBH holes (depth of 175 m to 290 m) 30

3.2 Fracture sets defined by the fracture data from all the faces of the ventilation drift and the fractures intersecting the drill cores from all the oriented R and HG holes. . . 41

3.3 Trace length statistics, by degree of censoring for the four fracture sets. 48

3.4 Main statistics of the spacing distribution for each fracture set in the bottom segment of each SBH hole, i.e., from a depth of 175 m to 290 m 59

3.5 Main statistics of the spacing distribution for each fracture set in each one of the oriented HG and R holes . . . 60

3.6 Analysis of variance of LSPAC between individual boreholes. . 63

3.7 Duncan multiple-range test for LSPAC (individual boreholes) . 65

3.8 Main statistics of the distributions of SPAC and LSPAC for each fracture set in each group of boreholes. 66

3.9 Analysis of variance of LSPAC between the three groups of boreholes HG, RN and RS 68

3.10 Duncan multiple-range test for LSPAC (groups of boreholes). . 69

3.11 Main statistics of the distributions of SPAC and LSPAC for each fracture set for all the oriented HG and R holes 72

3.12 Average fracture frequency for each fracture set. 81

ABSTRACT

Fracture data from Stripa, Sweden, have been analyzed to describe the nature and variation of the fracture system within the Stripa granite. Using both core log and fracture map data the type and the parameters of the distributions of fracture orientation, trace length and spacing have been determined. The core log data analysed in this report were obtained from three inclined surface boreholes, totaling 1065 meters in length, and fifteen subsurface boreholes drilled in a fixed pattern from the ventilation drift. These boreholes varied between 30 and 40 meters in length. The fracture map data came from detailed mapping of a 50-meter length of the ventilation drift. These map and core log data were compared with data that resulted from general mapping of the entire test area and with detailed map and core log data from other experimental rooms in the same test area.

The moving averages for three rock mass parameters, all based on the degree of fracturing, have been calculated for part of the borehole and core log data. These three parameters, the rock quality designation (RQD), the mean core length, and the fracture frequency, have been tentatively correlated with a fourth parameter, the rock mass permeability. However this study showed only a weak correlation between the three fracturing parameters and the rock mass permeability, presumably because no distinction was made between fractures belonging to different sets.

Using orientation data from both fracture maps and core logs, contoured pole diagrams were constructed and four fracture sets were delineated. For each fracture set the trace length and spacing data were analyzed. In the analysis of the trace length data, which were taken

from the fracture maps of the ventilation drift, three sampling biases: were considered censoring, truncation and size bias. For the spacing data obtained from the core logs of thirteen of the subsurface boreholes, the parameters of the distributions have been computed, and goodness-of-fit tests have been carried out for three theoretical models: the exponential, the lognormal and the Weibull distributions. Finally, the average fracture density has been estimated for each fracture set using core log data.

The orientation data from the vicinity of the test excavation permitted a reasonably clear definition of the various fracture sets. However fracture data taken from distances of 200 meters or more apart produced orientation diagrams that were more scattered, presumably due to the sampling of different lithologies and different structural domains. Significant differences in the distributions of spacings and trace lengths between the various fracture sets suggest that these geometric parameters are essential in the evaluation of the degree of fracture interconnection within the rock mass.

SELECTED NOMENCLATURE

CDF: Cumulative distribution function of a statistical model

CENS: Degree of censoring of the fracture traces:
= 0, both ends observable
= 1, only one end observable
= 2, neither end observable

ICDF: Inverse cumulative distribution function of a statistical model

LSPAC: natural logarithm of SPAC values (see below)

ML: Maximum Likelihood method of estimation of parameters

PDF: Probability density function of a statistical model

p,q,r: direction cosines of an oriented line

RQD: Rock quality designation (Deere, 1964): total length of all pieces of intact core that are 10 cm or greater in length from a given drill hole interval, divided by the length of that interval

SPAC: Fracture spacing defined as $\ell \cos \phi$, where ℓ is the distance between two consecutive intersections of fractures, from the same set, with a sampling line, and ϕ is the angle defined below.

α: probability of a lower value for a given variable

μ: mean of a statistical distribution

σ: standard deviation of a statistical distribution

Θ,$: scale and shape parameters, respectively, of a Weibull distribution

ϕ: angle between a borehole axis and the average pole of a fracture set

ACKNOWLEDGMENTS

The authors extend their thanks to N. Maerz for his assistance in processing and analyzing the core log data, and to A. Sweezey for assistance with data analysis. Special thanks are extended to S. Andrews for typing and assembling the report.

The primary sources of data for this study are Gale (1981) and Rouleau et al. (1981). Both reports form part of the SAC series of reports that is published by the Lawrence Berkeley Laboratory. People who contributed to the original data collection have been identified in these reports. Other sources of data have been acknowledged where appropriate in the text. Thanks and appreciation are extended to Mr. M. Wigley, scientific authority for this project, at the Battelle Memorial Institute, for his understanding and patience when delays were encountered in completing this report.

This project was funded by the Office of Nuclear Waste Isolation at the Battelle Memorial Institute, under Subcontract E515-04400 to the Waterloo Research Institute of the University of Waterloo.

EXECUTIVE SUMMARY

INTRODUCTION

At Stripa, Sweden, an old iron-ore mine whose ore is depleted has been the focal point of a comprehensive research and development program on the disposal of nuclear wastes in fractured granitic rocks (Witherspoon and Degerman, 1977). The two main objectives of the research have been to determine the thermomechanical response of the rock mass to the heat generated by simulated nuclear waste canisters (electrical heaters) and to determine the hydrogeologic characteristics of the rock mass. Fractures in granitic rocks have a controlling influence on the strength of the rock mass and hence on the stability of the excavated waste repository. Fractures also are the primary flowpaths along which radionuclides may migrate from the repository to the biosphere.

As part of the fracture-hydrology program at Stripa (Gale and Witherspoon, 1979), a considerable effort was devoted to characterizing the fracture system at that site. This consisted of applying various rock mass characterization schemes to the drill core data in order to assess the variation in the degree of fracturing within the rock mass. Data from fracture maps of the walls and the floor of the drifts were combined with the fracture data obtained from drill cores to delineate the main fracture sets in the Stripa granite. For each fracture set the statistics of spacings and trace lengths have been determined, and the average fracture density has been calculated. The results of this fracture analysis are presented in this report.

The test site and test boreholes are located on the north side of a northeast trending syncline. The experimental rooms, for much of the

research program, have been excavated at a depth of 338 meter below surface under the north limb of the syncline, in a small body of granitic rock adjacent to the metasedimentary-metavolcanic sequence in which the mined-out ore body was located. The general geology of the test site area and the general fracture system are described by Olkiewicz et al. (1979). The petrology of the granitic body is discussed by Wollenberg et al. (1982).

Sources of data for this rock mass and fracture system characterization include a limited number of surface outcrops, three surface boreholes (SBH-1 to SBH-3) and fifteen subsurface hydrology boreholes (HG1 to HG5 and R1 to R10) (Gale, 1981), a large number of boreholes drilled for the thermomechanical experiments and the fracture maps of the walls and the floor of the thermomechanical experimental rooms (Thorpe, 1979; Paulsson et al., 1982), as well as the maps of the ventilation experiment drift (Rouleau et al., 1981).

ROCK MASS CHARACTERIZATION

Rock mass characterization schemes generally constitute an essential part of rock mass classification systems. The main objective of these systems is to determine the characteristics that rock masses have in common in order that the experience gained at one site in assessing stability conditions and designing support systems can be applied to a different site. In most civil or mining engineering applications, the main parameters of interest in a rock mass are related to the stability of excavations or foundations. However in nuclear waste disposal,

particularly in crystalline rocks, the most important factor determining the suitability of a site is the rate of groundwater movement.

Since fractures in crystalline rock control both mechanical stability and the flow of groundwater, three rock mass fracturing parameters were compared. These parameters were the rock mass quality designation (RQD), mean core length, and fracture frequency. These parameters were computed using a moving average over intervals of 2 meters in length and using distance increments of 0.2 meter. The fracturing parameters were also compared with the permeability values calculated from packer injection test data. These injection tests were carried out using 2-meter packer intervals. While there is a good correlation between the RQD, mean core length and fracture frequency values, as one would expect, there is very weak correlation between these three parameters and the hydraulic conductivity values. The correlation between hydraulic conductivity and fracture frequency is only discernible on a scatter diagram including the data from all the fifteen hydrology boreholes together.

STATISTICAL CHARACTERIZATION OF THE FRACTURE SYSTEM

Using the basic data from the core logs of the surface and subsurface hydrology boreholes (Gale, 1981), and from the fracture maps of the ventilation drift (Rouleau et al., 1981), we have determined the number of fracture sets, based on orientation data, both for the immediate vicinity of the ventilation drift and for a larger volume of the granitic rock mass that forms roughly a cube of about 270 meters on a side. The definition of the fracture sets decreases considerably as the volume of rock mass

being considered increases. Combining the above data with the fracture data from Olkiewicz et al. (1979) and the orientation data from the thermomechanical experimental drifts (Thorpe, 1979; Paulsson et al., 1982), we have been able to correlate most of the fracture sets from one underground experimental room to another.

The fracture system was analyzed in greater detail for the rock mass surrounding the ventilation drift. Fracture trace lengths and fracture spacings were analyzed for each one of the four fracture sets defined on the basis of orientation data, as mentioned above. Using data from the fracture maps of the ventilation drift, the parameters of the trace length distributions were estimated for both an exponential and a lognormal model. The trace length distributions are truncated due to the fact that fracture traces shorter than 0.5 meter were not considered. Since many fracture traces have either one or both ends not observable, trace length distributions are also censored. Both truncation and censoring biases were accounted for in the estimation of the parameters of the trace length distributions.

The statistical analysis of fracture spacings was carried out using the data from the drill cores of the thirteen oriented hydrology holes drilled from the ventilation drift. In this study we define the fracture spacing (SPAC) as the distance between two consecutive fractures of the same set along the drill core, multiplied by the cosine of the angle between the borehole axis and the pole of the average plane of that fracture set. Statistics of spacing data were first computed for each fracture set in each borehole separately. Both analysis of variance and Duncan multiple-range test for the natural logarithm of spacing (LSPAC)

indicate significant difference in the mean of LSPAC from borehole to borehole. However this difference decreases considerably when, instead of individual boreholes, we consider groups of boreholes defined according to their location along the drift. Combining the data from all the oriented boreholes, we have computed the parameters of the spacing distributions assuming, in turn, exponential, lognormal and Weibull statistical models. Quantile plots and objective goodness-of-fit test (the Kolmogorov-Smirnov D-statistics) reveal that the lognormal distribution gives the best fit to spacing data.

Using core log data, an average value of fracture density (L^{-1}) has been computed for each fracture set. The method used has been described by Kiraly (1970). The basic data required are simply the number of fracture intersections with each borehole and a calculated "true" length for each borehole. This latter value is computed by multiplying the actual length of a borehole by the cosine of the angle between the borehole axis and the pole of the average plane of the fracture set being considered. As expected, fracture density was found to vary significantly from one fracture set to another.

CONCLUSIONS

The rock mass characterization scheme presented in this study suggests that there is only a weak correlation between fracture density and the hydraulic conductivity of the rock mass. This lack of correlation may result from the fact that the fracturing parameters that were considered do not distinguish between fractures of the various sets. In a more

systematic correlation analysis, some advantage could presumably be gained by considering each fracture set separately, especially if one fracture set is much more permeable than the others.

The statistical analysis of fracture orientation, using both core log and fracture map data, indicates that at least four fracture sets can be clearly defined in the rock mass immediately surrounding the main test excavations. The orientation data become much more scattered when one considers data obtained from distances of 200 meters or more apart, because these data represent presumably different structural domains of the rock mass.

For the rock mass surrounding the ventilation drift, the fracture spacing and trace length data were analysed for each one of the four fracture sets defined on the basis of orientation data. The spacing data, obtained from the drill cores of the fifteen hydrology boreholes, indicate significant differences in spacing distributions between boreholes for each fracture set. The difference becomes much less important when comparing groups of boreholes that are defined on the basis of their location along the drift. For the ventilation drift as a whole, both trace length and spacing data show substantial differences between fracture sets, as does the fracture density. Therefore these parameters, or a derivative of them, should be considered in any evaluation of the degree of fracture interconnection and hence hydraulic communication within the rock mass.

The results of this analysis can be used in numerical simulations of groundwater flow or rock mass stability where one needs to account for the variation in orientation and trace length as well as the variation in the fracture densities for different fracture sets.

PROJECT DESCRIPTION

After a brief review of the lithology and the structural geology of the Stripa area, three rock mass characterization schemes were applied to part of the borehole data from the Stripa site. Special attention was paid to the applicability of these characterization schemes to nuclear waste disposal problems in igneous rocks, especially the degree of correlation between the characterization parameters and rock mass permeability.

The fracture data from both core logs and fracture maps were then analyzed to determine the nature of, and the variation in, the fracture orientation data. For the four fracture sets defined in the area of the ventilation drift on the basis of orientation data, the statistics of fracture spacing and trace length distributions were determined. The variability of fracture spacings around the ventilation drift was also examined. The results of this analysis provide a three-dimensional description of the fracture system in the rock mass in the immediate area of the ventilation drift. The results are prerequisite to the evaluation of the degree of fracture interconnection, and hence hydraulic communication, within the rock mass.

1. INTRODUCTION

At Stripa, Sweden, an old iron-ore mine whose ore is depleted has been the focal point of a comprehensive research and development program on the disposal of nuclear waste in granitic rocks (Witherspoon and Degerman, 1978; Gale and Witherspoon, 1979). The main thrust of the research has been to determine the thermomechanical response of the rock mass to the heat generated by simulated nuclear-waste cannisters (electrical heaters) and to determine the fracture and hydrogeologic characteristics of the rock mass.

The success of underground storage of nuclear waste depends on the rock mass retaining its structural integrity while experiencing the thermomechanical loading that it will be subjected to during the operational phase of the repository and, more importantly, providing limited possibilities for groundwater transport of the radioactive materials from the repository to the biosphere. Fractures in granitic rocks have a controlling influence on the strength of the rock mass, and hence its stability. Fractures also are the primary flowpaths along which radionuclides may migrate from the repository to the biosphere.

It is also recognized that, in fractured crystalline rock, flow through the intact rock matrix will be so low that significant flows through the rock mass can only take place through the fracture system. Various studies (Davis and Turk, 1964; Snow, 1968; Raven and Gale, 1977; and Gale, 1981) have shown that there is a decrease of permeability with depth in fractured crystalline rocks. Factors that may contribute to this observed decrease in fracture permeability with depth include the following two possibilities: (1) a decrease in fracture apertures with increasing depth, and (2) a change in fracture density with depth. While

it is recognized (Gale, 1975; Iwai, 1976) that fracture apertures decrease with increasing stress (depth) and hence contribute to the observed decrease of fracture permeability with depth, there have been no fracture hydrology studies in which variations in fracture density within a given rock mass have also been documented. Also there have been no theoretical studies relating changes in observed fracture density to changes in rock mass permeability.

Recognizing that fractures have a finite length, i.e. they are discontinuous within their own planes, it is apparent that changes in observed fracture density can result from either a change in the spacing of fractures within each set, a change in the length of fractures within each set, or variations in the relative orientation of the fracture sets. The form and nature of the distributions of fracture spacings, lengths and orientations determine the degree of fracture interconnection and hence the degree of hydraulic communication within a given rock mass.

As part of the fracture-hydrology program at Stripa (Gale and Witherspoon, 1979), a considerable effort was devoted to characterizing the fracture system at that site. This consisted of applying various rock mass characterization schemes to the drill core data in order to assess the degree of variation in fracture intensity within the rock mass. Orientation data from fracture maps of the walls and the floor of the drifts were combined with the orientation data obtained from the drill cores to delineate the main fracture sets in the Stripa granite. For each fracture set the statistics of spacings and trace lengths have been determined. The results of this work are presented in this report.

1.1 General Geology and Sources of Data

The Stripa site is located about 150 kilometers west-northwest of Stockholm. The bedrock geology is typical of highly folded and deformed shield terrains. The regional geology (Figure 1.1A) is characterized by a northeast trending series of folded metamorphic rocks that have been intruded by a series of granitic rocks. The local bedrock structure around Stripa is dominated by a major northeast trending syncline (Figure 1.1B). Additional smaller synclines, trending both parallel and perpendicular to the major northeast trending synclines, add to the overall structural complexity of the region. Superimposed on the regional fold pattern is a series of fracture zones and lineaments (Figure 1.1B) with at least one major fracture zone trending perpendicular to the major synclinal feature that cuts across Lake Rasvalen. The overall trends of the lineaments are shown by the frequency-strike diagram (Figure 1.2).

The test site and test boreholes (Figure 1.3) are located on the north side of the local northeast trending syncline (Figure 1.4). The experimental rooms for much of the research program have been excavated at a depth of 338 meters below surface under the north limb of the syncline (Figure 1.4), in a small body of granite (quartz monzonite) adjacent to the metasedimentary-metavolcanic sequence in which the mined-out ore body was located. The general geology of the test site area and the general fracture system are described by Olkiewicz et al. (1979). The petrology of the granite body is discussed by Wollenberg et al. (1982).

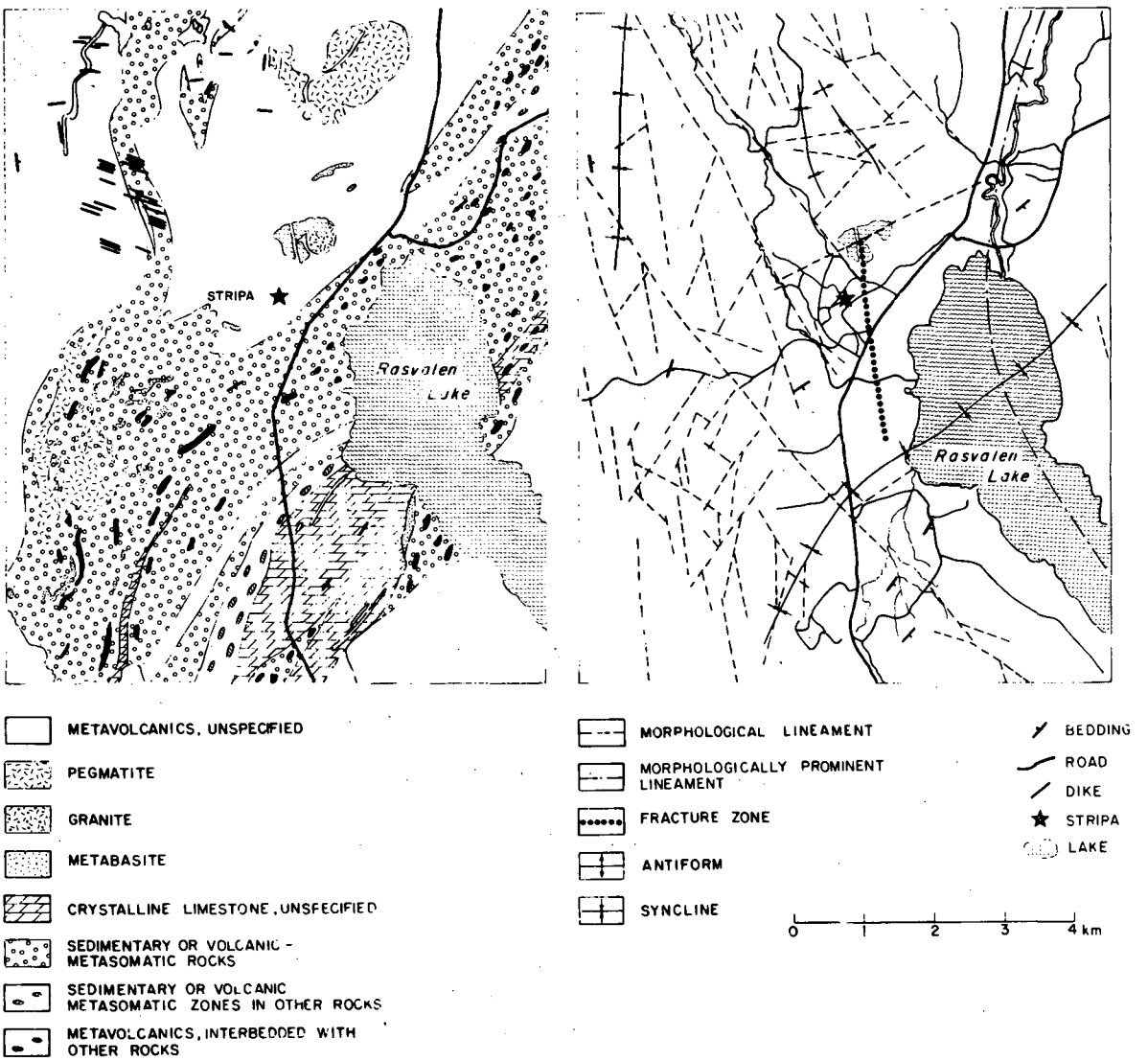

XBL 8411-5022

Fig. 1.1. Regional geology (A) and structural geology (B) maps of the Stripa area.

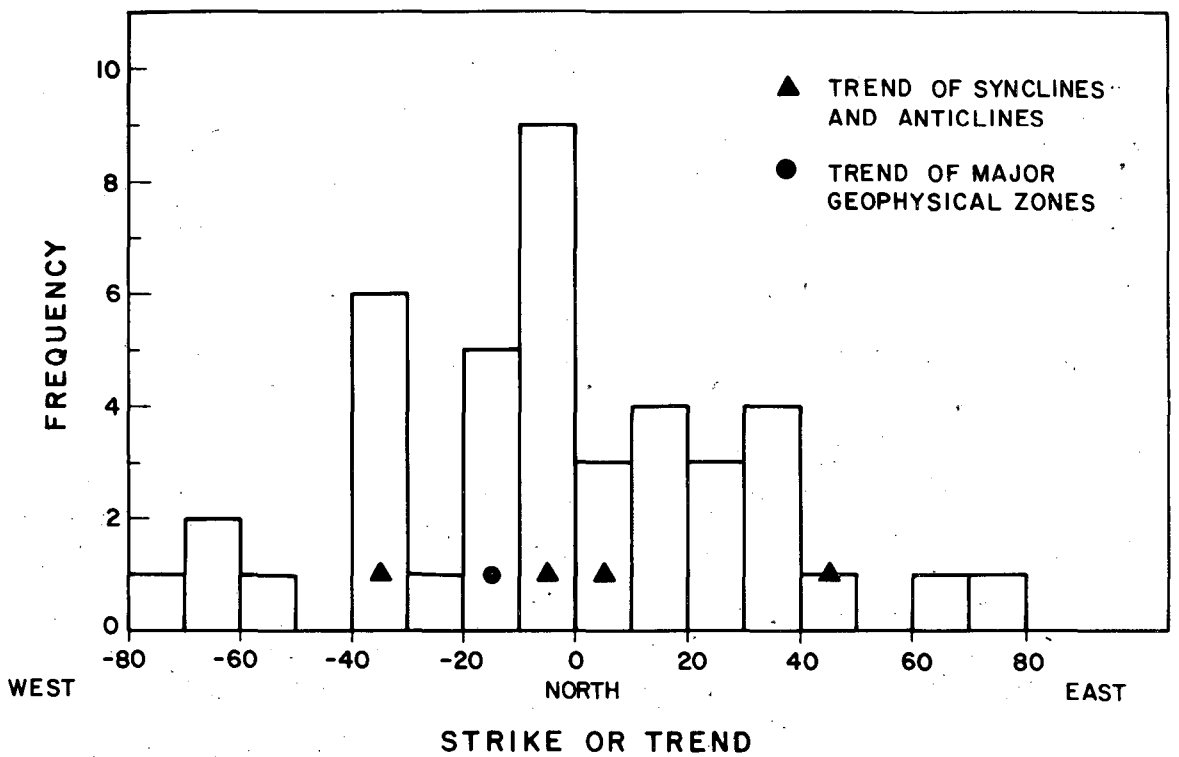

XBL 8411-5023

Fig. 1.2. Frequency-strike diagram for major lineaments.

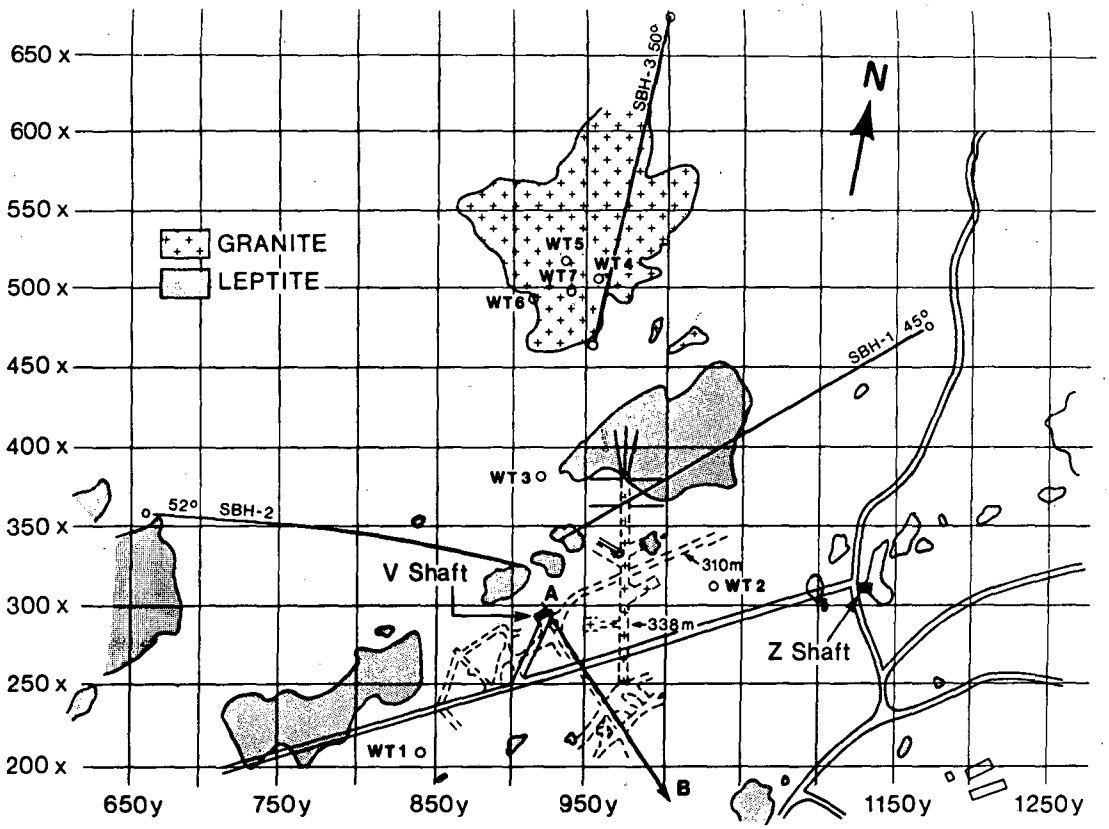

XBL 804-9434

Fig. 1.3. Plan map of the Stripa site showing rock outcrops, inclined surface boreholes and underground experimental drifts.

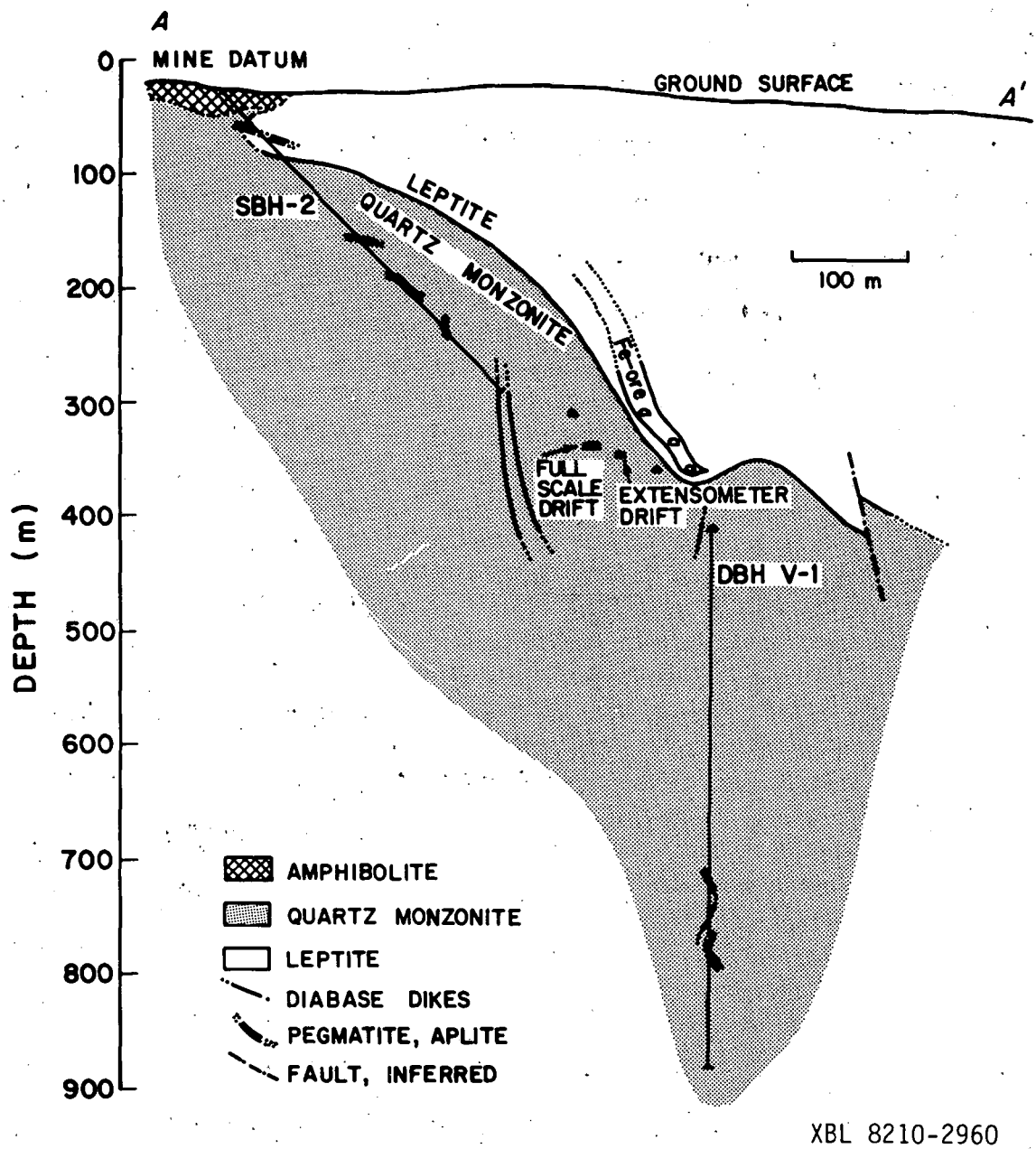

Fig. 1.4. Vertical cross-section bearing N89°E through boreholes SBH-2 and DBH V-1.

Sources of data for this rock mass and fracture system characterization include a limited number of surface outcrops (Figure 1.3), three surface boreholes and fifteen subsurface hydrology boreholes (Gale, 1981), a large number of boreholes drilled for the thermomechanical experiments and the fracture maps of the walls and the floor of the thermomechanical experimental rooms (Thorpe, 1979; Paulsson et al., 1982), as well as the maps of the ventilation experiment drift (Rouleau et al., 1981).

The surface boreholes used in this fracture study consist of three long inclined boreholes SBH-1, SBH-2 and SBH-3 (Figure 1.3). SBH-1 is an open, 76 mm diameter, diamond cored hole, 385 meters in length, that angles downward at 45 degrees and passes over the top of the test excavations and terminates at approximately the 290 meter level. SBH-2, also diamond cored, was drilled from the west toward the test excavations. This borehole is 365 meters in length, angles downward at 52 degrees and terminates in the position shown in Figure 1.3 at approximately the 290 meter level. SBH-3, 315 meters in length, also diamond cored, is drilled from the north at an angle of approximately 50 degrees south towards the test excavations, terminating in the position shown. All three inclined surface boreholes were oriented to optimize their intersection with the major fracture sets.

The subsurface hydrology boreholes (Figure 1.5) are located at the north end of the test excavations (Figure 1.6). Boreholes of this group are all diamond cored holes, 76 mm in diameter, and 30 meters in length, except R1 and R6 which are 40 meters in length. The surveyed coordinates and orientation data for all of the surface and subsurface hydrology boreholes are given in Table 1.1.

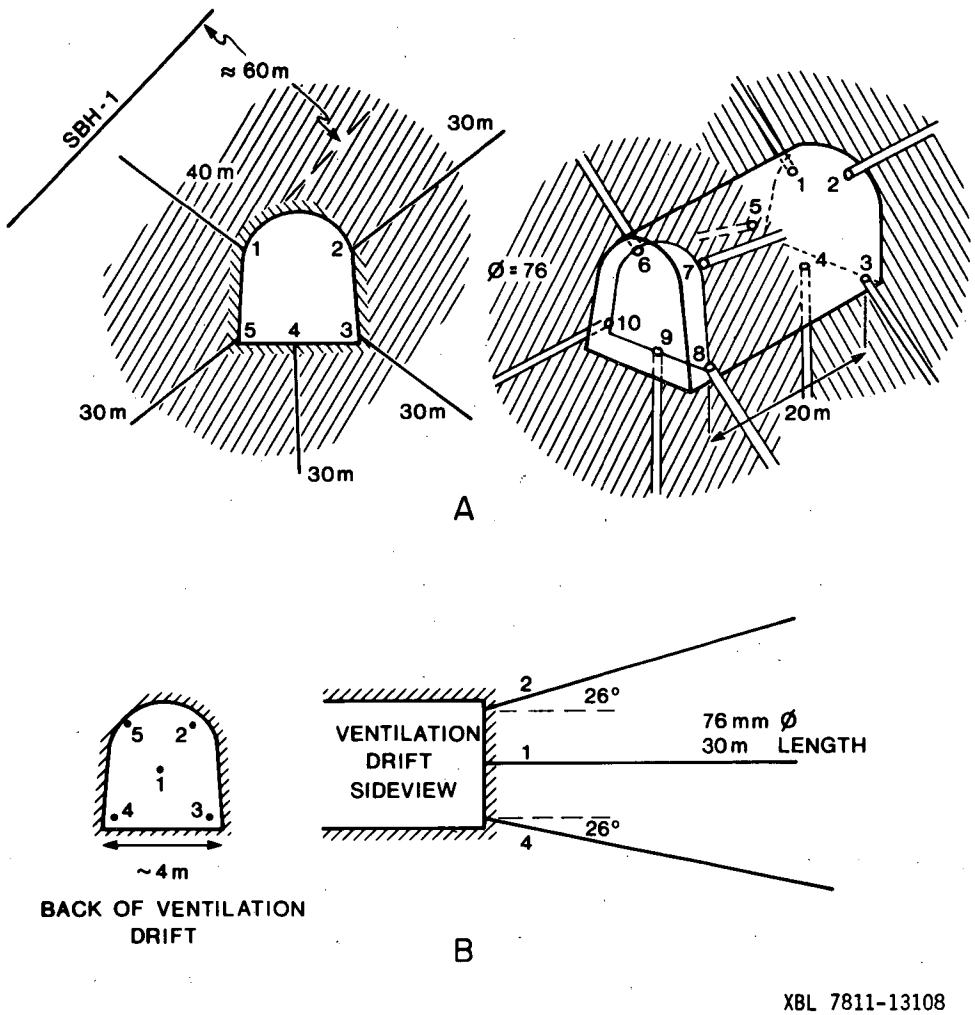

Fig. 1.5. Location and orientation of subsurface hydrology boreholes A: R-holes, B: HG-holes.

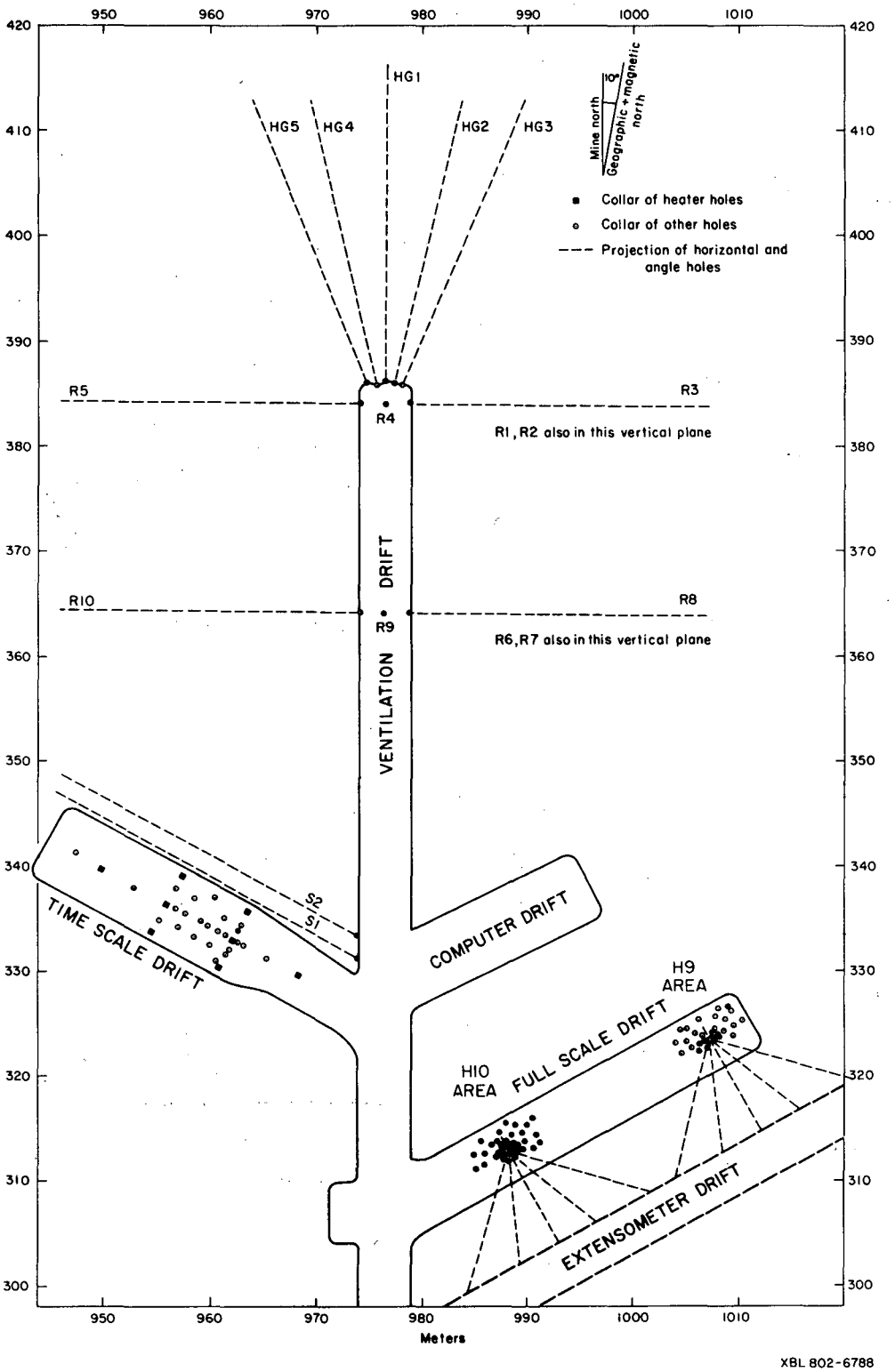

Fig. 1.6. Plan view of the experimental area at Stripa, 340 m undergound. The coordinate system on the edge of the figure is referenced to the original mine coordinates (in meters).

Table 1.1 Hydrology Borehole Coordinates and Survey Data (Gale, 1981)

Borehole No.	Mine Coordinates Top of hole			Bottom of hole			Hole Orientations (True North)	
	X(m)*	Y(m)	Z(m)	X(m)*	Y(m)	Z(m)	Bearing	Plunge**
R1	384.122	974.683	333.134	384.345	948.946	302.438	260.5°	+50.0°
R2	384.089	978.538	333.148	383.881	997.396	310.654	80.6°	+50.0°
R3	384.087	978.981	336.378	383.809	1007.215	346.620	80.6°	-19.9°
R4	384.097	976.577	336.496	384.072	976.654	366.605	98.0°	-89.8°
R5	384.125	974.363	336.368	384.353	946.110	346.666	260.5°	-20.0°
R6	364.116	974.583	333.089	364.479	948.895	302.447	260.8°	+50.0°
R7	364.099	978.192	333.135	363.933	997.282	310.267	80.5°	+50.1°
R8	364.089	978.732	336.405	363.780	1007.006	346.553	80.6°	-17.7°
R9	364.106	976.421	336.688	364.078	976.379	366.722	226.3°	-89.9°
R10	364.119	974.257	336.402	364.423	946.006	346.614	260.6°	-19.9°
HG1	386.220	976.593	334.376	416.204	976.629	334.383	350.1°	- 0.0°
HG2	385.988	977.456	332.683	412.836	983.738	321.017	3.2°	+22.9°
HG3	385.867	978.239	335.211	412.893	989.751	341.480	13.1°	-12.0°
HG4	385.788	975.776	335.985	412.799	969.536	347.788	337.0°	-23.1°
HG5	386.003	974.888	333.518	412.957	964.029	326.041	328.1°	+14.4°
SBH-1	482.60	1169.40	21.731	340.20	930.50	285.40	229.2°	-43.5°
SBH-2	363.50	662.30	26.657	326.90	902.40	290.40	88.7°	-47.4°
SBH-3	674.40	1001.20	29.138	464.20	954.20	259.60	182.6°	-46.9°
S-1	330.885	974.287	336.970	347.060	945.578	359.839	289.4°	-34.8°
S-2	332.799	974.968	337.196	348.699	946.217	359.977	288.9°	-34.7°

* + X axis: Mine North
** plunge: - down
+ up

A detailed discussion of the procedures used to log the fractures in the drill cores and to code the fracture data, and also all of the raw fracture data from the hydrology boreholes are presented in Gale (1981). Additional data on the fractures encountered during the mining activity are given in Geijer (1938).

2. ROCK MASS CHARACTERIZATION--AN ENGINEERING APPROACH

2.1 Rock Mass Characterization--Purpose and Procedures

The main objective of rock mass classification systems is to determine the characteristics that rock masses have in common in order that the experience gained at one site in assessing stability conditions and designing support systems can be applied to a different site. Thus a particular system must be useful in practical design, the terminology must be simple and direct, and the data needed to apply the classification system must be readily obtainable. While a number of rock mass characterization systems have been proposed, the most relevant to the nuclear waste disposal field are those by Terzaghi (1946), Lauffer (1958), Deere (1964), Knill and Jones (1965), Bieniawski (1973) and Barton et al. (1974).

Most of the systems described above evolved in order to deal with difficult ground conditions. Given proper screening in site selection it is unlikely that difficult ground conditions, similar to those encountered in civil and mining engineering practice, will be encountered during the development of a nuclear waste repository. However, since a large number of potential repository sites in a number of countries will be investigated, these systems provide a useful reference point for site comparisons. The primary inputs in many of these systems are the geologic logs of drill cores (Rose et al., 1981). Since the first data available from a potential repository site will be surface data and drill cores, these systems provide a means of making an initial assessment of the potential suitability of a site for a nuclear waste repository as the site is being investigated. What is needed is some experience in correlating rock mass

classification parameters with the parameters that are critical to nuclear waste disposal.

The parameter that is most critical to nuclear waste disposal is the rate of groundwater movement. In fractured crystalline rocks, fractures represent by far the most important potential pathways by which radionuclides can migrate. Fortunately nearly all rock mass characterization systems are based on the degree of fracturing in one form or another. Terzaghi's (1946) classification system for computing tunnel loads was based primarily on the degree of fracturing in a general and descriptive sense. Lauffer (1958) included fractures in his system and introduced the concept of standup time which, while it is of importance to the stability of the rock mass subjected to thermomechanical loads, will not be discussed here. The rock quality designation (RQD) system introduced by Deere (1964) is a practical and simple approach and consists of measuring the total length of all pieces of intact core that are 10 cm or greater in length. The result is then expressed as a percent of the length of the borehole section drilled. The RQD system is also incorporated into the geomechanics system proposed by Bieniawski (1973) and the Q-index proposed by Barton et al. (1974). Knill and Jones (1965) proposed several engineering logs, including mean core length and number of fractures per meter (fracture frequency) as a means of describing the variation in fracturing along the borehole length. In practice this variation is determined by calculating the RQD, mean core length and fracture frequency over fixed lengths of the borehole. A variation of this last approach has been adopted for the Stripa data.

2.2 Characterization of the Rock Mass at Stripa

In this study we have attempted to correlate the variations in RQD, mean core length and fracture frequency with the measured hydraulic conductivities. The RQD values for nearly all of the drill cores from Stripa have been calculated using a fixed 2-meter interval. These data are tabulated in the report by Olkiewicz et al., (1979), and show that RQD values very seldom fall below 80 percent indicating good to excellent rock mass conditions. However the RQD values decrease with a decrease in the size in the drill core, reflecting the susceptibility of the Stripa core to damage during drilling because of the large number of healed to partly healed fissures that pervade the rock mass.

Since flow occurs in discrete fractures or groups of fractures, using a fixed 2-meter interval approach in calculating RQD may smooth out the variation in the fracture characteristics and mask any real correlation with the variation in hydraulic conductivities. Thus, although the hydraulic conductivities were determined by using 2-meter packer intervals or greater (Gale, 1981), a moving average approach (Gale, 1983) was adopted in calculating RQD, mean core length and fracture frequency values. A 2-meter interval was selected and the RQD and other values were plotted at the mid-point of the interval. Both ends of the 2-meter interval were then advanced 0.2 meter, the values calculated and then plotted at the center of this new section. The interval was moved in 0.2 meter steps along the length of the drill core producing a plot with a series of values spaced 0.2 meter apart.

The data for three of the subsurface boreholes, R3, R5 and R7, have been plotted in Figures 2.1, 2.2 and 2.3. Boreholes R3 plunges 19.9

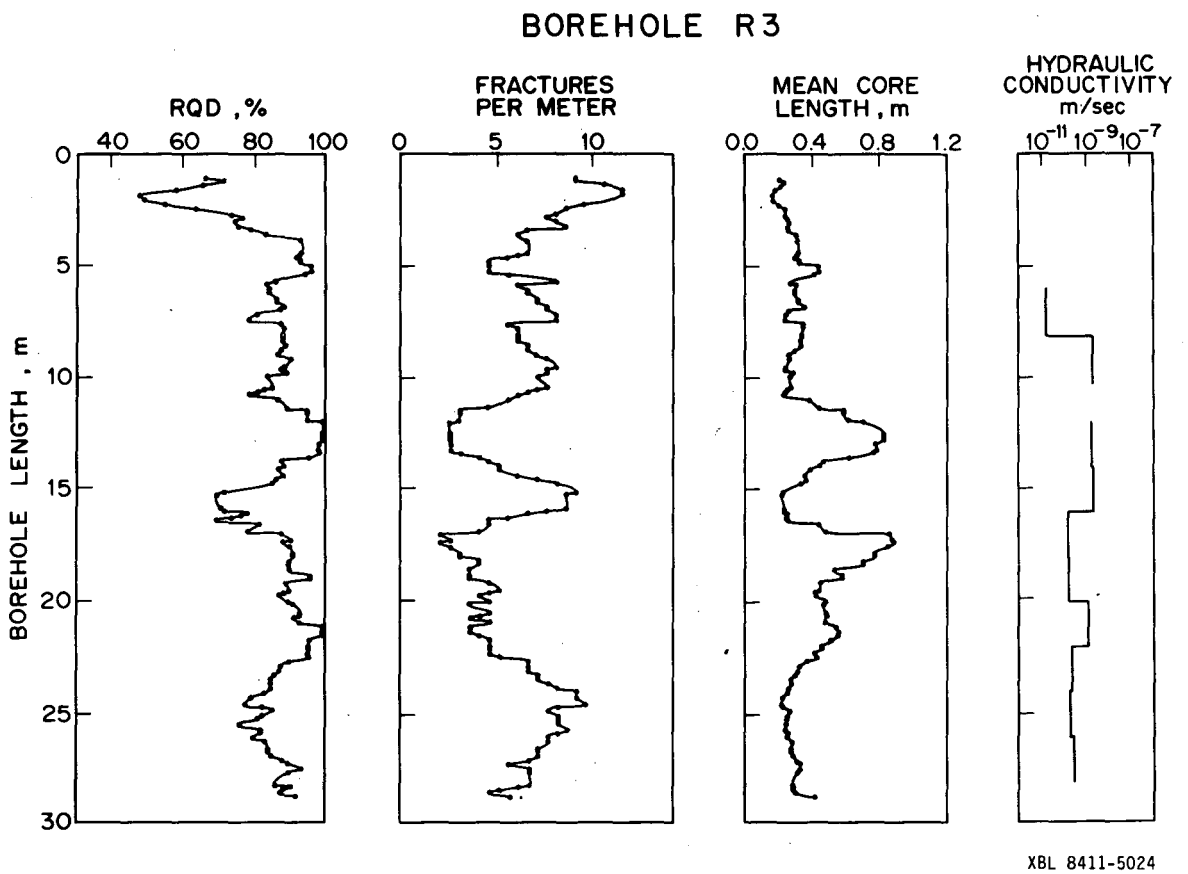

Fig. 2.1. Plot of RQD, fractures per meter, and mean core length using a moving average, with an interval of 2.0 m and a distance increment of 0.2 m; borehole R3.

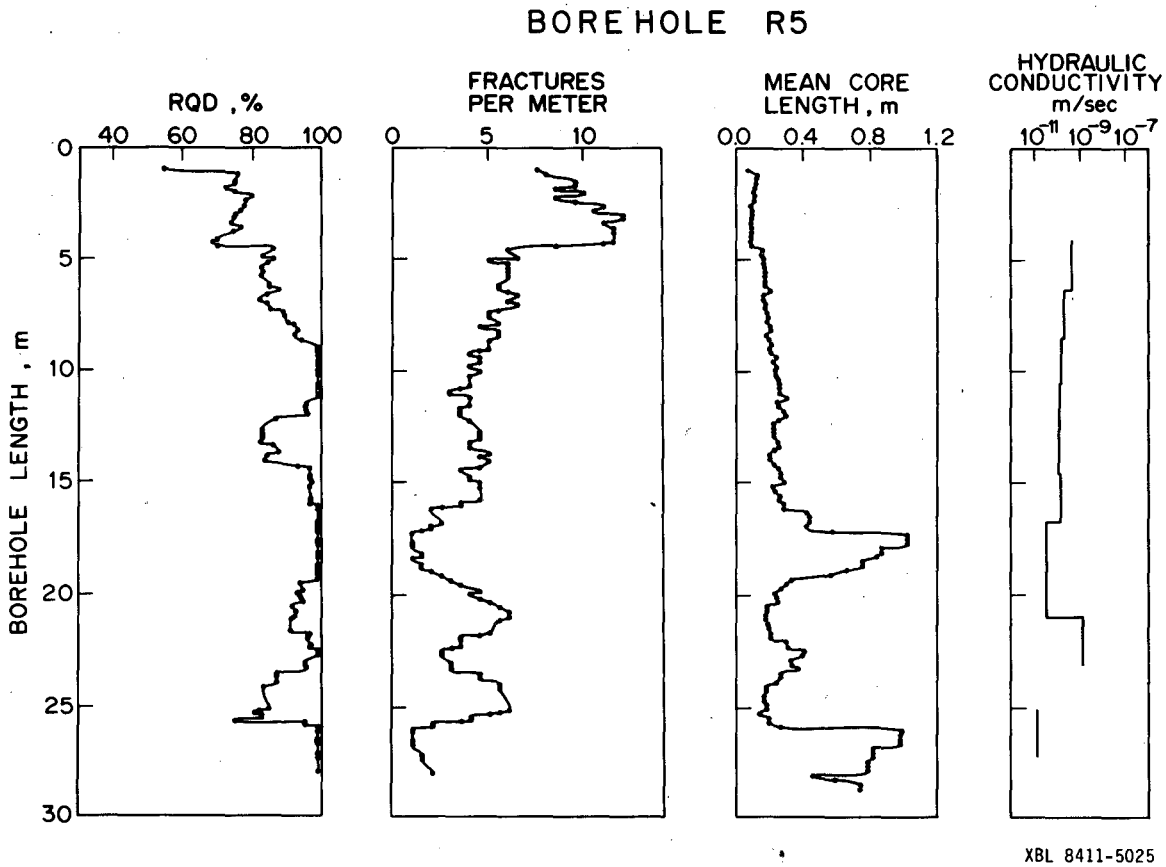

Fig. 2.2. Plot of RQD, fractures per meter, and mean core length using a moving average, with an interval of 2.0 m and a distance increment of 0.2 m; borehole R5.

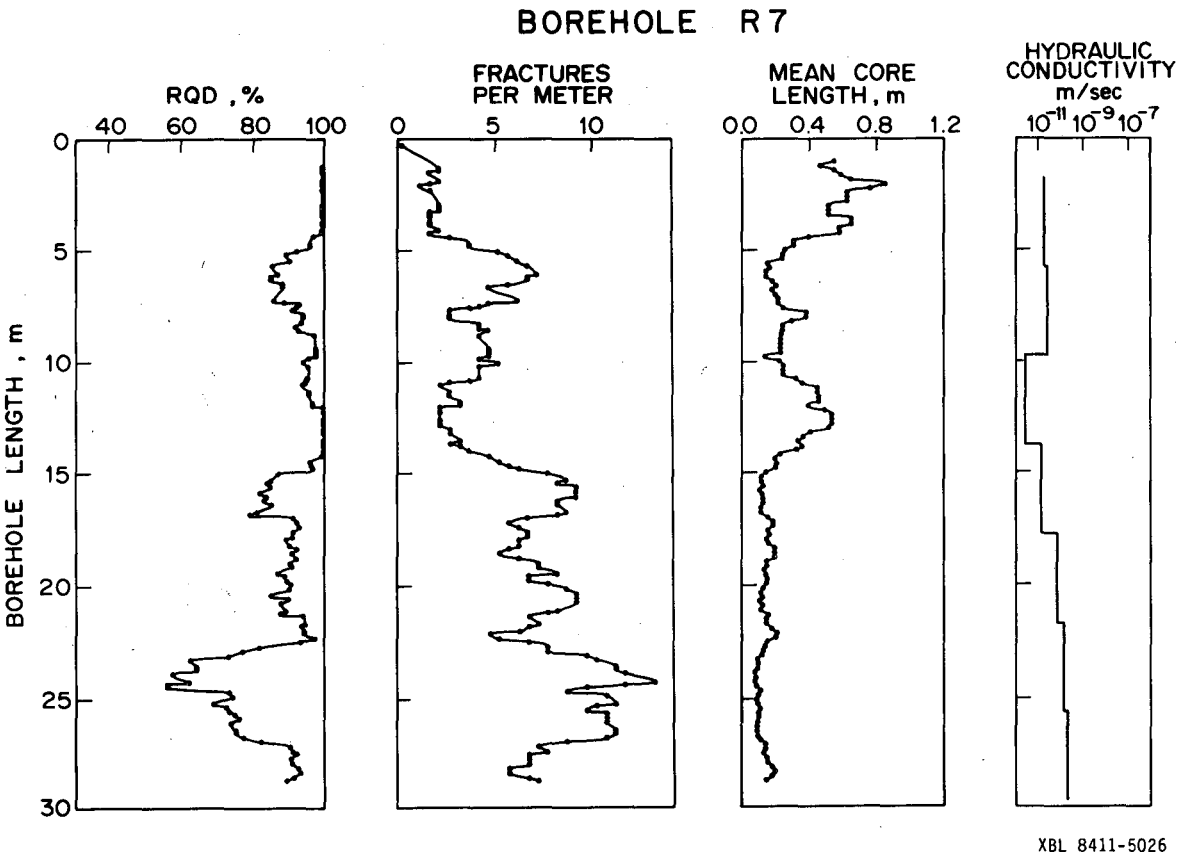

Fig. 2.3. Plot of RQD, fracture per meter, and mean core length using a moving average, with an interval of 2.0 m and a distance increment of 0.2 m; borehole R7.

degrees with a bearing of N 80.6 degrees. R5 plunges 20 degrees with a bearing of 260.5 degrees. R7 is directed 50.1 degrees above the horizontal with a bearing of 80.5 degrees, similar to R3. Both R3 and R5 are in the same vertical plane and R7 is located in a parallel vertical plane separated by a horizontal distance of 20 meters (Figure 1.5).

While there is good correlation among the RQD, fracture frequency and mean core length values, as one would expect, there is very little correlation of fracture characteristics with the hydraulic conductivity values along the borehole. However both R5 and R7 show decreasing hydraulic conductivity with (1) increase in RQD values, (2) decrease in the number of fractures per meter and (3) a general increase in the mean core length. The lowest hydraulic conductivity values in R5 and R7 are clearly associated with the high or low points on the other three plots. The overall trend of increasing permeability with increase in fracture frequency is shown in Figure 2.4. Figure 2.4 is a plot of the permeabilities determined from each injection test versus the number of fractures in that injection test interval. As can be seen in Figure 2.4, while the correlation between fracture frequency and permeability is very weak, the regression definitely does not have a zero slope. Table 2.1 shows that if the slope was exactly zero, the probability of getting a value of F greater than the one obtained would be as low as 0.0001. Nevertheless the wide scatter present in the data suggests that factors other than the raw fracture frequency also influence the rock mass permeability. This variability in the data may reflect the fact that neither RQD, mean core length, or fracture frequency distinguishes between the individual members of the different fracture sets--with their different permeabilities--

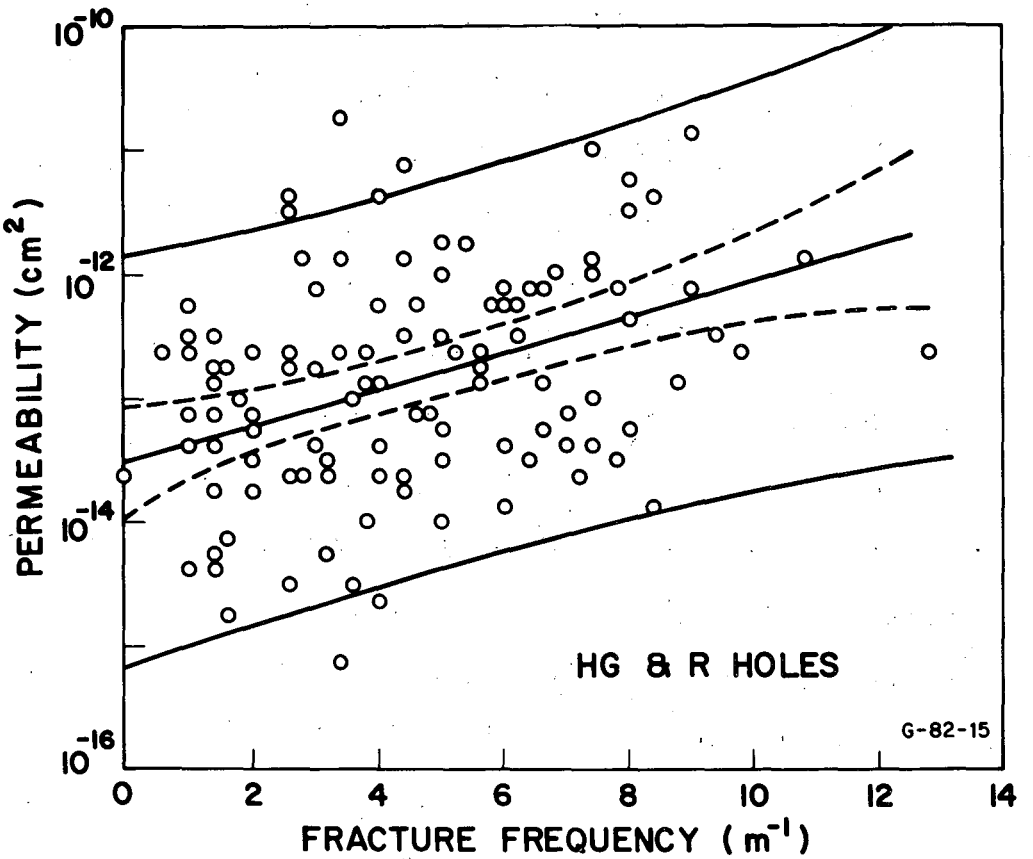

XBL 8210-2964

Fig. 2.4. Permeability versus fracture frequency data from the R and HG boreholes. The dashed lines indicate the 95 percent confidence limits for the mean values and the solid lines indicate the same confidence limits for the individual values.

Table 2.1. Analysis of variance for the linear regression of the natural logarithm of permeability versus fracture frequency

Source of Variation	Degree of Freedom	Sum of Squares	Mean Square	F Ratio	PR[> F]
Model	1	15.49	15.49	22.21	0.0001
Residual	121	84.41	0.70		
Total	122	88.90			

Notes

Dependent variable: ℓn (permeability)

Independent variable: fracture frequency

F Ratio = mean square (model)/mean square (residual) and follows the F distribution.

that may be present in a given test interval. This variation in fracture permeability from one set to another could be the result of a number of factors including (1) variation in infilling material, (2) variation in fracture aperture and (3) variation in the degree of interconnection between fracture sets. This may account for the lack of correlation between parameters in R3 since it has a different orientation than R5 and R7 and hence would tend to intersect a different set of fractures. To properly quantify the degree of correlation between each parameter for each borehole and to compare the correlation coefficients from borehole to borehole requires an approach that has yet to be developed. Separation of the individual members of each fracture set in the borehole data may show much stronger correlations with RQD and fracture frequency, especially if one fracture set is much more permeable than the others.

3. STATISTICAL CHARACTERIZATION OF THE FRACTURE SYSTEM

In geological studies the strike and dip of fractures in outcrops are routinely measured. However, very little other data on the fractures are recorded. Only in a few exceptional cases does one find statistical information on the length and spacing of individual fractures that is tied to the basic orientation data. Similarly, only in a few recent studies, (Kendorski and Mahtab (1976), and Raven and Gale (1977)), have workers collected fracture orientation data, both from the surface outcrops and subsurface excavations, and attempted to correlate both sets of data. It is obvious that the degree of variation in fracture geometry, both horizontally and vertically, in a given rock mass determines to a large extent how well one can make predictions about subsurface geometries and associated hydraulic and stability problems from surface and near surface data. Obviously, in the site selection and excavation process, it would be a considerable advantage to be able to predict subsurface conditions from surface or near surface conditions.

At Stripa, an extensive amount of fracture geometry data have been collected, both from the surface outcrops and the subsurface excavations, as well as from the analysis of the fractures intersecting the hydrology boreholes (Gale, 1981), and the numerous thermomechanical boreholes (Thorpe, 1979; Paulsson et al., 1982). Among other things these latter two studies analyzed the type of fracture infilling material. The type of infilling material is certainly a fundamental parameter for understanding the origin of the fracture system; it is also an important factor controlling the strength of the fractures and hence the mechanical behaviour of a rock mass. However, with the exception of argillaceous material, the

importance of infilling or coating material on fracture permeability is yet poorly understood. Paulsson et al. (1982) found that calcite-filled fractures are significantly more open in rock cores than chlorite-coated and epidote-filled fractures. This finding probably reflects the greater brittleness of calcite, and hence its greater susceptibility to drilling-induced breakage, than the two other infilling or coating minerals. Nevertheless that observation does not allow any conclusion concerning the fracture permeability of the undisturbed rock mass.

This report is primarily concerned with the rock mass surrounding the ventilation drift. Since this drift was used principally for hydrological testing, only the fracturing parameters clearly affecting the rock mass permeability have been considered. Using the basic data given in Gale (1981) and Rouleau et al. (1981) we have determined the number of fracture sets and their orientation, spacing, and length characteristics. Where possible we have attempted to detect variations in these characteristics throughout the rock mass. In collecting the data, distinction has been made between joints, veins, and fracture zones. We define joints as fractures that have not experienced significant displacement along their plane and that do not contain infilling material; they may however have coating material. Veins are simply open joints with some infilling material. Fracture zones are arbitrarily defined as those zones that contain many fractures shorter than 0.5 meter and with 0.05 to 0.10 meter spacings. Since the number of veins and fracture zones is relatively small, this statistical analysis is essentially concerned with joints. Thus, in the rest of the report, joints are referred to by the more general term "fractures".

3.1 Fracture Orientations

One of the accepted procedures in analyzing fracture orientation data is to plot and contour the poles to the fracture planes on an equal-area hemispheric orientation diagram (Phillips, 1972). The contour lines define areas of equal pole density and thus permit visual identification of fracture sets. The fracture data from Stripa were stored in a series of readily accessible computer files. This permitted rapid filtering and analysis of the basic data and the computer plotting and contouring of a number of lower-hemisphere pole diagrams from different data sets representing different areas of the test site.

3.1.1 SBH Boreholes

The orientation data collected from the whole length of the three SBH drill cores are presented in Figure 3.1. The diagram of Figure 3.1 shows only weak clustering of the fracture poles. The best defined cluster corresponds to the sub-horizontal fractures. This cluster however is located in the vicinity of the zone most favored by the orientation bias (Terzaghi, 1965). This zone is approximately defined by the spherical triangle formed by joining the points corresponding to the orientation of the three boreholes. The orientation bias, combined with the fact that the peak concentration of the cluster is only 3.9% (per 1% surface area), makes the significance of the sub-horizontal cluster very questionable. The scattering observed in Figure 3.1 is probably due to the mixing of fracture data collected from different lithologies and different struc- tural domains.

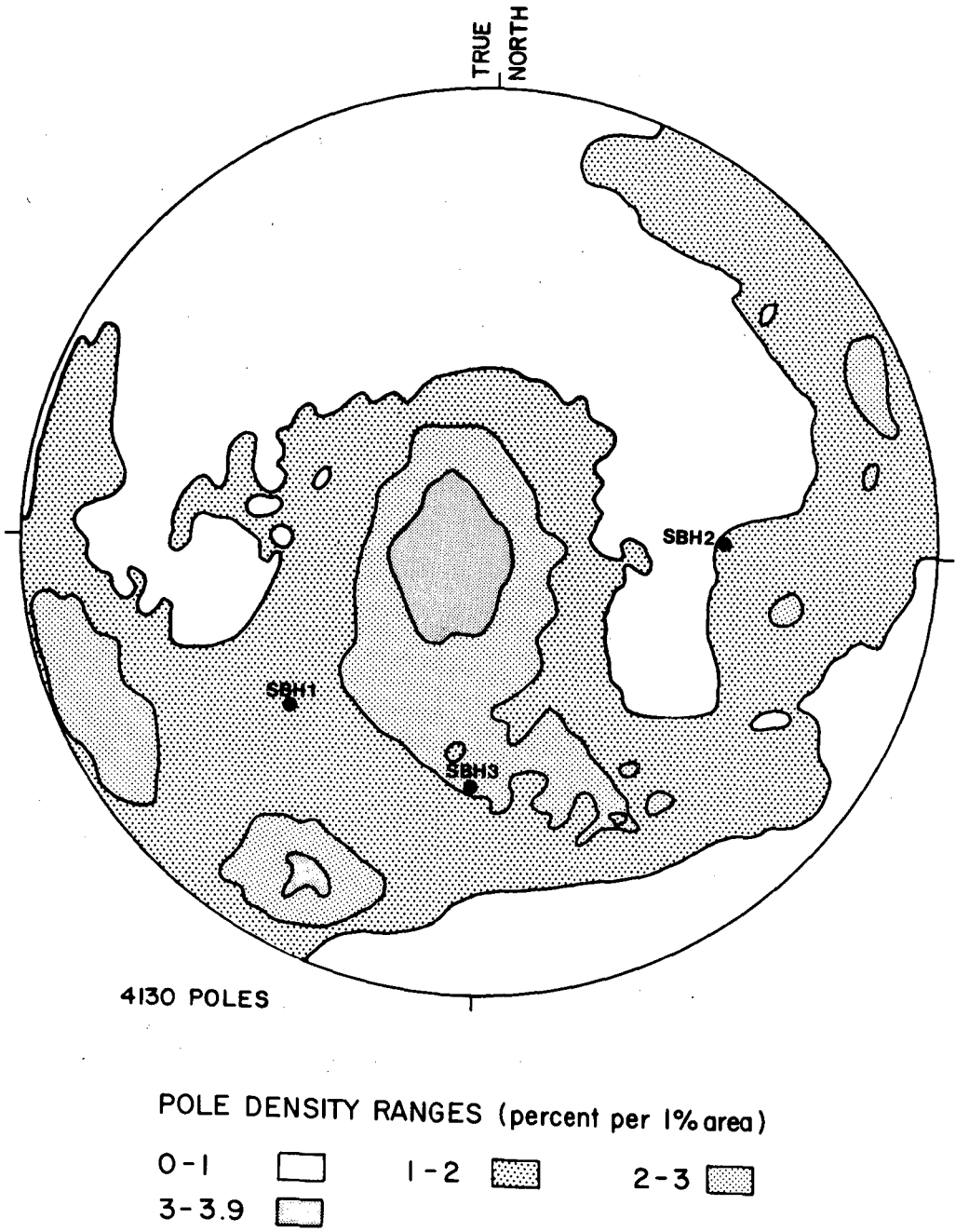

XBL 8411-5027

Fig. 3.1. Pole diagram for the fracture planes intersecting the drill cores of the three SBH holes (data from the entire length of the boreholes). Lower-hemisphere equal-area plot.

In order to eliminate some of the lithologic and structural variations, a pole diagram has been constructed for the fracture data obtained from the bottom segment only of the three SBH holes (Figure 3.2). These borehole segments correspond to the depth range of 175 meters to 290 meters in the mine coordinate system (see Figure 1.4). All the fracture data are from the granitic rock mass, and at 10 meters or more from a known contact with the leptite (Gale, 1981).

It can be seen on Figure 1.3 that using only the fractures from the bottom segment of the SBH holes decreases considerably the distance between the various points of the rock mass that are represented in the sample. Even then, at the top end of these bottom segments, some of the fracture data come from points that are as far apart as 270 meters in the rock mass. We will see in analyzing the data from the underground test excavation that the fracturing of the rock mass shows an appreciable variability even within a much smaller distance than 270 meters.

Four fracture sets are defined for the lower portion of the SBH holes. In order to facilitate the comparison of the SBH data with those from the underground excavations, the number of each fracture grouping in Figure 3.2 is the same as the number assigned to the fracture grouping having a similar orientation on the orientation diagram for the rock mass surrounding the ventilation drift (see Figure 3.8).

In spite of the large volume of sampled rock mass, the orientation diagram of Figure 3.2 shows two well-defined clusters, corresponding to fracture sets 1 and 4. Two other clusters, somewhat weaker, corresponding to fracture sets 2 and 3 are also identified on Figure 3.2. Since the 1 contour corresponds to the average concentration of poles on the

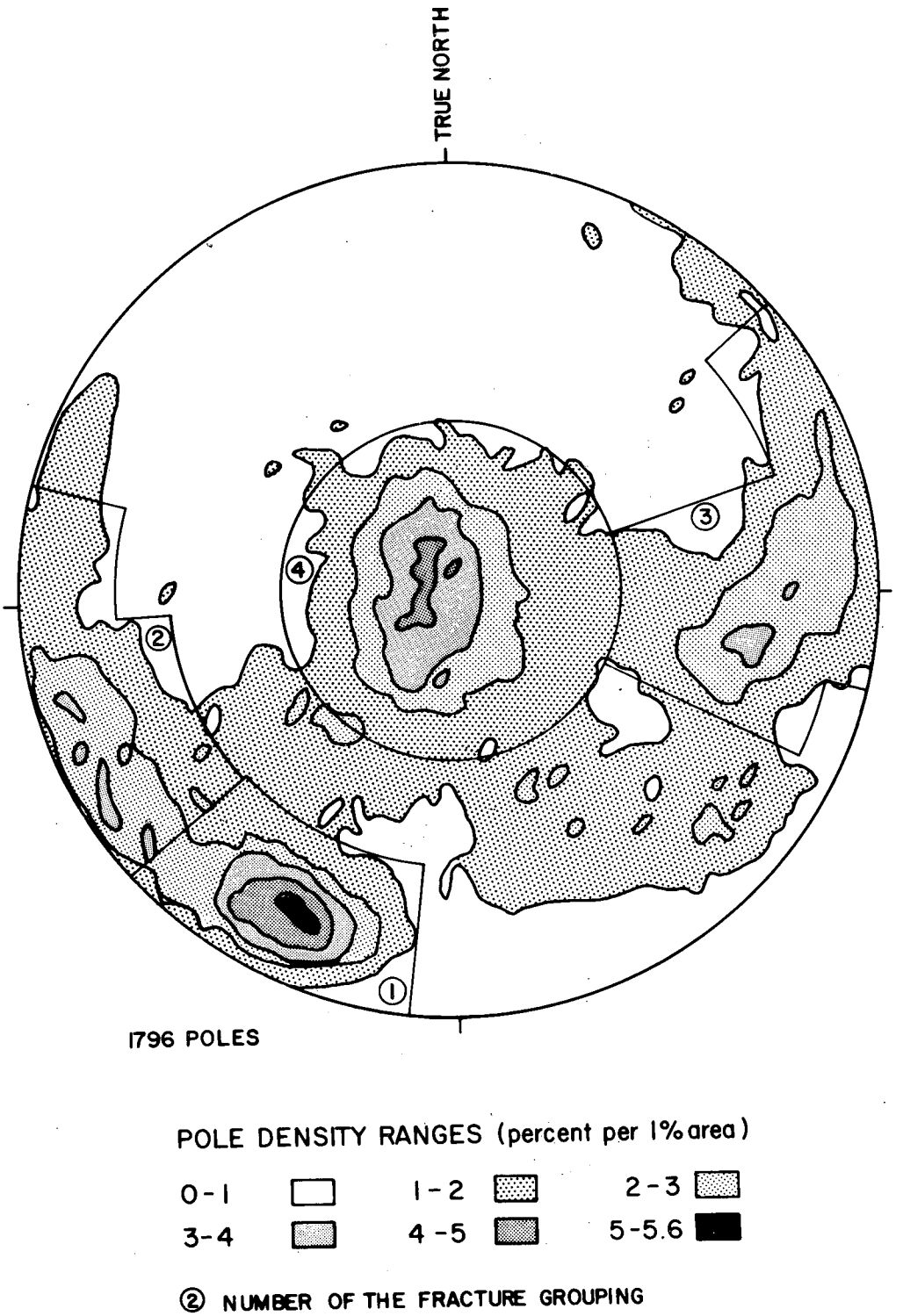

XBL 8411-5028

Fig. 3.2. Pole diagram for the fracture planes intersecting the drill cores from the bottom segment of the three SBH holes, i.e., from a depth of 175 m to 290 m. Lower-hemisphere equal-area plot.

diagram, this contour has been taken as the significant threshold for the clusters and thus as the logical boundary of the fracture sets. The set boundaries have been linearized (Figure 3.2) in order to facilitate the automatic assignment of the appropriate set number to each fracture, so that each set can be analyzed separately (see Section 3.3). Linear boundaries between two adjacent clusters have been drawn by visual inspection. A major limiting assumption here is that fracture sets do not overlap. Table 3.1 gives the boundaries of the fracture sets delineated on Figure 3.2, in terms of orientation, as well as a visually determined average orientation for each fracture set.

3.1.2 Test Excavations

3.1.2.1 Ventilation Drift

The contoured lower-hemisphere orientation diagram of the data collected in the floor and the walls of the ventilation drift (see Figure 3.7 below) is given in Figure 3.3. This figure incorporates only joints and no other structural discontinuities such as veins and fracture zones. Orientation diagrams for the veins and fracture zones are presented in Appendix A.

On Figure 3.3, two clusters are more clearly defined than the other clusters. The bottom cluster corresponds to the fractures which strike approximately N 70° W and dip steeply to the north. The other well defined cluster corresponds to sub-horizontal fractures that generally dip to the southeast. Some clustering is also apparent for the fractures oriented at N 10° E, with dip 55° W. The drift from which these data

Table 3.1. Fracture sets defined by the fracturs intersecting the drill cores from the bottom segment of the SBH holes. (depth of 175m to 290 m).

Set	Dip Direction		Dip		Visual Average	
	From	To	From	To	Dip Direction	Dip
1	6	48	53	90	29	71
2	49	87	54	90	66	76
	88	106	66	90		
3	229	251	68	90	274	66
	252	284	32	90		
	285	296	32	78		
4	0	359	0	32	125	4

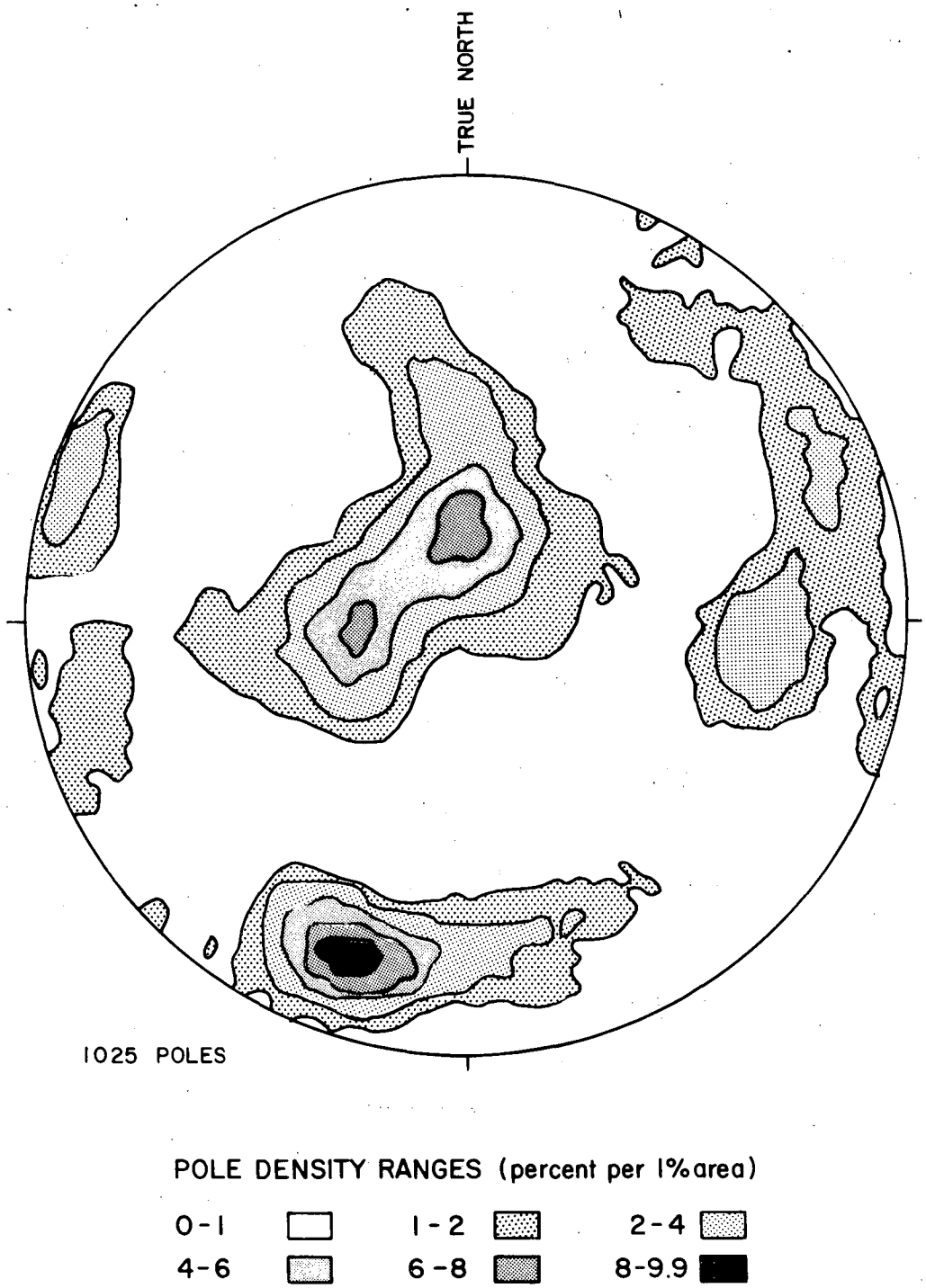

XBL 8411-5029

Fig. 3.3. Pole diagram for all the fracture planes measured on the faces of the ventilation drift. Lower-hemisphere equal-area plot.

were collected is oriented N 10° W. This orientation introduces a bias in the sample favoring vertical fractures that are striking approximately east, like those forming the cluster at the bottom of Figure 3.3.

Figure 3.4 presents the pole diagram for a completely different data set, the data taken from the thirteen oriented HG and R drill cores. The data from the drill cores and the data from the drift maps can be considered independent in the sense that they have been collected by different workers using two different sampling techniques. In Appendix A, two additional orientation diagrams are given, one for the R holes only and one for the HG holes only. Since about 80% of the data included in Figure 3.4 comes from the radial (R) holes (1293 of the 1623 poles), we may consider the bias of Figure 3.4 as complementary to the bias of Figure 3.3. In spite of the completely different orientation bias and the independence of the data sets, the clusterings in both figures are remarkably similar.

3.1.2.2 Full-Scale Drift

Figure 3.5 presents the orientation data obtained from the cores of the boreholes drilled around the full-scale drift. Fifty-eight percent of these data come from horizontal holes (679 of the 1176 poles), the remaining come from vertical holes. Separate plots for the vertical and the horizontal holes are shown in Appendix A. A thorough analysis of the fracturing in the full-scale drift is given in Paulsson et al., (1982).

A comparison of Figure 3.5 with Figures 3.3 and 3.4 reveals that the fracture groupings are essentially the same in the ventilation drift and in the full-scale drift. The only exception seems to be the fracture set oriented N 10° E, dip 55° W, that is clearly present in the ventilation

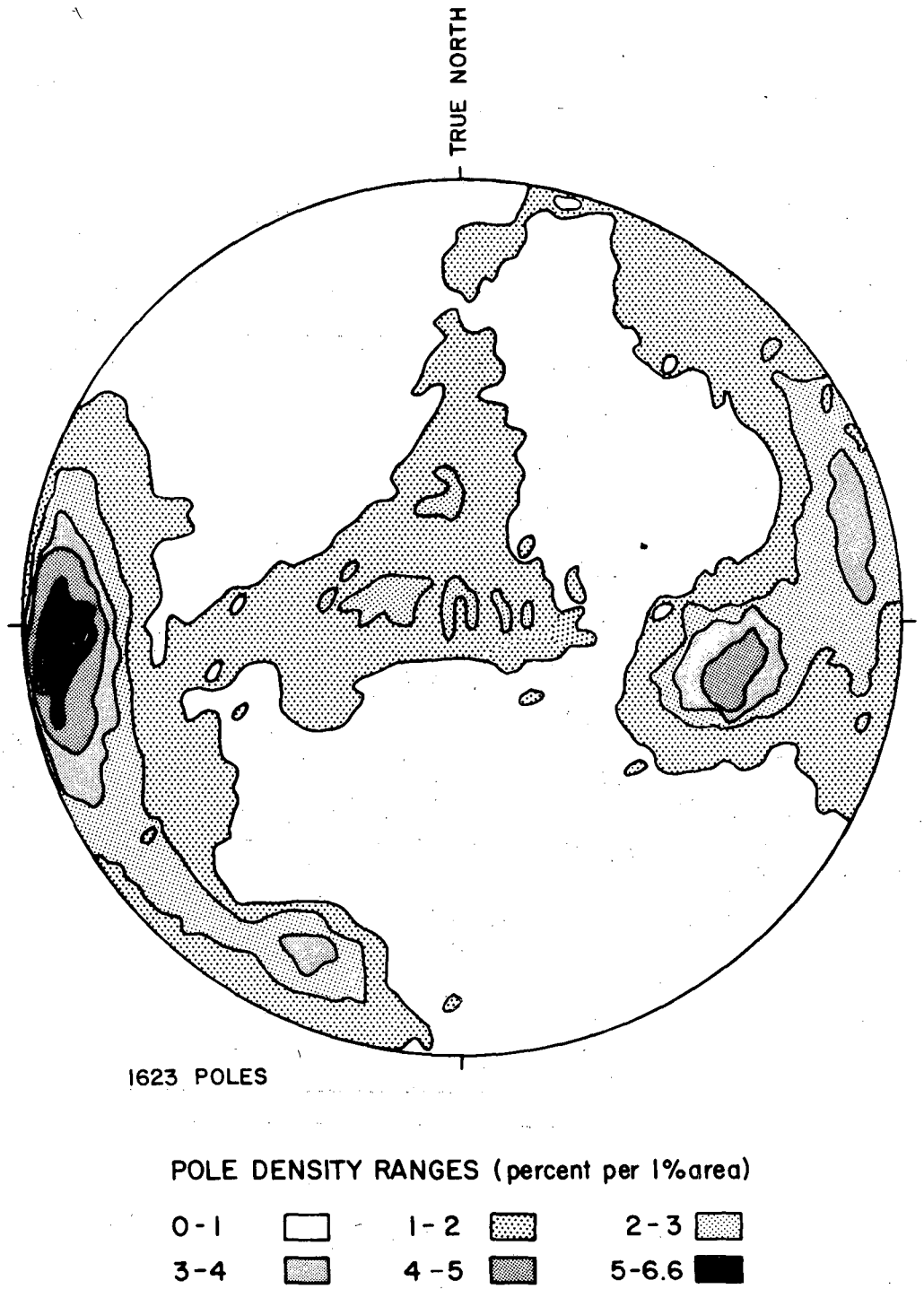

XBL 8411-5030

Fig. 3.4. Pole diagram for all the fracture planes intersecting the drill cores from all the HG holes and all the R holes, except R4 and R9. Lower-hemisphere equal-area plot.

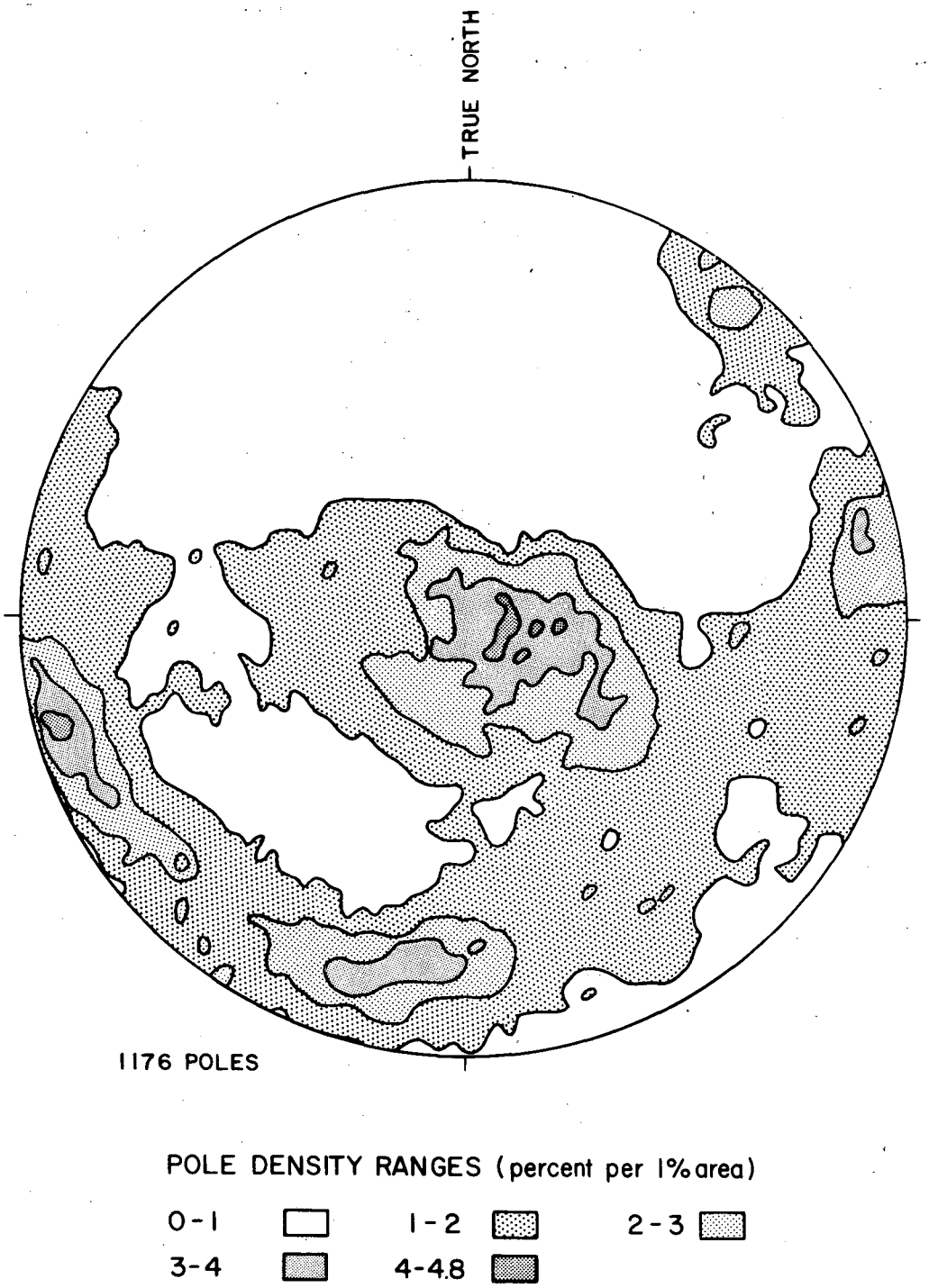

XBL 8411-5031

Fig. 3.5. Pole diagram for fracture planes intersecting the drill cores from the full-scale drift. Lower-hemisphere equal-area plot.

drift in both of the data sets, but is very weakly represented in the full-scale drift.

3.1.2.3 Time-Scale Drift

Detailed mapping, core logging, and analysis of the fracture system in the time-scale drift have been reported by Thorpe (1979). Figure 3.6, taken from Thorpe (1979), gives the contoured orientation diagram for the poles of 827 fractures in the time-scale vertical boreholes. This figure shows the numbers, in Roman numerals, assigned by Thorpe (1979) to the various fracture sets. Since all the sampling lines (boreholes) are vertical, this sample is heavily biased toward horizontal fractures. Indeed, essentially no vertical fractures are present on Figure 3.6. Thus one must recognize that the various clusters shown in Figure 3.6 are to some extent shifted towards the center of the diagram with respect to what would have been obtained had the sample been unbiased. Nevertheless, keeping this orientation bias in mind, we can correlate qualitatively the clustering of Figure 3.6 with that of Figures 3.3, 3.4 and 3.5. Fracture set I in the time-scale drift corresponds to the fracture set oriented N 10° E, dip 55° W, that is clearly shown in Figures 3.3 and 3.4. As mentioned above, this fracture set is at best weakly represented in the full-scale drift. Set II of Thorpe (1979) is probably formed by the shifting toward the center of the diagram of two fracture sets, one essentially oriented north and steeply dipping to the east, and one oriented N 70° W and dipping steeply to the north. Both of these fracture sets are present in the ventilation drift and in the full-scale drift. The sub-horizontal fracture set IV in Figure 3.6 is present everywhere in the test

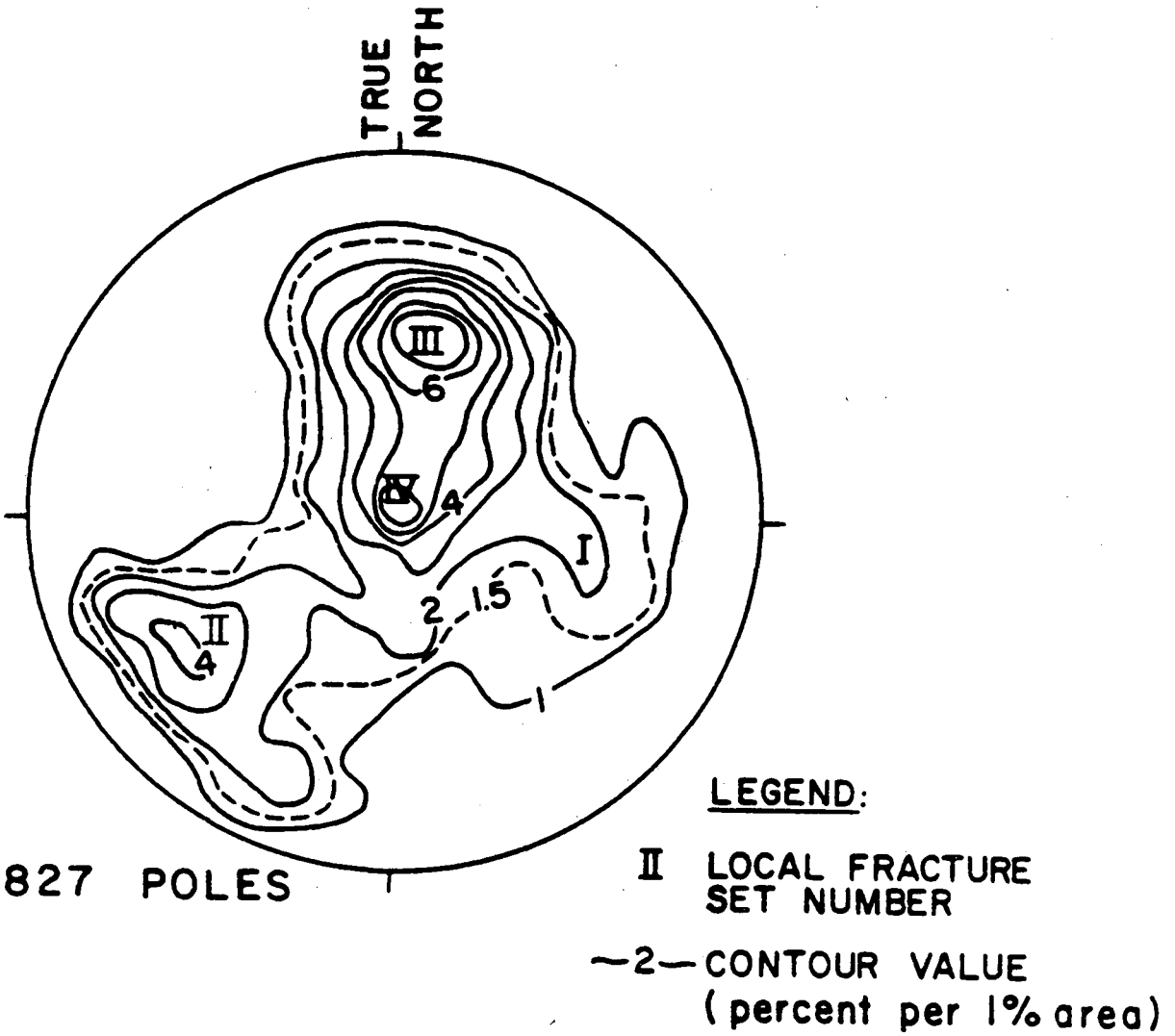

XBL 8411-5043

Fig. 3.6. Pole diagram for the fracture planes intersecting the cores of the boreholes drilled in the floor of the time-scale drift (from Thorpe, 1979).

3.1.3 Summary and Conclusion

Figure 3.7 presents a composite diagram of the contour plots of poles to fracture planes summarizing the fracture orientation data from the Stripa site. The orientation diagrams of Figures 3.1 to 3.6 are shown side by side in Figure 3.7 in order to facilitate their comparison.

Since the following sections of this report deal essentially with the analysis of the fracture trace lengths, spacings and density in the vicinity of the ventilation drift, we have created in Figure 3.8 an orientation diagram containing all the orientation data available from the HG and R holes (Figure 3.4) and from the faces of the ventilation drift (Figure 3.3). As pointed out above, the diagrams of Figures 3.3 and 3.4 are affected by complementary orientation bias. Therefore their combination in the same diagram (Figure 3.8) presumably gives a relatively unbiased picture of the actual importance and orientation of the various fracture sets permeating the rock mass around the ventilation drift. The linearized boundaries shown in Figure 3.8 for the four identified fracture sets have been drawn by visual inspection, as discussed in relation with Figure 3.2. Table 3.2 gives the boundaries of the fracture sets delimited on Figure 3.8, in terms of orientation, as well as a visually determined average orientation for each fracture set.

Finally, it is also interesting to note the relatively good agreement between the orientation of the various fracture sets in Figure 3.2, presenting data from the bottom segment of the three SBH holes, and in Figure 3.8, constructed with data from the immediate vicinity of the ventilation drift. Fracture sets 1 and 4 in both diagrams are essentially the same, whereas the pole clusters for the fracture sets 2 and 3 are not as clearly defined in Figure 3.2 as they are in Figure 3.8.

excavation. The prodominant cluster in Figure 3.6, corresponding to the fracture set III, seems to be absent in the full-scale drift. On Figures 3.3 and 3.4 showing ventilation drift data, this fracture set is not defined. The presence of southward dipping fractures with very shallow dip and fractures striking N 70° W and dipping steeply to the south suggests that the fractures representing fracture set III of the time-scale drift may also be present in the ventilation drift, but combined with the other sets. South dipping fractures, that strike N 70° W, at the north end of the ventilation drift and in the time-scale drift were observed in the preliminary fracture survey of the test excavation (Olkiewicz et al., 1979). Only the orientation diagram for the HG holes given in Appendix A confirms the presence of these south dipping fractures. The downward lobe in the top part of this latter pole diagram suggests the presence of a separate set corresponding to set III in the time-scale drift (Figure 3.6). This fracture set would therefore be present mainly in the northwest portion of the rock mass surrounding the test excavation.

3.1.2.4 Other Drifts

Other non-contoured orientation diagrams have been presented in Olkiewicz et al. (1979), for the ventilation tunnel and the lower tunnel, both at the 360 meter level. Fractures corresponding to the N 70° W, north dipping set in the main test excavation are clearly present in all mapped areas. The sub-horizontal and the north-oriented sub-vertical fractures also seem to be present at this greater depth, and the existence of a set oriented N 10° E and dipping to the east at an intermediate angle is suggested.

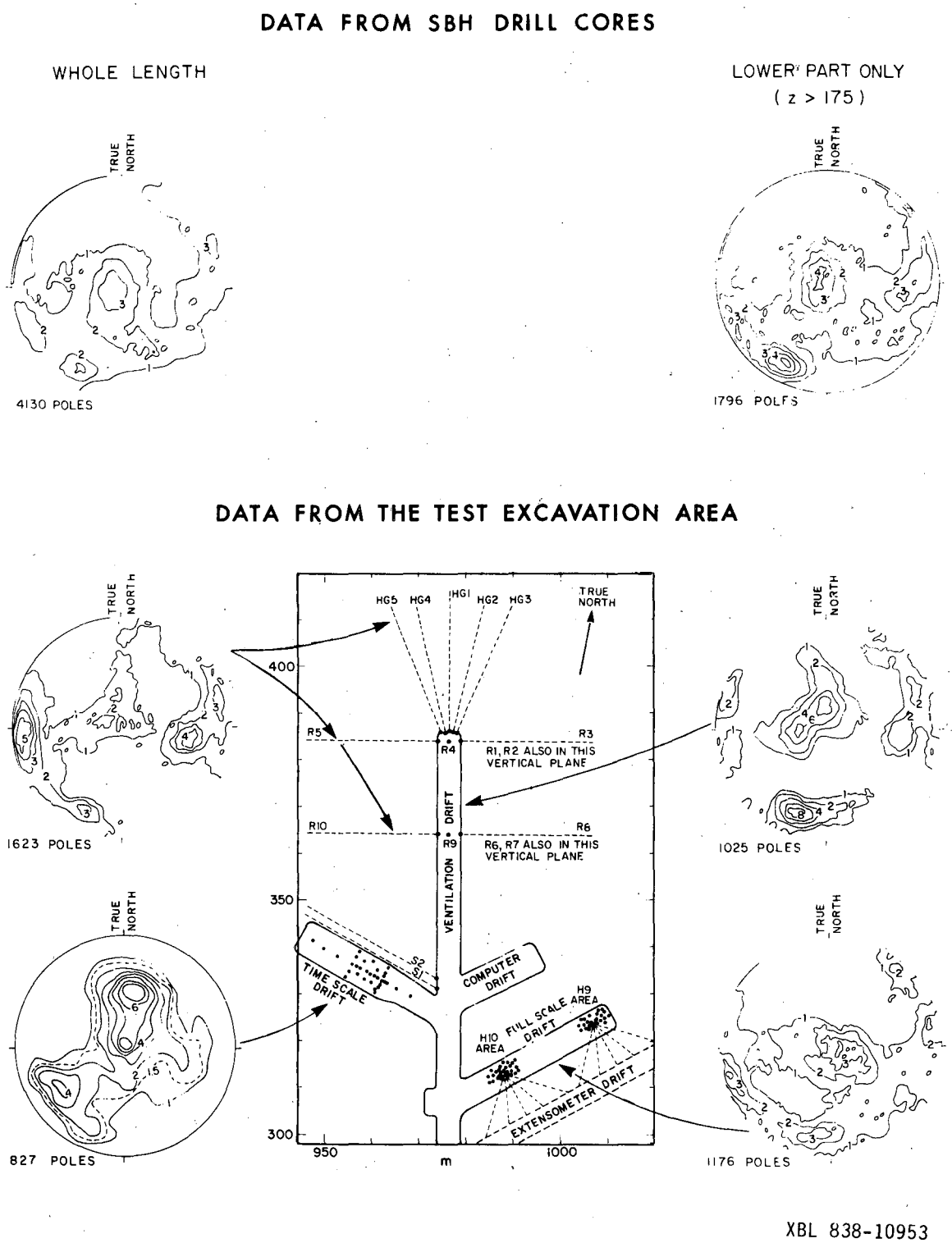

Fig. 3.7. Composite diagrams showing the fracture orientation data from different areas of the test excavation.

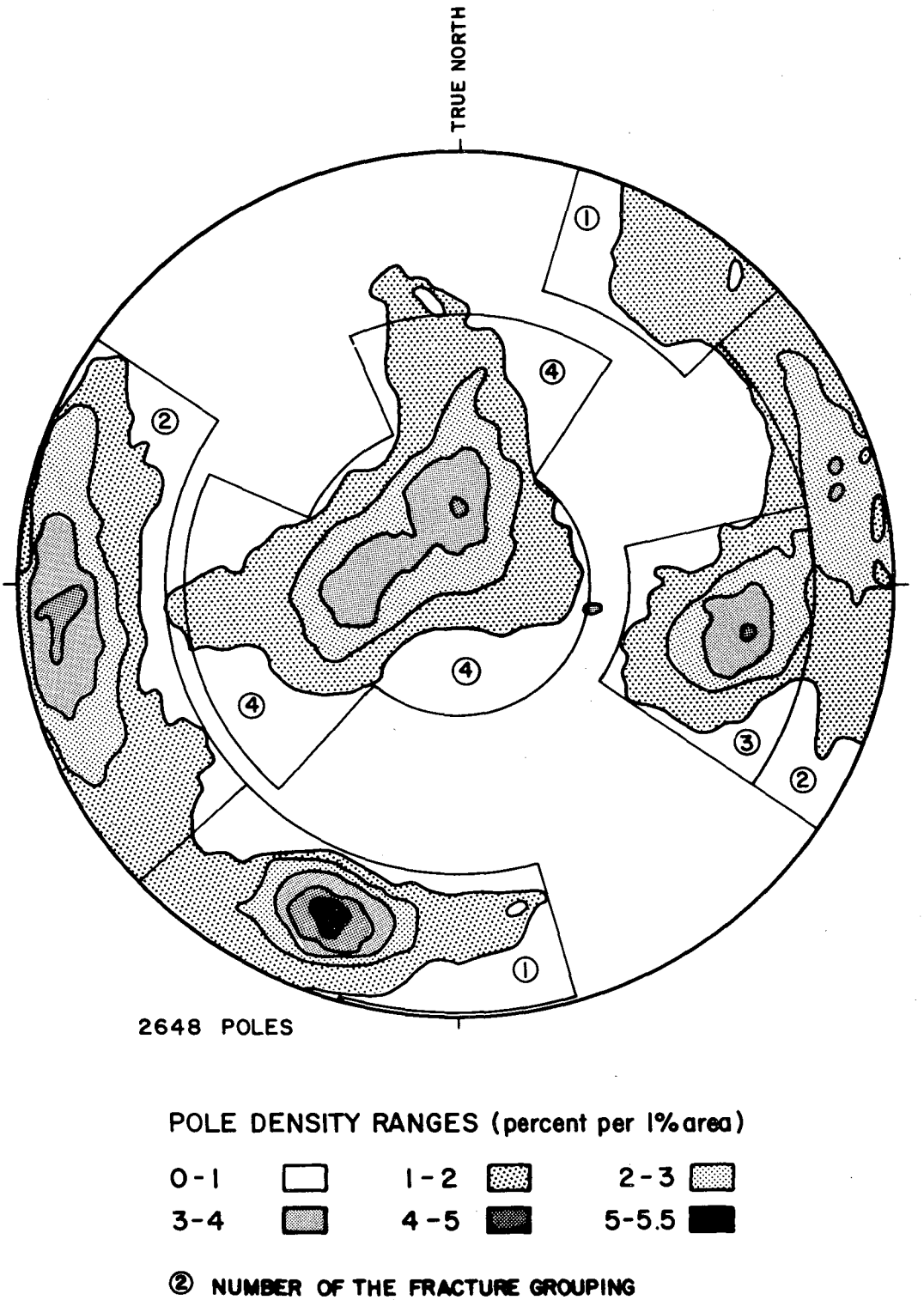

XBL 8210-2961

Fig. 3.8. Pole diagram for all the joint planes intersecting the faces of the ventilation drift and the fracture planes intersecting the drill cores of all the HG holes and all the R holes, except R4 and R9. Lower-hemisphere equal-area plot.

Table 3.2. Fracture sets defined by the fracture data from all the faces of the Ventilation drift and the fractures measured on the drill cores from all the oriented R and HG holes.

Set	Dip Direction		Dip		Visual Average	
	From	To	From	To	Dip Direction	Dip
1	342	359	56	88	23	76
	0	46	56	88		
	16	46	89	90		
	196	226	60	90		
2	47	124	56	90	83	95
	227	304	69	90		
3	257	304	32	68	278	53
4	212	359	0	25		
	0	40	0	25	155	12
	41	115	0	53		
	116	146	0	32		
	147	211	0	52		

3.2 Trace Length Analysis

3.2.1 Bias and Sources of Error

The fracture mapping of the walls and the floor of the ventilation drift provided data that were used for fracture trace length analysis. The data from the fracture mapping was presented in the forms of maps drafted on the site at a 1:20 scale (Figure 3.9) and of a coded data file (Rouleau et al., 1981). The data file is related to the map through a one to one fracture numbering system. The digitization of the fracture maps allowed the calculation of trace lengths to be made with an accuracy of ± 0.1 meter.

The limitation in accuracy in the estimation of individual trace lengths constitutes a source of measurement errors. Many other sources of error affect the results of a fracture survey. This is especially true in the estimation of fracture size. Biases, for instance, are systematic sources of error that theoretically can be accounted for in the analysis stage, provided that appropriate information has been collected during sampling. The orientation bias (Terzaghi, 1965), caused by the preferential sampling of fractures perpendicular to the measurement lines (e.g., borehole axes) or to the sampling faces, has been pointed out in the section on orientation analysis and will be briefly discussed in the section on spacing analysis. As far as fracture size is concerned, many of the sources of error have been discussed in Baecher and Lanney (1978) and in Rouleau and Gale (1981). We will briefly discuss the three more important biases affecting the estimation of fracture size from field data: the size bias, the trace length censoring, and the trace length truncation.

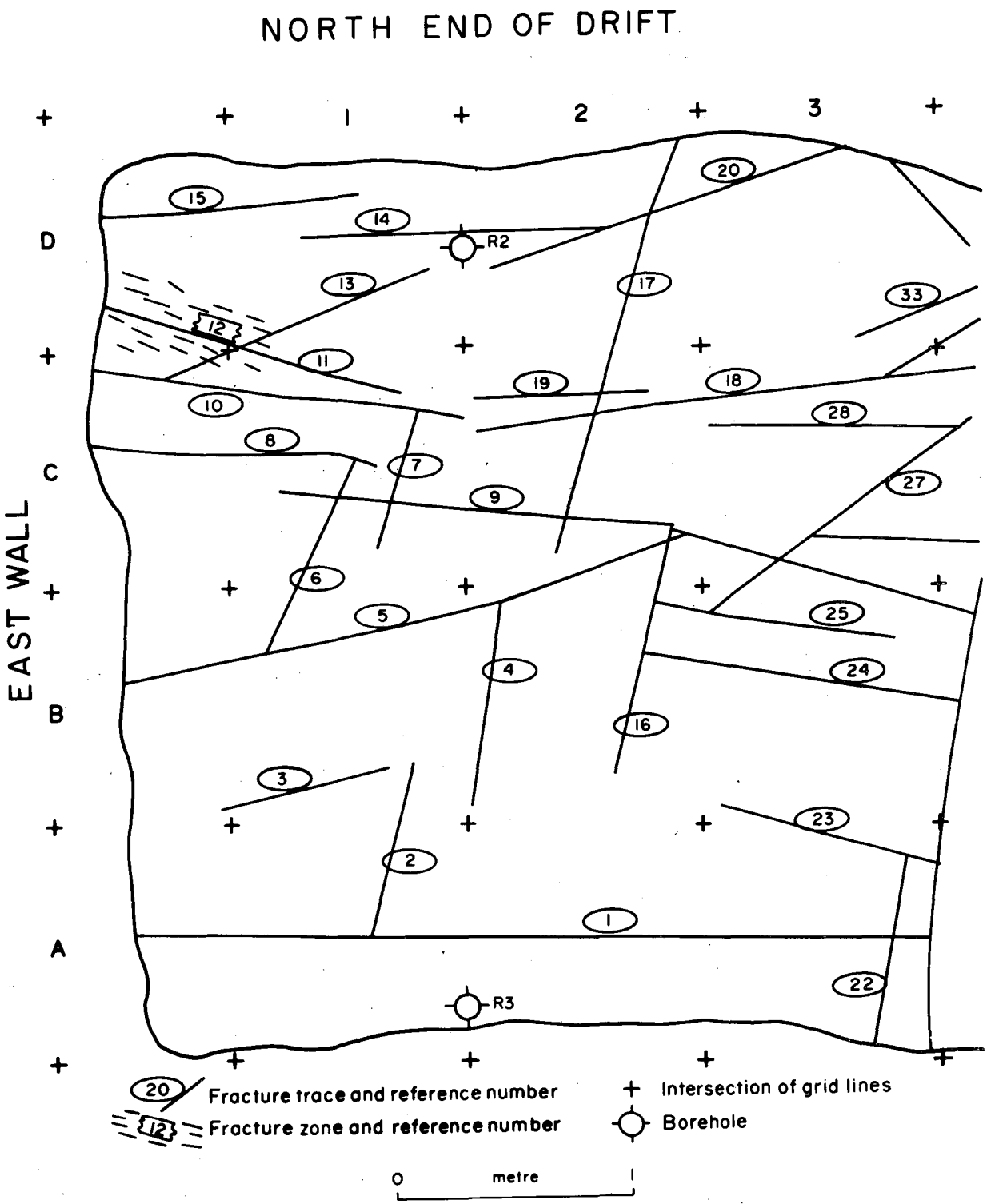

XBL 8411-5032

Fig. 3.9. Portion of the fracture map of the ventilation drift.

A size bias arises from the fact that large fractures, or long fracture traces, have a greater probability of being sampled than smaller fractures, or shorter fracture traces. If, for instance, one considers two parallel disc-shaped fractures in a rock mass, one of diameter D and the other of diameter 2D, clearly the chances of a random surface intersecting the fracture with diameter 2D are twice that of the fracture with diameter D.

Size bias occurs at two levels. As discussed above, the larger the surface area of the fracture the greater the probability that it will be intersected by the sampling surface; this is the first level. Also, since the portion of the surface that is actually sampled is limited in size, it intersects preferentially longer fracture traces; this is the second level. The first level of size bias is of interest for studies involving real three-dimensional descriptions of the fracture system. Warburton (1980a and 1980b) presented an adaptation of mathematical relationships developed in the field of stereology by which one can estimate the parameters of a fracture size distribution from trace length data, assuming a given convex shape for the fracture planes and a given type of size distribution. Methods for correcting size bias for trace lengths, at the sampling line or rock exposure level, are discussed below.

Generally, because of time limitation when measuring rock discontinuities over a large area, one must intentionally omit short discontinuities. For instance, the cutoff length in the fracture map of the ventilation drift was 0.5 meter (Rouleau et al., 1981). The error produced by this practice is called the trace length truncation error.

For many long discontinuities, one or both ends cannot be seen because they are covered by soil or because they extend beyond the edge of

the sampling face. Thus their measured trace length provides only a lower bound on their actual trace length. This source of error is called trace length censoring.

Various methods have been proposed in the literature on fracture analysis to overcome some of the biases mentioned above. Priest and Hudson (1981) presented a method of correction for size bias applied to fracture trace lengths. Their method is applicable to line survey data and allows the computation of an estimate for the actual mean trace length based on the mean trace length of the sample, assuming a negative exponential, a normal or an uniform distribution. The same authors also proposed a method of correction for censoring that is an extension of a method proposed earlier by Cruden (1977). Their method however assumes a constant censoring point--i.e., always the same length value--and consequently it is not applicable to our data. Pahl (1981) suggested a distribution-free method of computing the actual mean trace length of a sample, accounting for size bias, censoring and truncation. Pahl's method however requires also a constant point of censoring, and if that requirement is not met the method cannot be applied to any of the biases. Moreover being distribution-free, Pahl's method is not appropriate in a study where the results of the statistical analysis are to be used in probabilistic simulations of the fracture system in which trace length distribution is an input parameter. Steffen et al. (1975) and Baecher (1980) proposed the method of maximum likelihood (ML) to account for censoring at any point. Baecher (1980) presented a closed-form expression to compute an estimate of the actual mean of a progressively censored sample assuming an exponential distribution of trace lengths. This latter method, described in greater detail below, has been applied to the Stripa data.

3.2.2 Analysis of Ventilation Drift Data

Using the fracture sets (Figure 3.8) described in Table 3.2, each fracture trace on the ventilation drift maps was assigned to one of the defined fracture sets, if its orientation fell into the range of orientation for that set. A computer program using the SAS system (SAS Institute, 1979; see Appendix B) was written to extract the relevant data for each fracture set, from both the field data and the digitized data files (see Section 3.2.1). The same computer program also constructed the frequency histograms (Figure 3.10) and computed the basic statistics for each fracture set (Table 3.3), for different degrees of censoring. The censoring is zero for traces with both ends observable, 1 for traces with only one end observable, and 2 for traces with neither end observable. The histograms of Figure 3.10 present different shadings corresponding to these different degrees of censoring.

The shape of the histograms in Figure 3.10, as well as a literature review reported in Baecher and Lanney (1978), suggests that the exponential and the lognormal models can be fitted to trace length distributions. An estimate of the parameters of these two models has been computed (Table 3.3). Censoring bias and truncation bias have been corrected in the calculation of these estimates. Size bias was not considered because no simple method has been derived yet to estimate the parameters of an exponential and a lognormal distributions accounting simultaneously for progressive censoring, truncation and size bias. The error introduced by size bias is important in the case of data obtained by line sampling (Priest and Hudson, 1981; Pahl, 1981). This error is certainly less when the data, like the ventilation drift data, come from the complete mapping

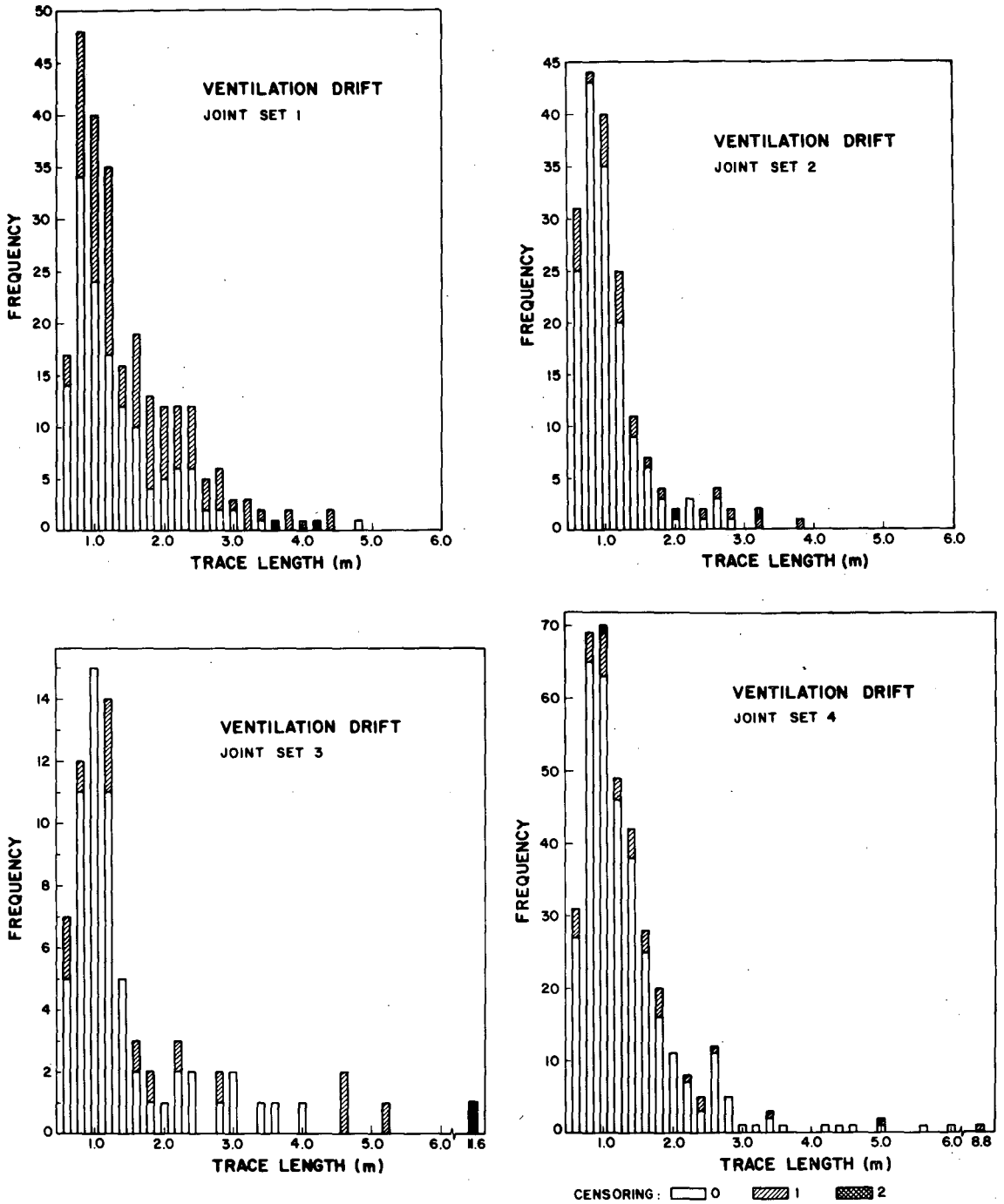

XBL 8210-2962

Fig. 3.10. Histograms of fracture trace lengths on the faces of the ventilation drift.

Table 3.3. Trace length statistics, by degree of censoring (CENS = 0,1 and 2) for the four fracture sets.

	Set 1			Set 2			Set 3			Set 4		
	Basic Statistics											
Censoring	0	1	2	0	1	2	0	1	2	0	1	2
No. of Obs.	140	109	2	150	26	2	61	13	1	327	35	2
Sum (m) [1]	181.55	183.25	7.89	158.12	36.38	5.04	82.40	28.79	11.51	435.42	59.14	5.96
Max (m)	4.78	4.44	4.28	2.93	3.85	3.11	3.95	5.22	11.51	6.04	8.88	5.02
Mean (m)	1.30	1.68	3.95	1.05	1.40	2.52	1.35	2.22	11.51	1.33	1.69	2.98
Std. dev. (m)	0.68	0.86	---	0.45	0.88	---	0.77	1.71	----	0.73	1.53	---
	Bias-Corrected Parameters[4]											
Exponential model $\hat{\mu}_E$(m) [2]	2.16			0.83			1.51			1.03		
Log-normal model $\hat{\mu}_{LN}$ [3]	0.4261			- 0.0471			0.0583			0.1648		
$\hat{\sigma}_{LN}$	0.8459			0.5543			0.9124			0.5583		
$\hat{\mu}$ (m) [4]	2.190			1.113			1.607			1.378		
$\hat{\sigma}$ (m)	2.269			1.039			1.852			1.125		

[1] Sum: total length, in meters

[2] $\hat{\mu}_E$: estimate of the mean trace length, assuming an exponential model.

[3] $\hat{\mu}_{LN}$ & $\hat{\sigma}_{LN}$: estimate of the mean and standard deviation of the natural logarithm of trace lengths.

[4] $\hat{\mu}$ & $\hat{\sigma}$: estimate of the mean and standard deviation of the original distribution, computed from: $\hat{\mu}_{LN}$ & $\hat{\sigma}_{LN}$ using equations 3.10 and 3.11

[4] All the parameter estimates are corrected for censoring and truncation biases.

of surfaces that are at least 2 or 3 times larger than the mean value of trace length.

The probability density function (PDF) of an exponential distribution with mean μ is:

$$f_E(x;\mu) = (1/\mu)\ \mathrm{EXP}\ (-x/\mu) \tag{3.1}$$

The cumulative density function (CDF) is simply:

$$F_E(x;\mu) = \int_0^x f_E(t;\mu)\ dt = 1 - \mathrm{EXP}\ (-x/\mu) \tag{3.2}$$

The availability of a simple CDF permits the derivation of a closed-form expression for the ML estimate of the mean of a censored exponential distribution (Epstein, 1954; Baecher, 1980):

$$\hat{\mu}'_E = L\ /\ N_o \quad , \tag{3.3}$$

where N_o is the number of traces with both ends observable and L is the sum of all the trace lengths.

In order to account also for truncation bias in the sample, a relationship was derived between the mean of a truncated sample from an exponential distribution and the actual mean of the complete distribution. The PDF of a left-truncated portion of an exponential distribution is:

$$f^T_E(x;a,\ \mu) = K\ f_E(x;\mu) \tag{3.4}$$

where a is the point of truncation. K is a normalizing factor that insures that the truncated portion obeys one of the axioms of a probability function that can be stated as:

$$\int_a^\infty f^T_E(x;\ a,\mu)\ dx = 1 \tag{3.5}$$

In equation (3.4),

$$K = 1 \big/ (1 - F_E(a;\mu)) \quad . \tag{3.6}$$

The mean of the truncated exponential distribution (3.4) is:

$$\mu_E^T = \int_a^\infty x \, f_E^T \, dx \tag{3.7}$$

$$\text{or} \quad \mu_E^T = \int_a^\infty \frac{(x/\mu) \text{ EXP } (-x/\mu)}{\text{EXP } (-a/\mu)} \, dx \quad . \tag{3.8}$$

After integration one is left with the simple expression:

$$u^T{}_E = \mu_E + a$$

$$\text{or} \quad \mu_E = \mu^T{}_E - a \tag{3.9}$$

Taking the value of $\hat{\mu}'_E$ obtained by (3.3) as an estimate of $\mu^T{}_E$, values of $\hat{\mu}_E$ have been computed with (3.9) (see Table 3.3).

Incidentally, the assumption of an exponential distribution can be interpreted as indicating that the propagation of the traces of the fractures is a purely random process. This could occur if obstacles to the propagation of the discontinuity traces were distributed at random (Cruden, 1977).

Estimating the parameters of a lognormal distribution presents more difficulties because no closed-form expression has been derived for the ML estimate of these parameters. However, since a variable is lognormally distributed when the logarithm of its values are normally distributed, the parameters of the lognormal distribution are the mean and the standard

deviation of the log-transformed variable (μ_{LN} and σ_{LN} respectively). Using appropriate transformation of the parameters μ and σ, a set of ML equations have been derived to estimate the parameters of a left-truncated and progressively right-censored distribution (J.G. Kalbfleish, 1982, personal communication). This set of ML equations can be solved with an iterative procedure like the Newton-Raphson method (e.g., Jennings, 1977, p. 65). The values of μ_{LN} and σ_{LN} in Table 3.3 have been computed with this latter method. Then the mean and the standard deviation of the original distribution have been estimated with the following relationships (Bury, 1975, p. 279):

$$\mu = \mathrm{EXP}[\hat{\mu}_{LN} + \hat{\sigma}^2_{LN}/2] \tag{3.10}$$

and $$\sigma = \left\{ \mathrm{EXP}(2\hat{\mu}_{LN} + \hat{\sigma}^2_{LN})[\mathrm{EXP}(\hat{\sigma}^2_{LN})-1] \right\}^{1/2} \tag{3.11}$$

The results of this trace length analysis can only be considered as approximate, since not all the sampling biases have been accounted for and no goodness-of-fit test has been carried out because of complexities introduced by the presence of the various biases. Nevertheless the resulting figures suggest that there is a significant difference in trace length from one fracture set to another.

3.3 Spacing Analysis

3.3.1 Selecting the Data Set

Two principal sources of data are available to study the variability of fracturing around the test excavation at Stripa: the fracture maps and

the drill core data. However, as discussed below, the fracture maps are not suited for the calculation of exact spacing values between fractures, and therefore are not included in this discussion.

Fracture maps of the Stripa granite are presented in Olkiewicz et al. (1979), Thorpe (1979), Rouleau et al. (1981) and Paulsson et al. (1982). Besides their illustrative role, these maps are useful in a deterministic analysis of the larger fractures where the density of boreholes is relatively high (see Thorpe, 1979; and Paulsson et al., 1982). They are also useful in attempting to identify local, dense fractured zones, or to carry out detailed fracture analyses around selected boreholes (see Rouleau et al., 1981, for example). However, as pointed out by Rouleau et al. (1981), fracture maps are generally affected by various round off errors that can be corrected only at considerable expense, which precludes their use in computing exact spatial relationships between fractures. One such cause of round off error is the sub-circular shape of the drift walls, which introduces a distortion in the fracture map of these faces. Also, even if very careful blasting techniques are used during excavation, the sampling faces are rather uneven. In such a situation, an exact representation of the spatial relationship between fractures could only be achieved by projecting all the fractures onto a planar reference plane, which in the case of Stripa was not feasible because of time limitation. Finally, also because of time and financial limitations, it is generally impossible to show absolutely all the fracture traces on a map. Defining a cut-off length below which no fracture is measured is an accepted sampling technique (see Section 3.2). This sampling procedure however prevents the densely fractured zones from being sampled since they generally consist of

many short and closely spaced fractures. While the trace length truncation bias introduced by this cut-off length is relatively easy to correct in the statistical analysis, the bias concerning the spacing would be more complex to define and to correct. For all the reasons mentioned above, the fracture maps have not been used in our statistical analysis of fracture spacing. Therefore, only the borehole data were used for the analysis described in this section.

3.3.2 Selecting the Method of Analysis

A study of the spatial variability of a measured parameter can take many different approaches. In the case of the analysis of rock fractures measured along boreholes, the density approach requires the computation of many values of fracture frequency, i.e. number of fracture intersections per unit interval; the distance approach necessitates many calculated values of the distance between fracture intersections. The density approach in turn can use various methods of analysis such as spatial time-series, spectral analysis and geostatistics. Jamier (1975), Miller (1979), Brière and Razack (1980), La Pointe (1980) have presented studies in which geostatistics, using variograms (a variant of autocorrelation plots), has been applied to the analysis of rock fracturing. However, the estimates of the range of influence of various parameters seem to be quite variable and, as pointed out by Beacher and Einstein (1981), almost nothing is known about the variation of estimators for variograms. The sensitivity to the size of the measuring intervals introduces further complications in a density-based analysis. Since one of the principal objectives of this statistical analysis of rock fracturing is to obtain input parameters for simulation of discrete fracture networks, which will also include dis-

tributed fracture sizes and fracture orientations, geostatistics and the other methods based on fracture density were not considered suitable for this study.

The distance approach has been developed primarily in the field of biostatistics to study the ecology of populations (Bartlett, 1975). Workers in that field are mainly interested in point patterns. For example, they may try to evaluate the interaction between individuals (attraction or repulsion). For that reason the problems of line patterns (e.g., two dimensional fracture traces) have been considered only by a few statisticians, and they have considered almost exclusively lines of infinite extent (Bartlett, 1975), or purely random sets of lines of finite length (Corte and Kallmes, 1961, Parker and Cowan, 1976).

Sophisticated mathematical tools for the analysis and modeling of spatial point processes and series of events based on distance methods have been proposed (Cox and Lewis, 1966; Bartlett, 1975; Ripley, 1977; Diggle, 1979). However even if fracture intersections with the borehole axes form what we may call one-dimensional point patterns, our geometrical problem is more complex than the two-dimensional patterns found in ecology. Indeed our data sets represents a series of one-dimensional expressions of three-dimensional structures (fracture planes in three-dimensional space) that we want to model eventually at least in two dimensions, if not in three dimensions. Therefore, even a thorough analysis, using state-of-the-art techniques, of the spatial pattern of our one-dimensional samples would not contribute much information for an eventual discrete modeling of the fracture system.

The two previous paragraphs demonstrate the lack of existing techniques for the analysis and the realistic simulation of both two-

dimensional patterns of lines of finite length and three-dimensional patterns of planes of finite extent. For that reason we have adopted a relatively simple method based on spacings or the distance between consecutive fractures measured along the drill cores. Because it is simple to measure or to compute, fracture spacing has become a rather common parameter during the last decade in the quantitative description of fracture systems (Kiraly, 1970; ISRM, 1978). Moreover, analysis of spacings can provide a first insight into the randomness of the fracture system and into the variability in fracture density from one area to the other in the same rock mass. Following the ISRM (1978) convention we define spacing as the perpendicular distance between adjacent discontinuities. This definition implies that spacings are measured, or computed, for fractures that are sub-parallel. Since our fracture sets (see Section 3.2) are defined on the basis of fracture orientation, all the fractures in a given set being roughly sub-parallel, the spacings of each fracture set were analyzed separately.

3.3.3 Analysis of Spacing for Individual Boreholes

Spacing values have been computed and analyzed for the bottom segment (i.e., depth greater than 175 meters) of the three surface boreholes, SBH-1, SBH-2, and SBH-3, and for all the oriented HG and R holes, i.e., HG1 to HG5, R1 to R3, R5 to R8, and R10. In each borehole, the true spacing between consecutive fractures of the same set was computed using the method described below.

First the direction cosines (p, q, r) of the borehole axis and of the pole of the average plane of each fracture set were computed using the

general formula (see Koch and Link, 1971):

$$p = \cos u \cos v$$

$$q = \sin u \cos v$$

$$r = \sin v, \tag{3.12}$$

where u is the bearing of the oriented line, from 0 to 360 degrees, and v is the plunge of that line, positive downward, negative upward.

The bearing and plunge of the boreholes are given in Table 1.1. The bearing and plunge of the average pole to a fracture set are easily calculated from the dip directions and the dip values of the average fracture plane given in Tables 3.1 and 3.2. Since the spacing between fractures is a scalar, the direction of the oriented lines (either the borehole or the pole of the fracture plane) is immaterial. The bearing of the pole of an average fracture plane is simply taken as the dip direction of the fracture plane. The plunge v_f of that pole is calculated with the simple expression v_f = DIP-90, where DIP is the dip value of the average fracture plane.

The angle ø between a borehole axis and the average pole of a fracture set can be computed using the following relationship derived from the definition of the dot product of two unit vectors:

$$\cos \phi = p_h \cdot p_f + q_h \cdot q_f + r_h \cdot r_f \tag{3.13}$$

where the subscript h and f of the direction cosines refer to the borehole axis and to the pole of the average fracture plane respectively.

The "true" spacing (SPAC) between two consecutive fractures of the same set separated by a distance ℓ along the borehole axis is defined as:

$$\text{SPAC} = \ell \cos \phi$$

In these calculations of spacings the assumption is made that all the fractures of a set are parallel and oriented according to the average

orientation of the set. The definition of spacing presented here is similar to that of Kiraly (1970) and of ISRM (1978). Here however we compute a spacing value for each pair of consecutive fractures in a set, instead of simply a mean or a modal spacing for that set. Obviously, the individual spacing values calculated with this method are not the same as what would have been obtained by using only sampling lines perpendicular to the fracture sets. However, if one makes the assumption that the frac- tures of a set are independently and homogeneously distributed in space at the scale of a sample, then, for a large sample, the distribution of spacing values obtained by this method is essentially the same as what would have been obtained had the sampling lines been exactly perpendicular to that fracture set.

A computer program using the SAS system (SAS Institute, 1979) has been written to carry out the calculations described above for each borehole (see Appendix B). The program assigns each fracture to a fracture set, according to its orientation, computes the angle between the borehole and the average pole of each one of the four fracture sets, and computes the spacing value between each pair of consecutive fractures of the same set. The same program also computes the main statistics of the spacing distribution for each fracture set. Tables 3.4 and 3.5 presents a selection of these statistics for each fracture set in each borehole separately.

3.3.4 Detailed Analysis of Spacing Around the Ventilation Drift

In order to obtain a more concise description of fracturing for the whole rock mass surrounding the ventilation drift, we must combine the

spacing data from all the HG and R drill cores. However, before proceeding further in that direction, it may be instructive to look at the variability of spacing values obtained from individual boreholes.

3.3.4.1 Spacing Variability

To analyze the variability of the spacing samples, the first obvious step is to make a one-way analysis of variance to test the hypothesis (H_0) that, for each fracture set, all the populations of spacings sampled from the different drill cores have the same mean. An assumption that is specified for this type of analysis is that the variables are normally distributed. Therefore, in order to improve the validity of the test we will carry out the calculations using the natural logarithm of the spacing values (LSPAC). This transformation reduces the skewness and the variance, and improves the normality of these distributions. The diagram of Figure 3.11 shows the distribution of LSPAC for each fracture set in each borehole. Table 3.6 summarizes the analysis of variance of LSPAC between and within boreholes. The last column in Table 3.6 gives the significance level, or the probability of a value of F larger than that observed if H_0 holds. If we choose arbitrarily 0.05 as a reasonable significance level, we see that, for all the fracture sets except set 3, we have strong indications that the different population means are unequal. These results suggest that the individual boreholes sample a volume of rock that is too small to give spacing distributions that are representative.

We will now place the various spacing samples into groups, so that the samples within a group will be more or less alike, whereas those in

Table 3.4 Main statistics of the spacing distribution for each fracture set in the bottom segment of each SBH hole, i.e. from a depth of 175 m to 290 m

Borehole	SBH-1 (bottom end)				SBH-2 (bottom end)				SBH-3 (bottom end)			
Fracture Set	1	2	3	4	1	2	3	4	1	2	3	4
ϕ (d°)[1]	29.80	32.80	79.00	45.60	85.20	64.70	23.80	45.90	35.60	62.10	71.40	45.40
No. of obs.	222	160	63	132	2	39	244	191	12	30	9	106
Max (m)	7.05	11.97	2.12	15.34	4.39	9.45	4.80	8.57	33.99	3.59	4.98	11.67
Min (m)	0.000	0.008	0.006	0.007	2.915	0.015	0.015	0.014	0.285	0.070	0.045	0.007
Mean (m)	0.63	0.86	0.49	0.75	3.65	1.80	0.62	0.57	6.93	1.05	2.05	0.71
Std. dev. (m)	0.92	1.54	0.54	1.68	---	2.26	0.78	1.03	9.55	0.95	1.81	1.34
Skewness	3.68	3.86	1.48	6.04	---	2.10	2.48	4.37	2.41	0.92	0.47	5.87
Unassigned Fractures	147				308				101			

[1] ϕ: angle between borehole and pole of average fracture plane

Table 3.5 Main statistics of the spacing distribution for each fracture set in each one of the oriented HG & R holes

Borehole	HG1				HG2				HG3			
Fracture Set	1	2	3	4	1	2	3	4	1	2	3	4
φ (d°)	35.40	87.10		78.40	20.80	82.60	72.80	77.80	27.80	60.00		68.70
No. of obs.	21	6	0	2	35	18	5	16	23	9	0	5
Max (m)	3.60	0.39		1.08	5.14	0.80	2.54	1.15	7.08	3.97		6.75
Min (m)	0.057	0.002		0.096	0.000	0.012	0.003	0.017	0.053	0.025		0.171
Mean (m)	1.057	0.10		0.59	0.80	0.19	0.59	0.36	1.10	0.84		1.95
Std. dev.(m)	1.09	0.16		----	1.19	0.22	1.09	0.37	1.55	1.39		2.74
Skewness	1.06	1.63		----	2.37	1.49	2.21	0.96	2.91	1.91		2.04
Unassigned Fractures	19				24				14			

Borehole	HG4				HG5			
Fracture Set	1	2	3	4	1	2	3	4
φ (d°)	58.30	77.40		54.90	53.10	64.70	49.80	87.50
No. of obs.	10	10	0	12	11	16	5	4
Max (m)	4.80	3.56		9.29	6.73	3.28	3.83	0.23
Min (m)	0.205	0.004		0.103	0.024	0.051	0.045	0.019
Mean (m)	1.46	0.61		1.22	1.11	0.56	1.27	0.08
Std. dev.(m)	1.59	1.11		2.57	1.96	0.79	1.53	0.10
Skewness	1.52	2.55		3.31	2.78	3.09	1.63	1.82
Unassigned Fractures	10				36			

Borehole	R1				R2				R3			
Fracture Set	1	2	3	4	1	2	3	4	1	2	3	4
φ (d°)	81.40	45.10	18.10	44.50	58.70	55.00	88.30	38.30	66.00	15.10	22.90	73.70
No. of obs.	5	94	60	30	14	67	1	43	25	83	18	16
Max (m)	2.27	3.05	3.06	5.70	2.77	2.25	0.13	2.70	2.13	1.89	8.59	1.51
Min (m)	0.117	0.007	0.019	0.021	0.036	0.000	0.13	0.063	0.004	0.000	0.009	0.008
Mean (m)	1.08	0.29	0.56	0.86	0.95	0.25	0.13	0.52	0.42	0.34	1.25	0.52
Std. dev.(m)	0.90	0.40	0.61	1.17	0.95	0.37	----	0.66	0.51	0.39	2.52	0.53
Skewness	0.17	4.17	2.22	2.74	0.82	3.26	----	2.29	2.03	2.34	2.49	0.95
Unassigned Fractures	29				16				22			

Table 3.5. (continued)

Borehole	R5				R6				R7			
Fracture Set	1	2	3	4	1	2	3	4	1	2	3	4
ϕ (d°)	55.10	25.10	59.30	67.20	81.50	45.00	17.90	44.50	58.70	55.10		38.20
No. of obs.	14	76	5	20	11	35	61	67	8	68	0	79
Max (m)	3.15	2.35	4.76	3.73	0.94	4.42	3.29	5.13	5.82	1.67		2.31
Min (m)	0.023	0.009	0.199	0.016	0.019	0.050	0.057	0.014	0.172	0.000		0.000
Mean (m)	1.12	0.34	2.26	0.47	0.49	0.78	0.61	0.42	1.56	0.23		0.28
Std. Dev.(m)	1.24	0.44	2.19	0.89	0.35	0.90	0.73	0.74	1.87	0.36		0.33
Skewness	0.69	2.82	0.51	3.13	0.03	2.47	2.08	4.44	2.11	2.70		3.69
Unassigned Fractures	8				25				9			

Borehole	R8				R10			
Fracture Set	1	2	3	4	1	2	3	4
ϕ (d°)	62.20	6.20	30.60	82.70	55.20	25.00	59.20	67.30
No. of obs.	21	85	13	13	11	52	9	12
Max (m)	2.64	3.11	6.21	1.30	4.47	3.45	5.32	2.55
Min (m)	0.028	0.020	0.017	0.022	0.143	0.027	0.046	0.012
Mean (m)	0.61	0.34	1.07	0.28	1.41	0.50	1.33	0.90
Std. Dev.(m)	0.71	0.52	1.67	0.42	1.39	0.59	1.64	0.00
Skewness	2.25	3.19	2.77	2.15	1.38	2.90	2.11	0.68
Unassigned Fractures	20				8			

ϕ: angle between borehole and pole of average fracture plane

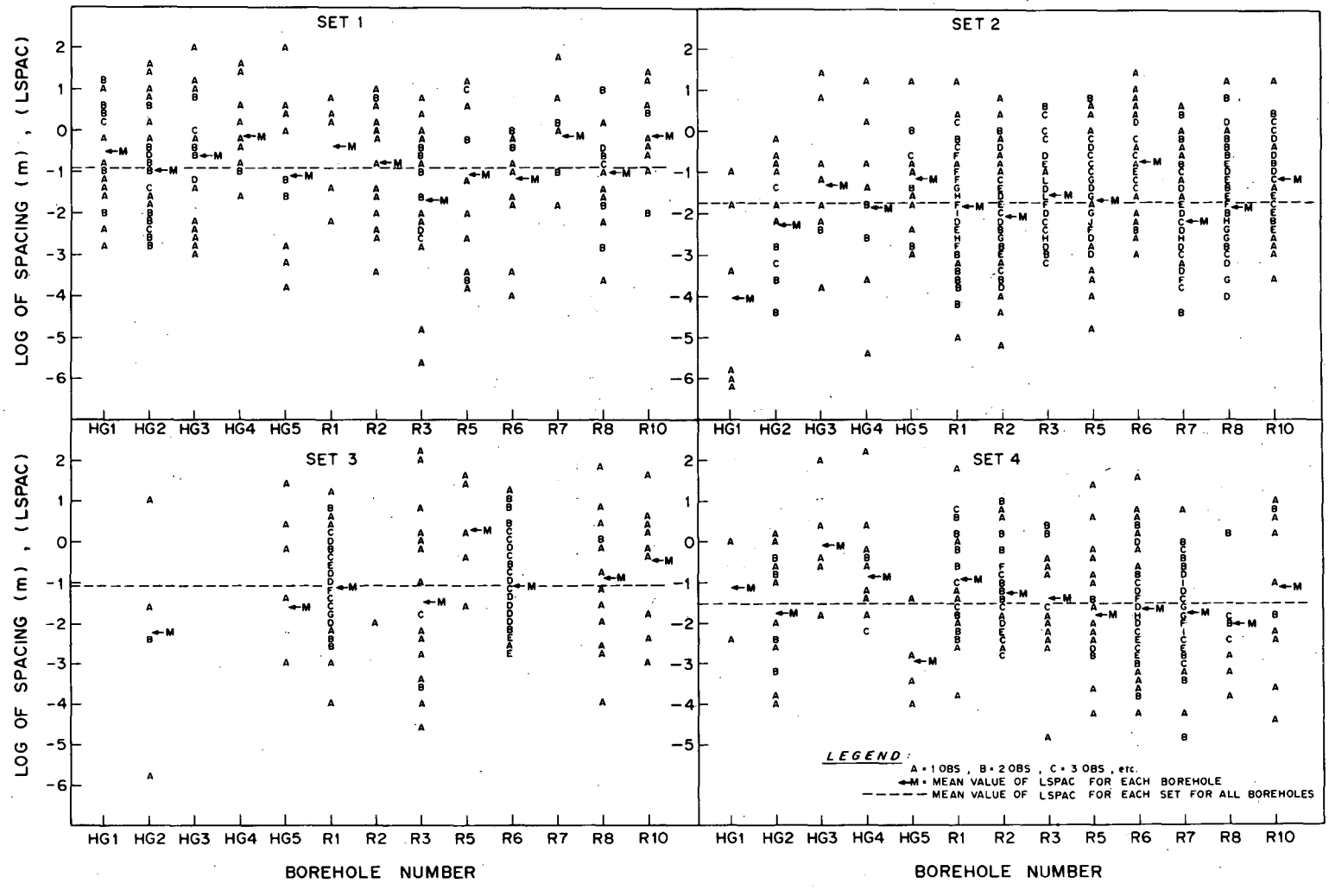

XBL 8411-5033

Fig. 3.11. Distribution of LSPAC for each fracture set in each borehole.

Table 3.6 Analysis of variance of LSPAC between individual boreholes

Set	# of obs.	$\frac{DF(b)}{DF(w)}$	$\frac{SS(b)}{SSE(w)}$	$\frac{MS(b)}{MSE(w)}$	F Ratio	Prob. [>F]
1	208	$\frac{12}{195}$	$\frac{41.20}{366.01}$	$\frac{3.43}{1.88}$	1.82	0.0458
2	614	$\frac{12}{601}$	$\frac{119.92}{812.75}$	$\frac{9.99}{1.35}$	7.39	0.0001
3	177	$\frac{8}{168}$	$\frac{24.37}{299.81}$	$\frac{3.05}{1.79}$	1.71	0.1001
4	318	$\frac{12}{305}$	$\frac{52.34}{451.82}$	$\frac{4.36}{1.48}$	2.94	0.0007

DF: degrees of freedom

(b): between boreholes

(w): within boreholes

SS and MS: between sample sum of squares and mean squares respectively

SSE and MSE: error sum of squares and mean squares respectively

F Ratio: MS(b)/MSE(w), follows F distribution for corresponding two values of d.f.

different groups will be somewhat different. For this purpose, the Duncan multiple-range test (see for instance Miller and Freund, 1977) has been carried out on the variable LSPAC, and the results are shown in Table 3.7. In Table 3.7 the boreholes are arranged by increasing value of mean LSPAC. The means with the same grouping letter are not significantly different, at a level of significance of 0.05. The results of this test show that for each fracture set there are boreholes for which the mean value of LSPAC is significantly different from that of other boreholes, supporting the results of the analysis of variance presented above. Also, a closer look at Table 3.7 reveals that there does not seem to be a relationship between the mean value of LSPAC and the number of observations, the position, or the orientation of the borehole.

A similar series of analyses as the ones described in the previous paragraphs for individual boreholes has been carried out on groups of boreholes. The groups are defined according to the location along the drift. The three groups being the HG holes, the boreholes in the northern transverse plane (RN), i.e. R1, R2, R3 and R5, and the boreholes in the southern transverse plane (RS), i.e. R6, R7, R8 and R10. First, the main statistics have been computed for each fracture set in each one of these three groups of boreholes for both SPAC and LSPAC (Table 3.8), and a summary plot of the distributions of LSPAC in the different groups is shown in Figure 3.12. Then an analysis of variance and a Duncan multiple-range tests have been carried out for LSPAC on these groups of boreholes. The results are given in Tables 3.9 and 3.10.

Table 3.7. Duncan multiple-range test for LSPAC (individual boreholes)

Set 1 DF = 195					Set 2 DF = 601						
Grouping			Mean	N	Hole	Grouping				Mean	N	Hole
		N	-0.100792	8	R7			P		-0.769042	35	R6
		N	-0.123369	10	HG4			P		-1.206894	52	R10
		N	-0.159525	11	R10	Q		P	R	-1.214238	16	HG5
O		N	-0.413961	5	R1	Q	S	P	R	-1.369934	9	HG3
O		N	-0.497885	21	HG1	Q	S		R	-1.535408	82	R3
O		N	-0.664529	23	HG3	Q	S		R	-1.629877	76	R5
O		N	-0.776012	14	R2		S		R	-1.826018	94	R1
O		N	-1.016320	34	HG2		S		R	-1.860495	85	R8
O		N	-1.057132	21	R8		S		R	-1.861786	10	HG4
O		N	-1.117293	14	R5		S			-2.110896	65	H2
O		N	-1.120012	11	HG5		S			-2.199837	66	R7
O		N	-1.235434	11	R6		S			-2.336717	18	HG2
O			-1.665801	25	R3			T		-4.001377	6	HG1

Set 3 DF = 168					Set 4 DF = 305						
Grouping			Mean	N	Hole	Grouping				Mean	N	Hole
		U	-0.242906	5	R5			W		-0.080414	5	HG3
V		U	-0.532032	9	R10			W		-0.808152	12	HG4
V		U	-0.609724	5	HG5	X		W		-0.898106	30	R1
V		U	-0.948930	13	R8	X		W	Y	-1.129564	2	HG1
V		U	-1.064491	60	R1	X		W	Y	-1.164140	12	R10
V		U	-1.102912	61	R6	X		W	Y	-1.239277	43	R2
V			-1.519634	18	R3	X		W	Y	-1.315727	16	R3
V			-2.017507	1	R2	X			Y	-1.663118	67	R6
V			-2.236401	5	HG2	X			Y	-1.727389	16	HG2
									Y	-1.750847	78	R7
									Y	-1.777661	20	R5
									Y	-2.008375	13	R8
									Y	-2.926650	4	HG5

Note: N to R = Groups of samples (inside each group the means are not significantly different)

DF = Degree of freedom

N = Number of observations

Level of Significance = 0.05

Table 3.8. Main statistics of the distributions of SPAC and LSPAC for each fracture set in each group of boreholes .

Set	Statistic	HG1 to HG5		R1 to R5		R6 to R10	
		SPAC	LSPAC	SPAC	LSPAC	SPAC	LSPAC
1	N	100	99	58	58	51	51
	Max	7.08	1.96	3.15	1.15	5.82	1.76
	Min	0.00	-3.73	0.004	-5.51	0.0019	-3.96
	Mean	1.03	-0.75	0.77	-1.21	0.91	-0.75
	Std. dev.	1.38	1.32	0.91	1.61	1.41	1.25
	Skewness	2.38	-0.01	1.25	-0.40	2.60	-0.45
	Kurtosis	6.27	-0.78	0.35	-0.46	7.65	0.26
2	N	59	59	320	317	240	238
	Max	3.97	1.38	3.05	1.11	4.42	1.49
	Min	0.002	-6.21	0.00	-5.16	0.00	-4.47
	Mean	0.45	-1.97	0.31	-1.67	0.41	-1.65
	Std. dev.	0.84	1.71	0.40	1.10	0.60	1.26
	Skewness	3.13	-0.41	3.13	-0.07	3.21	0.13
	Kurtosis	9.60	0.27	12.41	0.09	13.67	-0.63
3	N	10	10	84	84	83	83
	Max	3.83	1.34	8.59	2.15	6.21	1.83
	Min	0.003	-5.82	0.009	-4.69	0.0017	-4.06
	Mean	0.93	-1.42	0.81	-1.10	0.76	-1.02
	Std. dev.	1.30	2.15	1.42	1.36	1.06	1.25
	Skewness	1.61	-0.70	3.77	-0.04	3.05	0.10
	Kurtosis	1.81	0.60	15.98	0.17	11.47	-0.67
4	N	39	39	109	109	171	170
	Max	9.29	2.23	5.70	1.74	5.13	1.63
	Min	0.017	-4.08	0.008	-4.78	0.00	-4.85
	Mean	0.81	-1.33	0.60	-1.26	0.37	-1.70
	Std. dev.	1.77	1.50	0.86	1.25	0.60	1.18
	Skewness	4.05	0.41	3.01	0.06	4.16	0.11
	Kurtosis	16.80	-0.17	12.21	-0.22	24.29	0.30

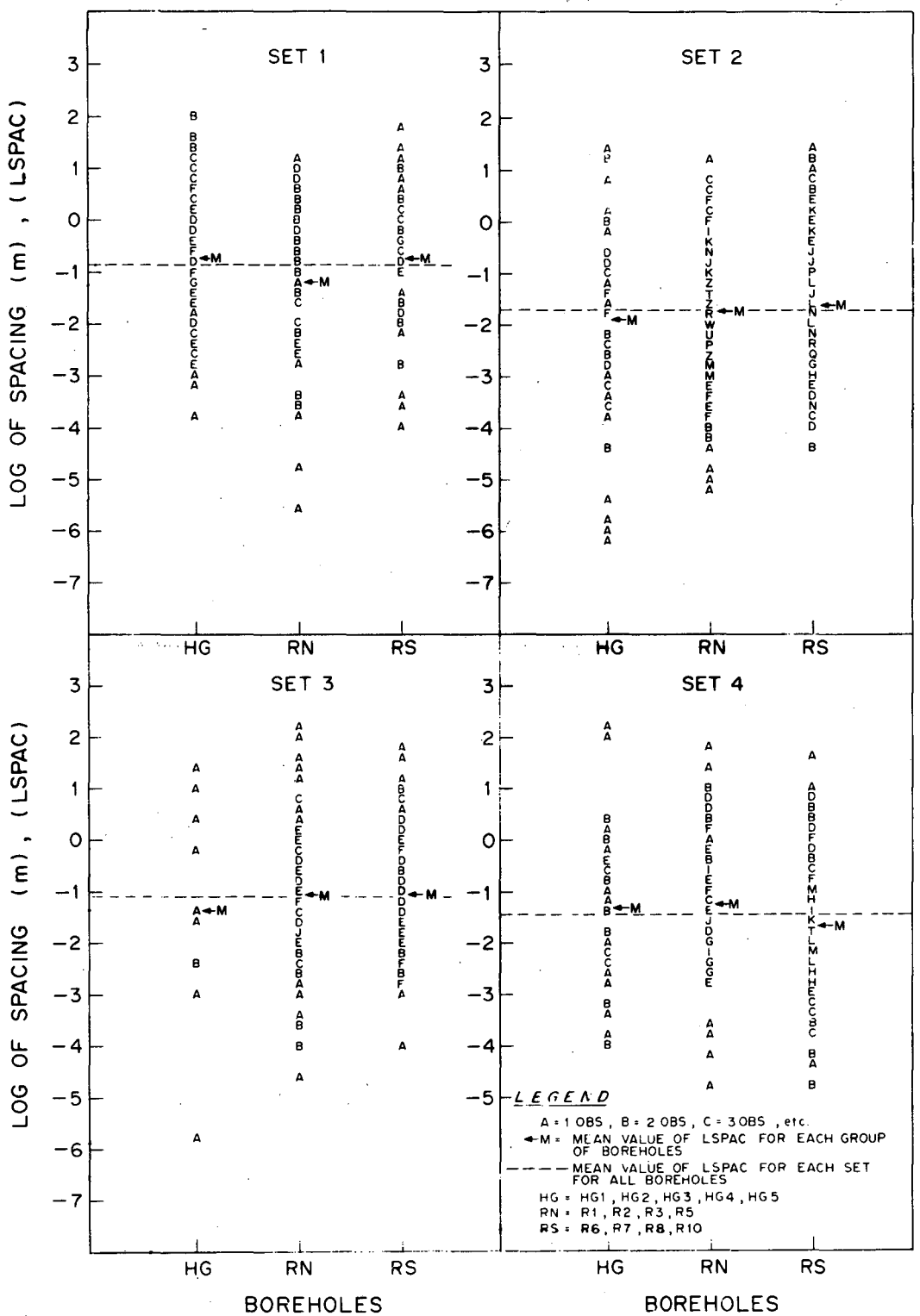

XBL 8411-5034

Fig. 3.12. Distribution of LSPAC for each fracture set in each group of boreholes.

Table 3.9 Analysis of variance of LSPAC between the three groups of boreholes HG, RN and RS

Set	# of obs.	$\frac{DF(b)}{DF(w)}$	$\frac{SS(b)}{SSE(w)}$	$\frac{MS(b)}{MSE(w)}$	F Ratio	Prob. [>F]
1	208	$\frac{2}{205}$	$\frac{8.96}{298.25}$	$\frac{4.48}{1.94}$	2.31	0.1023
2	614	$\frac{2}{611}$	$\frac{5.24}{927.43}$	$\frac{2.62}{1.52}$	1.72	0.1790
3	177	$\frac{2}{174}$	$\frac{1.55}{322.62}$	$\frac{0.77}{1.85}$	0.42	0.6594
4	318	$\frac{2}{315}$	$\frac{14.14}{490.02}$	$\frac{7.07}{1.56}$	4.54	0.0113

DF: degrees of freedom

(b): between boreholes

(w): within boreholes

SS and MS: between sample sum of squares and mean squares respectively

SSE and MSE: error sum of squares and mean squares respectively

F Ratio: MS(b)/MSE(w), follows F distribution for corresponding two values of DF

Table 3.10. Duncan multiple-range test for LSPAC (groups of boreholes)

Set 1 DF = 205				Set 2 DF = 611			
Grouping	Mean	N	Hole	Grouping	Mean	N	Hole
N	-0.745944	99	HG	O	-1.651287	238	RS
N	-0.751974	51	RS	O	-1.761296	317	RN
N	-1.210745	58	RN	O	-1.973631	59	HG

Set 3 DF = 174				Set 4 DF = 315			
Grouping	Mean	N	Hole	Grouping	Mean	N	Hole
P	-1.016892	83	RS	Q	-1.255385	109	RN
P	-1.101970	84	RN	R Q	-1.325740	39	HG
P	-1.423063	10	HG	R	-1.694550	170	RS

Note: N to R = groups of samples (inside each group the means are not significantly different)

DF = degree of freedom

N = number of observations

Level of significance = 0.05

Contrary to the analysis for individual boreholes, the results of this analysis for groups of boreholes do not indicate significant differences between the means of LSPAC, except for fracture set 4. Indeed, except for fracture set 4, the levels of significance (Prob [> F]) in Table 3.9 are greater than 0.05, and Table 3.10 shows that all three groups of boreholes do not show significantly different LSPAC means. These results suggest that, contrary to individual boreholes, the three groups of boreholes sample a volume of rock that is large enough to give representative spacing distributions. As far as fracture set 4 is concerned, the significant difference of mean LSPAC is between the two groups of radial holes, RN and RS. The mean LSPAC for the HG holes, the northernmost group of holes, is in between. This latter observation suggests that fracture spacing for set 4 reaches both high and low values along the length of the drift. Therefore it is reasonable to consider the volume of rock sampled by all the HG and R boreholes as statistically homogeneous with respect to fracturing. Thus, combining the spacing values from all the boreholes should yield reasonably good average values for the parameters of the spacing distribution.

3.3.4.2 Analysis of Fracture Spacings from all the Oriented HG and R Holes Combined

The spacing values from all the boreholes around the ventilation drift were combined and a frequency histogram was constructed for each fracture set (Figure 3.13). Table 3.11 presents the main statistics computed for SPAC and LSPAC for each fracture set. Based on the shape of the histograms of Figure 3.13, these empirical distributions have been

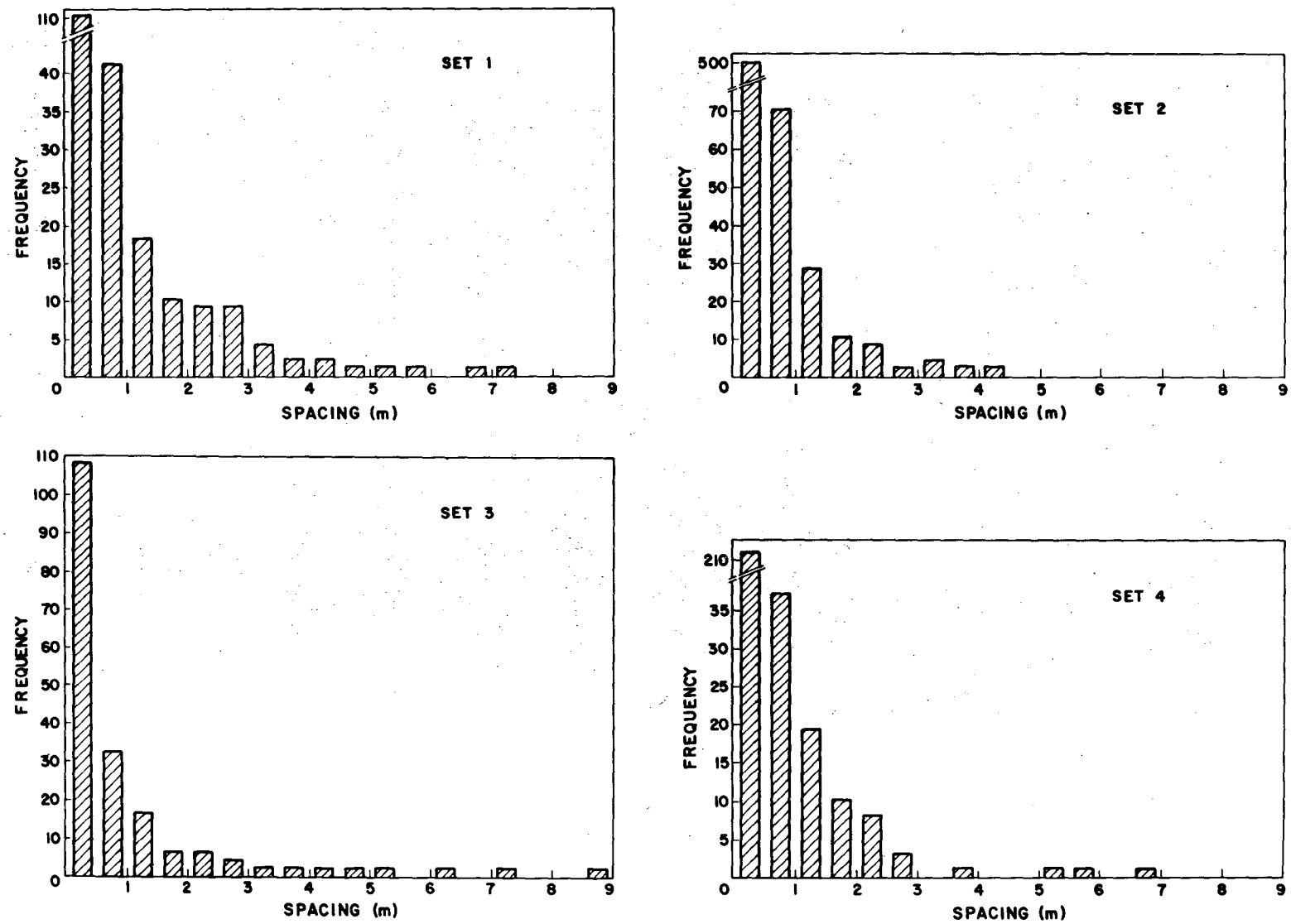

Fig. 3.13. Frequency histograms for the spacings between consecutive fractures of the same set (SPAC) intersecting all the oriented HG and R drill cores. XBL 838-10954

Table 3.11. Main statistics of the distributions of SPAC and LSPAC for each fracture set for all the oriented HG and R holes.

Statistic	Set 1		Set 2		Set 3		Set 4	
	SPAC	LSPAC	SPAC	LSPAC	SPAC	LSPAC	SPAC	LSPAC
No. of obs.	209	208	619	614	177	177	319	318
Max (m)	7.08	1.96	4.42	1.49	8.59	2.15	9.29	2.23
Min (m)	0.00	-5.51	0.00	-6.21	0.003	-5.82	0.00	-4.85
Mean (m)	0.93	-0.88	0.36	-1.74	0.79	-1.08	0.51	-1.50
Std. dev. (m)	1.21	1.40	0.54	1.23	1.25	1.36	0.92	1.26
Skewness	2.42	-0.34	3.58	-0.11	3.51	-0.17	5.21	0.15
Weibull								
Shape (λ)	.830		.856		.797		.798	
Scale (θ)	.769		.317		.625		.408	
D-Statistics and [P(>D)]*								
exponential	.126 [.002]		.126 [<.001]		.182 [<.001]		.200 [<.001]	
normal		.043 [>.15]		.019 [>.15]		.048 [>.15]		.055 [>.15]
Weibull	.043 [>.15]		.066 [>.01]		.075 [>.15]		.095 [<.01]	

*Results of the Kolmogorov-Smirnov goodness-of-fit test for the exponential, the log-normal and the Weibull models

compared to various theoretical models that are bounded at zero to the left and are skewed to the right. Accordingly, the exponential, the lognormal and the Weibull models have been tested. The computed parameters for these models are included in Table 3.11. The exponential distribution has been briefly discussed in Section 3.3. The estimate of the parameter of the exponential distribution is simply the inverse of the mean value of SPAC. Since a variable is lognormally distributed when the logarithm of its values are normally distributed, the estimates of the parameters of the lognormal distribution is the mean and the standard deviation of LSPAC. Since the Weibull model is less known than the two other models, the following paragraph presents more information about the Weibull distribution.

A variable X follows a Weibull distribution when its probability density function has the form:

$$f_W(x;\Theta,\lambda) = (x/\Theta)^{\lambda-1} \text{ EXP}[-(x/\Theta)^{\lambda}] \tag{3.14}$$

where Θ and λ are called scale and shape parameters respectively. When the shape parameter λ takes the value one, the Weibull model reduces to the one-parameter exponential model mentioned above. The parameters Θ and λ for the spacing distributions have been estimated with a specially written FORTRAN program using the maximum likelihood method (Appendix B), and the results are included in Table 3.11.

The goodness-of-fit of these three statistical models to our spacing distributions can be evaluated with the quantile plots shown in Figure 3.14. The quantile plots are easy to make by computer and since they are a variation of the better known probability plots usually constructed on special probability paper, their interpretation is as simple as these latter plots (Kalbfleisch, 1979). The straight line on each one of the

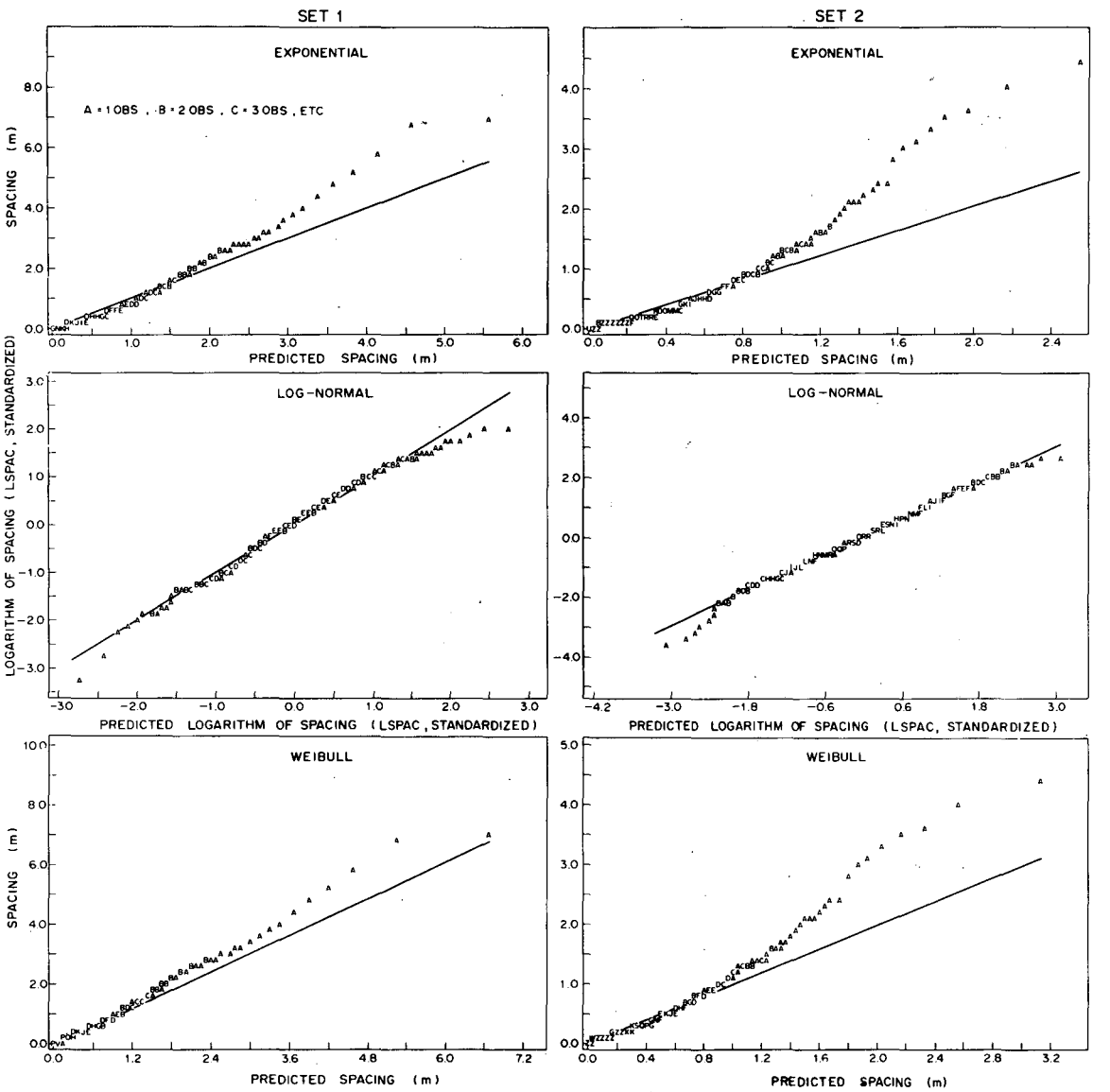

Fig. 3.14. Quantile plots for the exponential, the lognormal and the Weibull models fitted to the spacing distribution of the four fracture sets.

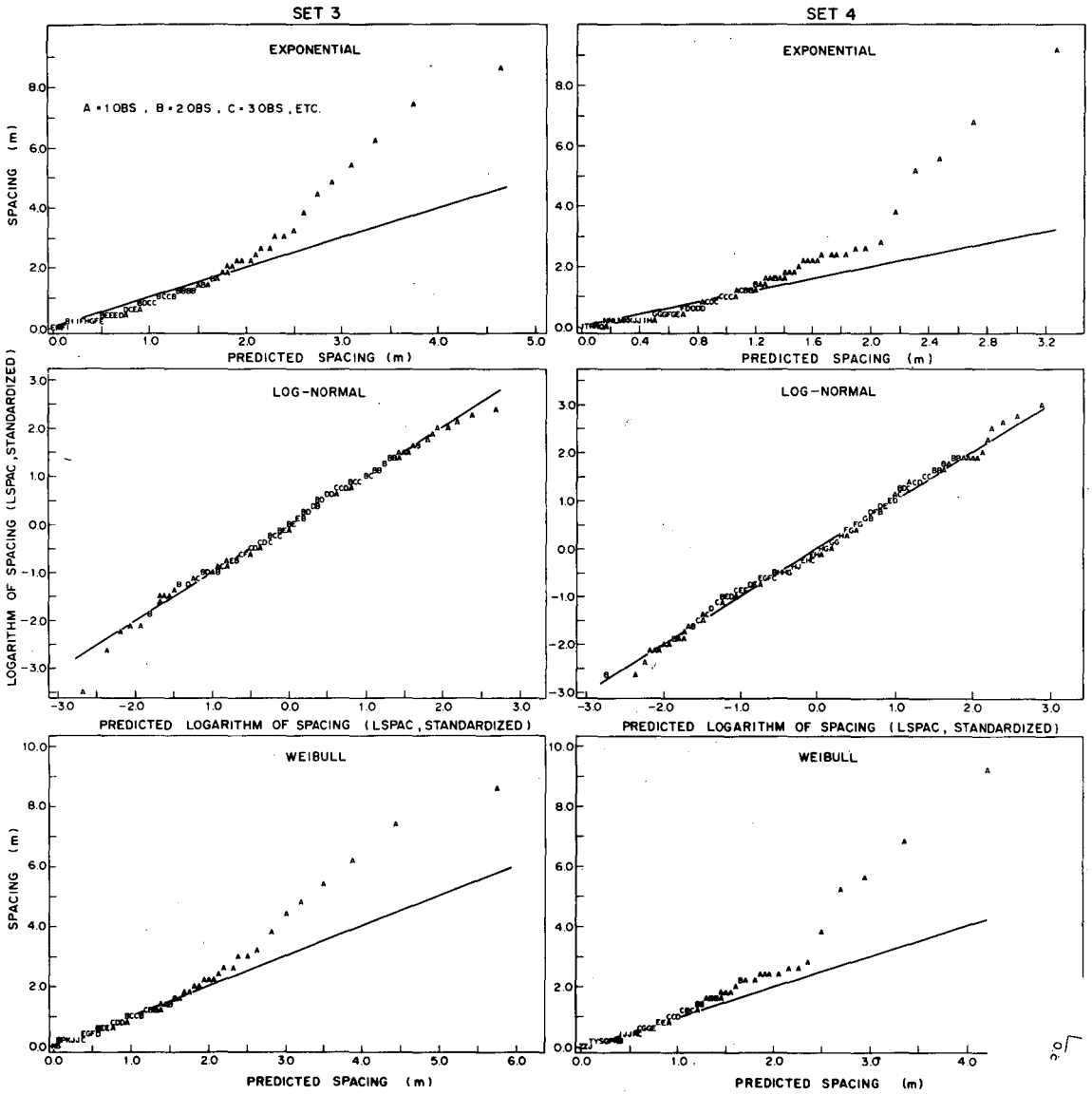

XBL 8411-5036

Fig. 3-14. (continued)

plots of Figure 3.14 is simply a reference line with a slope of one. The more the empirical line is curved and the further away from the reference line, the stronger is the indication that the theoretical model does not fit the data.

The construction of the quantile plots requires the use of the inverse cumulative distribution function (ICDF). In the cases of the exponential and the Weibull distributions, the ICDF is represented by the relatively simple expressions:

$$X = -\mu \, \ell n(1-\alpha) \qquad \text{(exponential)} \qquad (3.15)$$

and

$$X = \Theta \left\{ \ell n[1/(1-\alpha)] \right\}^{1/\lambda} \qquad \text{(Weibull)} \qquad (3.16)$$

where

$$\alpha = \text{Prob } (x \leq X) \quad ,$$

and μ, Θ and λ are the parameters of the distributions.

The case of the lognormal distribution (or the normal distribution fitted to the logarithm of the variable) is complicated by the fact that no closed-form expression exists for the CDF. Numerical approximation techniques have been developed to compute the normal score, i.e., the expected values of a standard normal population (mean zero and variance one), given the α values. The procedure RANK of SAS (SAS Institute, 1979) includes some of these numerical techniques.

The goodness-of-fit evaluated visually in Figure 3.14 have also been tested objectively using the Kolmogorov-Smirnov D-statistics (see for instance Bury, 1975). The results of these tests are included in Table 3.11. The end result of the test is given in the form of the probability of a value of D larger than that observed (Prob (> D) if the empirical distribution was exactly following the tested theoretical model. As

mentioned for the F test in Tables 3.6 and 3.10, the probability of a larger D is also known as the level of significance.

The quantile plots of Figure 3.14 and the goodness-of-fit test (Table 3.11) indicate that the exponential distribution does not fit our data at all. For two of the four fracture sets the Weibull model passes the test at a level of significance larger than 0.05. Finally the lognormal distribution fits our data very well for all of the fracture sets, at a level of significance larger than 0.15.

A series of computer programs using the SAS System (SAS Institute, 1979) was written to make the necessary computations for the goodness-of-fit test and to construct the quantile plots of Figure 3.14. The listing of these programs is given in Appendix B.

The results of the goodness-of-fit tests presented above allow some comments to be made concerning the spatial distribution of the fractures. Indeed, we know from probability theory that if points are randomly distributed along a line (a Poisson process), the distances between consecutive points follow an exponential distribution (see for instance Ross, 1980; and Priest and Hudson, 1976). Therefore the failure of the goodness-of-fit test of the exponential distribution to our spacing data is an indication that the fracture intersections are not randomly distributed along the boreholes. This simple spacing analysis however does not indicate what type of spatial process is responsible for the distribution of the fracture intersections along the boreholes and more so for the distribution of fracture planes in a three-dimensional space.

3.4 Fracture Density

The preceding section presented an analysis of the spatial variability of the fracture system around the ventilation drift based on fracture spacings. Because of its greater complexity, the density approach, which makes use of many computed values of fracture frequency (i.e., number of fracture intersections divided by length of borehole interval) was not used. Nevertheless, fracture density* is an important parameter on its own and at least an average value for the whole rock mass must be estimated.

In this section, first we demonstrate that fracture density is in fact equivalent to fracture frequency as computed along boreholes; then we present the calculations made to estimate an average value of fracture frequency for the rock mass surrounding the ventilation drift.

Using geometric probabilities, one can demonstrate that, for a three-dimensional structure formed by many planar surfaces with the same orientation (Figure 3.15), the volumetric surface area (S_V) is equal to the average number of intersections with the plane surface system per unit length of perpendicular test line ($\bar{P}_{L_\perp}$) (see Underwood, 1968), i.e.,

$$S_V = \bar{P}_{L_\perp} \quad . \tag{3.17}$$

One can also demonstrate that, for a set of surfaces with completely random orientation, the equivalent relationship is:

---

*Fracture density (dimension L^{-1}) is defined as the total area of fractures divided by the volume of rock (S_V) in three dimensions, or the total length of fracture traces divided by the surface area of rock exposure (L_A) in two dimensions.

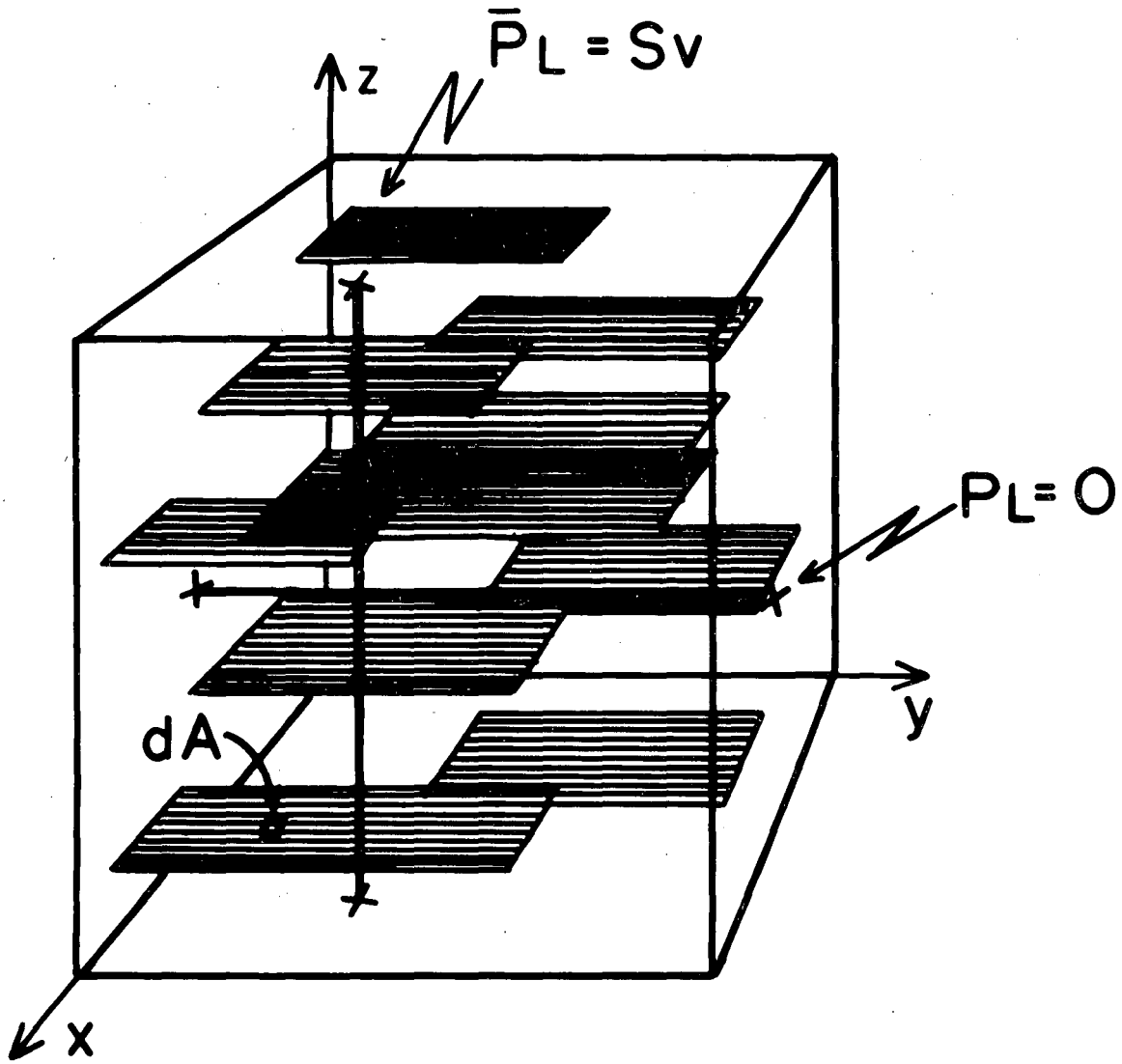

XBL 8411-5044

Fig. 3.15. A three-dimensional structure consisting of parallel surfaces.

$$S_V = 2\bar{P}_L \quad (3.18)$$

where $\bar{P}_L$ is the number of point intersections per unit length of test line of any orientation. When applied to fracture data, S_V and $\bar{P}_L$ refer respectively to fracture density and average fracture frequency.

Since the fracture sets in the Stripa granite have been defined on the basis of fracture orientation, all the fractures in a set being roughly sub-parallel, relation (3.17) is more appropriate than relation (3.18) to estimate fracture density. Because of the dispersion in orientation data in each set, however, the value of S_V obtained with (3.17) is slightly underestimated.

To estimate the values of $\bar{P}_{L\perp}$, a method described by Kiraly (1970) has been applied to the core log data. This method first requires the calculation of a "true" length (L') for each measurement line (or borehole). L' is simply the projection of the actual borehole length (L) on the normal to the average plane of the fracture set being considered and it is computed with the relationship

$$L' = L \cos \phi \ , \quad (3.19)$$

where ϕ is the angle between the borehole axis and the normal to the average plane of the fracture set. For M boreholes and a total of N fractures intersected in a given set,

$$S_V = \bar{P}_{L\perp} = N / \sum_{i=1}^{M} L'_i \quad . \quad (3.20)$$

The values of S_V calculated with (3.20) are 1.026, 2.639, 0.905 and 1.829 (m^{-1}) for fracture sets 1, 2, 3 and 4 respectively. Data used in the calculation are given in Table 3.12.

Table 3.12. Average fracture frequency for each fracture set.

Borehole	Set 1				
	ϕ	$\cos\phi$	L(metre)	L'(metre)	N
HG1	35.4	0.8147	29.98	24.43	22
HG2	20.8	0.9351	29.94	28.00	36
HG3	27.8	0.8847	30.04	26.58	24
HG4	58.3	0.5251	30.13	15.82	11
HG5	53.1	0.6006	30.01	18.02	12
R1	81.4	0.1498	40.07	6.00	6
R2	58.7	0.5195	29.96	15.56	15
R3	66.0	0.4065	30.01	12.20	26
R5	55.1	0.5727	30.03	17.20	15
R6	81.5	0.1470	40.00	5.88	12
R7	58.7	0.5200	29.98	15.59	9
R8	62.2	0.4660	30.00	13.98	22
R10	55.2	0.5712	30.03	17.15	12
Summation				216.41	222

$\overline{P_{L\perp}} = 1.026\ m^{-1}$

Borehole	Set 2				
	ϕ	$\cos\phi$	L(metre)	L'(metre)	N
HG1	87.1	0.0504	29.98	1.51	7
HG2	82.6	0.1286	29.94	3.85	19
HG3	69.3	0.3530	30.04	10.60	10
HG4	77.4	0.2184	30.13	6.58	11
HG5	64.7	0.4279	30.01	12.84	17
R1	45.1	0.7065	40.07	28.31	95
R2	55.0	0.5730	29.96	17.17	68
R3	15.1	0.9656	30.01	28.98	84
R5	25.1	0.9054	30.03	27.19	77
R6	45.0	0.7066	40.00	28.26	36
R7	55.1	0.5715	29.98	17.13	69
R8	6.2	0.9942	30.00	29.83	86
R10	25.0	0.9062	30.03	27.21	53
Summation				239.47	632

$\overline{P_{L\perp}} = 2.639\ m^{-1}$

Table 3.12 (continued)

Borehole	Set 3				
	ϕ	$\cos\phi$	L(metre)	L'(metre)	N
HG1	75.8	0.2455	29.98	7.36	1
HG2	72.8	0.2957	29.94	8.85	6
HG3	78.8	0.1946	30.04	5.85	1
HG4	81.8	0.1422	30.13	4.29	0
HG5	49.8	0.6459	30.01	19.38	6
R1	18.1	0.9506	40.07	38.09	61
R2	88.3	0.0289	29.96	0.87	2
R3	22.9	0.9214	30.01	27.65	19
R5	59.3	0.5099	30.03	15.31	6
R6	17.9	0.9514	40.00	38.06	62
R7	88.5	0.0269	29.98	0.81	0
R8	30.6	0.8606	30.00	25.82	14
R10	55.2	0.5117	30.03	15.37	10
Summation				207.71	188

$\overline{P_{L\perp}} = 0.905\ m^{-1}$

Borehole	Set 4				
	ϕ	$\cos\phi$	L(metre)	L'(metre)	N
HG1	78.4	0.2007	29.98	6.02	3
HG2	77.8	0.2118	29.94	6.34	17
HG3	68.7	0.3634	30.04	10.92	6
HG4	54.9	0.5749	30.13	17.32	13
HG5	87.5	0.0433	30.01	1.30	5
R1	44.5	0.7136	40.07	28.59	31
R2	38.3	0.7852	29.96	23.53	44
R3	73.7	0.2804	30.01	8.42	17
R5	67.2	0.3868	30.03	11.62	21
R6	44.5	0.7129	40.00	28.52	68
R7	38.2	0.7860	29.98	23.56	80
R8	82.7	0.1267	30.00	3.80	14
R10	67.3	0.3855	30.03	11.58	13
Summation				181.52	332

$\overline{P_{L\perp}} = 1.829\ m^{-1}$

Note: ϕ = angle between the borehole axis and the normal to the average plane of the fracture set,

L = length of the borehole,

L' = L cos ϕ,

N = the number of fracture intersections,

P_L = average number of intersections with fractures of the set per unit length of L'.

4. CONCLUSIONS AND RECOMMENDATIONS

Rock fractures are important in nuclear waste disposal in deep geological formations for two main reasons: they control the stability of underground excavation and they may constitute flow paths for the migration of radionuclides in groundwater from the repository to the biosphere. Various rock mass characterization schemes, considering rock fracturing in one form or another, have been reviewed and applied to selected sets of the Stripa data, in order to facilitate the comparison with different sites. Also, based on core log and fracture map data, three fracture parameters, i.e., fracture orientation, trace length and spacing, have been analyzed statistically, in order to describe the geometric structure of the fracture system.

The parameters used in the rock mass characterization are the rock quality designation (RQD), the mean core length, the fracture frequency, and the rock mass permeability. The first three parameters, all dealing with rock fracturing, were computed using a moving average method with intervals of 2 meters and distance increments of 0.2 meter. The rock mass permeability was determined from packer injection tests, using successive 2-meter packer intervals. Inspection of the logs of these four parameters for three of the hydrology boreholes reveals a good correlation between RQD, mean core length and fracture frequency, as one could expect. However the correlation of these three parameters with hydraulic conductivity is very weak and is discernible only on a scatter diagram of permeability versus fracture frequency using data from all the fifteen hydrology boreholes together.

The analysis of the fracture orientation data, using both core log and fracture map data, indicate that at least four fracture sets can be

clearly defined in the rock mass immediately surrounding the main test excavations. The orientation data become much more scattered when one considers data obtained from distances of 200 meters or more apart, because these data sample different lithologies and presumably different structural domains of the rock mass.

For the rock mass surrounding the ventilation drift, the fracture spacing and trace length data were analysed for each one of the four fracture sets defined on the basis of orientation data. The spacing data, obtained from the drill cores of the thirteen oriented hydrology boreholes, indicate significant differences in spacing distributions between boreholes for each fracture set. The difference becomes much less important when comparing groups of boreholes that are defined on the basis of their location along the drift. Therefore it is reasonable to consider the volume of rock surrounding the ventilation drift and sampled by all the hydrology boreholes as statistically homogeneous with respect to fracturing. For the ventilation drift as a whole, both trace length and spacing data show substantial differences between fracture sets. Fracture density, for which an average value was computed for each fracture set, also shows significant differences from one fracture set to the other. These differences between the fracture sets suggest that all these geometric parameters, or a derivative of them, should be considered in any evaluation of the degree of fracture interconnection and hence hydraulic communication within the rock mass.

The results of this analysis of the geometric parameters of the fracture system can be used in numerical simulations of groundwater flow or

rock mass stability that include orientation and trace length distributions, as well as different fracture densities for different fracture sets.

The study described in this report permits one to point out some of the areas where further research could prove to be productive. As far as the general rock mass characterization is concerned, an approach must be developed to quantify systematically the correlation between parameters for each borehole and to compare the correlation coefficients from borehole to borehole. In this latter correlation analysis, some advantage could presumably be gained by considering each fracture set separately.

Good fracture orientation data is essential to the assessment of the degree to which various theoretical distributions fit actual field data. To this end, additional efforts must be made to ensure in future studies both good core recovery and systematic orientation of the fractures intersecting the cores. Also, quick and efficient methods must be designed to generate accurate fracture maps that account for the irregularity and the curvature of the sampling surfaces.

The statistical analysis of trace length data would be greatly improved by a properly designed statistical computation package that accounts for truncation, censoring, and size bias. This package should include the estimation of the parameters for standard statistical models and provide tests for the goodness-of-fit of these models. Both functions should account for the three important bias mentioned above.

Finally, the spatial variability of fracturing has not been considered in a systematic manner in this study because of the lack of statistical methods based on sound geometrical probability theory. Therefore a

prerequisite to a study of spatial variability of fracturing seems to be theoretical work in geometrical probability that could shed light on the relationship between series of one-dimensional (borehole axis) or two-dimensional (rock exposure) sets of data, and the distributions of fracture planes in a three-dimensional space.

REFERENCES

Baecher, G.B., 1980. Progressively Censored Sampling of Rock Joint Traces; Mathematical Geology, v. 12/1, p. 33-40.

Baecher, G.B. and Einstein, H.H., 1981. Statistical and Probabilistic Method in Rock Engineering; notes for a short course given at the Massachusetts Institute of Technology, Cambridge, MA, June 1981.

Baecher, G.B. and Lanney, N.A., 1978. Trace Length Biases in Joint Surveys; 19th U.S. Rock Mechanics Symposium, p. 56-65.

Baecher, G.B., Lanney, N.A., Einstein, H.H., 1977. Statistical Description of Rock Properties and Sampling; 18th U.S. Rock Mech. Symp., p. 5c1-1 to 5c1-8.

Bartlett M.S., 1975. The Statistical Analysis of Spatial Pattern; Chapman and Hall, London, 90 p.

Barton, N., Lien, R. and Lunden, J., 1974. Engineering Classification of Rock Masses for the Design of Tunnel Support; Rock Mechanics, v. 6/4, p. 189-236.

Bieniawski, Z.T., 1973. Engineering Classification of Jointed Rock Mass; Trans. S. Afr. Inst. Civ. Engrs. v. 15/2, p. 335-344

Brière, G. and Razack, M., 1980. Application de la Théorie des Variables Régionalisées à l'Etude de la Fracturation des Magasins Aquifères en Roches Fissurées; Compte-rendus de l'Académie des Sciences, série D; Paris, p. 925-928

Bury, K.V., 1975. Statistical Models in Applied Sciences; John Wiley, 625 p.

Call, R.D., Savely, J.P., Nicholas, D.E., 1976. Estimation of Joint Set Characteristics from Surface Mapping Data; 17th U.S. Rock Mechanics Symp., p. 2B2-1 - 2B2-9.

Corte, H. and Kallmes, O.J., 1961. Statistical Geometry of a Fibrous Network; in The Formation and Structure of Paper, F. Bolam editor; Trans. of Symp. held at Oxford, UK, by British Paper and Board Makers Ass. Inc.; p. 13-52.

Cox, D.R. and Lewis, A.W., 1966. The Statistical Analysis of Series of Events; Chapman and Hall, London.

Cruden, D.M., 1977. Describing the Size of Discontinuities; Int. J. Rock Mech. Min. Sci. and Geomech. Abstr., v. 14, p. 133-137.

Davis, S.N. and Turk, L.S., 1964. Optimum Depth of Wells in Crystalline Rocks; Ground Water v. 2/2, p. 6-11.

Deere, D.U. 1964. Technical Description of Rock Cores for Engineering-Purposes; Rock Mechanics and Engineering Geology. v. 1/1 p. 17-22.

Diggle, P.J., 1979. On Parameter Estimation and Goodness-of-Fit Testing for Spatial Point Patterns; Biometrics v. 35, p. 87-101.

Epstein, B., 1954. Truncated Life Tests in the Exponential Case; Annal of Math. Statistics v. 25, p. 555.

Gale, J.E., 1975. A Numerical, Field and Laboratory Study of Flow in Rocks with Deformable Fractures; Ph.D. dissertation, University of California, Berkeley, 255 p. (Also Scientific Series no. 72, Inland Waters Directorate, Water Resources Branch, Environment Canada, Ottawa, 1977).

Gale, J.E., 1981. Fracture and Hydrology Data from Field Studies at Stripa, Preliminary Results; Lawrence Berkeley Laboratory report, LBL-13101, SAC-46.

Gale, J.E., Rouleau, A., Witherspoon, P.A., Wilson, C.R., 1982. Progress in the Hydrogeologic Characteristics of the Stripa Site; Lawrence Berkeley Laboratory report, LBL-14878, SAC-49.

Gale, J.E., (In Preparation). Correlation of rock mass fracturing with measured permeabilities and in-situ fluid pressures.

Gale, J.E. and Witherspoon, P.A., 1979. An Approach to the Fracture Hydrology at Stripa --Preliminary Results; Lawrence Berkeley Laboratory report LBL-7079, SAC-15.

Gale, J.E., Rouleau, A. and Witherspoon, P.A., 1982. Hydrogeologic Characteristics of a Fractured Granite; Proceedings of the Conference on Groundwater in Fractured Rock, sponsored by the Australia Water Resources Council, Canberra, Sept. 1982.

Geiger, P., 1938. Stripa Odalfaeltsgeologi (Stripa Mine District Mapping); Stripa Mine File, Stora, S-71050, Sweden.

ISRM, 1978. Suggested Methods for the Quantitative Description of Discontinuities in Rock Masses; Int. J. Rock Mech. Min. Sci. and Geomech. Abstr. v. 15, p. 319-368.

Iwai, K., 1976. Fundamental Studies of Fluid Flow through a Single Fracture; Ph.D. dissertation, University of California, Berkeley, 208 p.

Jamier, D., 1975. Etude de la Fissuration, de l'Hydrogéologie et de la Géochimie des Eaux Profondes des Massifs de l'Arpille et du Mont-Blanc; D.Sc. thesis, Université de Neuchatel, Switzerland, 153 p.

Thorpe, R., 1979. Characterization of Discontinuities in the Stripa Granite - Time-Scale Heater Experiment; Lawrence Berkeley Laboratory report LBL-7083, SAC-20.

Underwood, E.E., 1968. Surface Area and Length in Volume; in Quantitative Microscopy, R.T. Dehoff and R.N. Rhines, editors; McGraw-Hill, p. 77-127.

Warburton, P.M., 1980a. A Stereological Interpretation of Joint Trace Data; Int. J. Rock Mech. Min. Sci. and Geomech. Abstr., v. 17, p. 181-190.

Warburton, P.M., 1980b. Stereological Interpretation of Joint Trace Data; Influence of Joint Shape and Implications for Geological Surveys; Int. J. Rock Mech. Min. Sci. and Geomech. Abstr., v. 17, p. 305-316.

Witherspoon, P.A. and Degerman, O., 1978. Swedish-American Cooperative Program on Radioactive Waste Storage in Mined Caverns - Program Summary; Lawrence Berkeley Laboratory report LBL-7049, SAC-01.

Wollenberg, H., Flenser, S. and Andersson, L., 1982. Petrology and Radiogeology of the Stripa Pluton; Lawrence Berkeley Laboratory report LBL-11654, SAC-36.

APPENDIX A. ORIENTATION DIAGRAMS

N.B. All diagrams in this appendix are lower-hemisphere, equal-area plots.

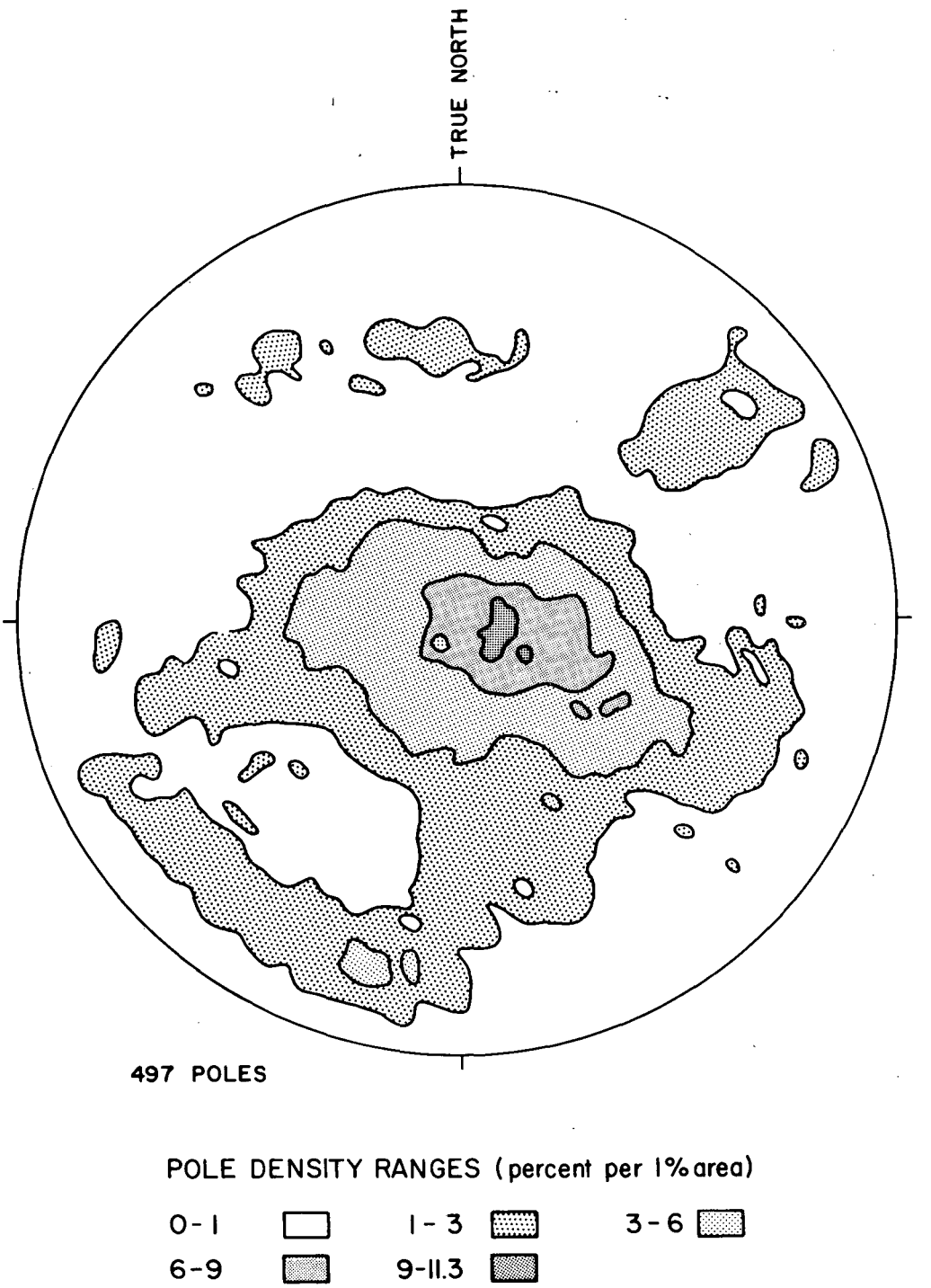

XBL 8411-5037

Fig. A.1. Pole diagram of fracture planes intersecting the drill cores of vertical boreholes in the full-scale drift.

XBL 8411-5038

Fig. A.2. Pole diagram for fracture planes intersecting the drill cores of subhorizontal boreholes around the full-scale drift.

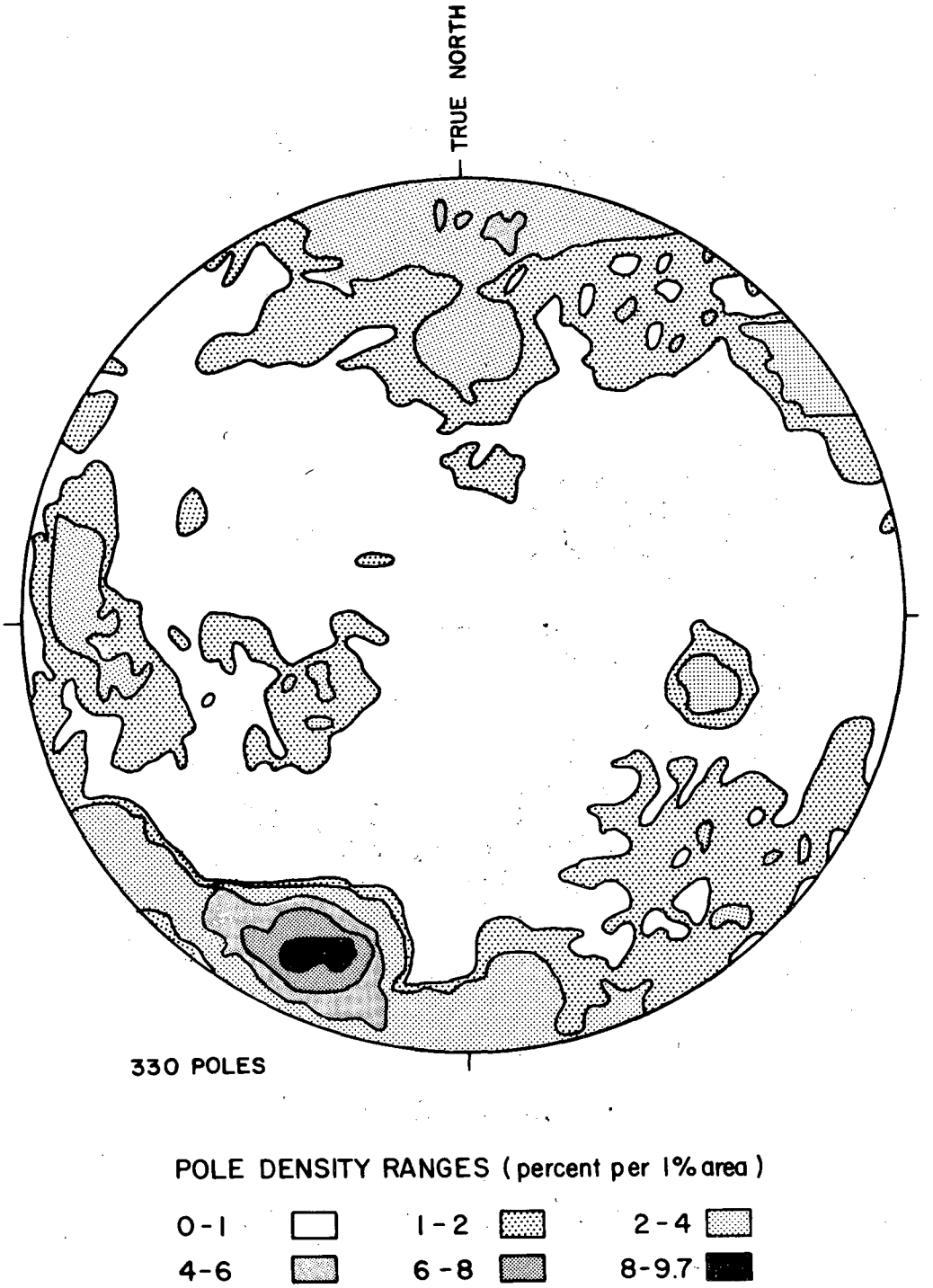

XBL 8411-5039

Fig. A.3. Pole diagram for the fracture planes intersecting the drill cores of the boreholes HG1 to HG5.

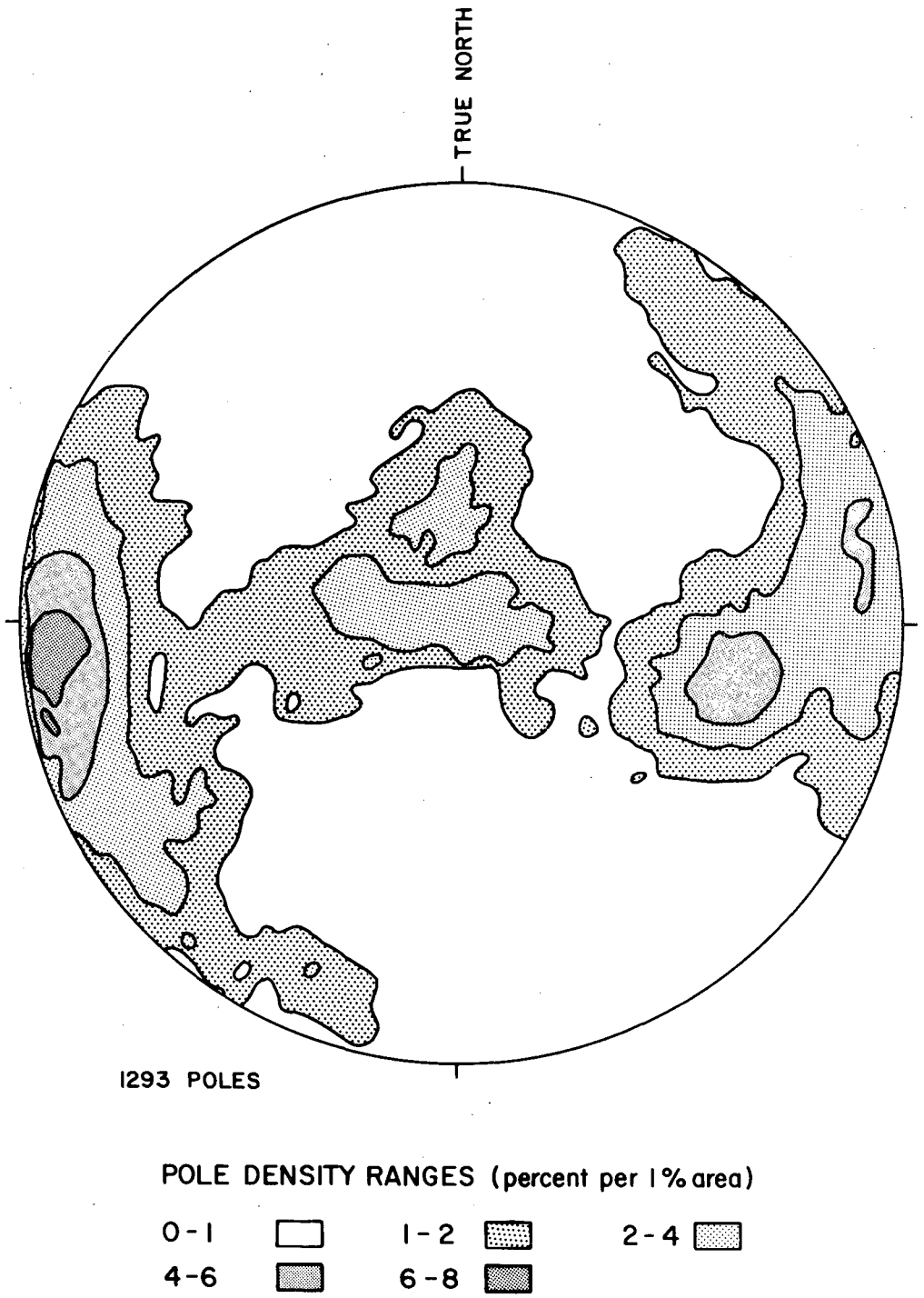

XBL 8411-5040

Fig. A.4. Pole diagram for the fracture planes intersecting the drill cores of the boreholes R1 to R10, except R4 and R9.

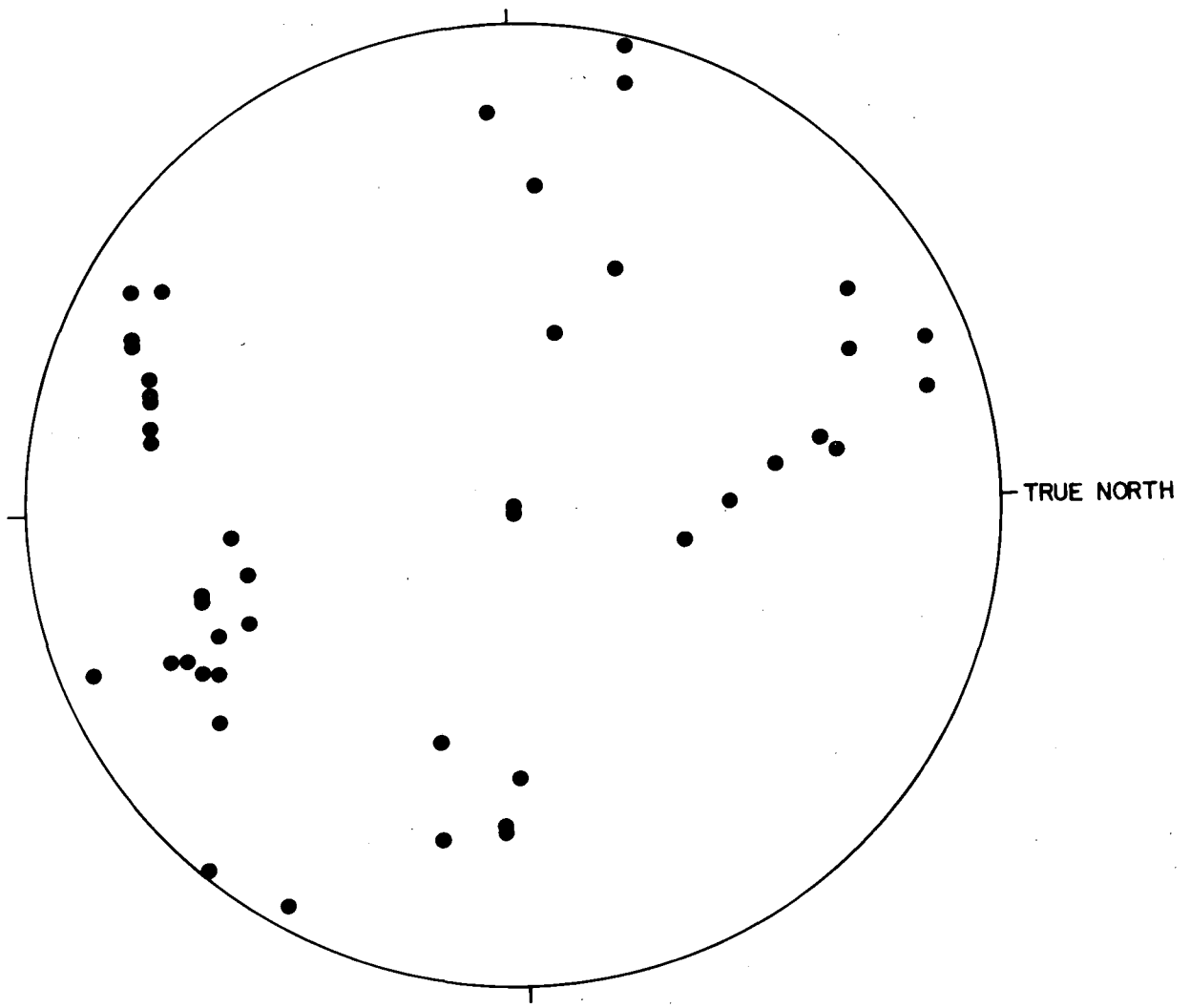

XBL 8411-5041

Fig. A.5. Poles to veins measured on the faces of the ventilation drift.

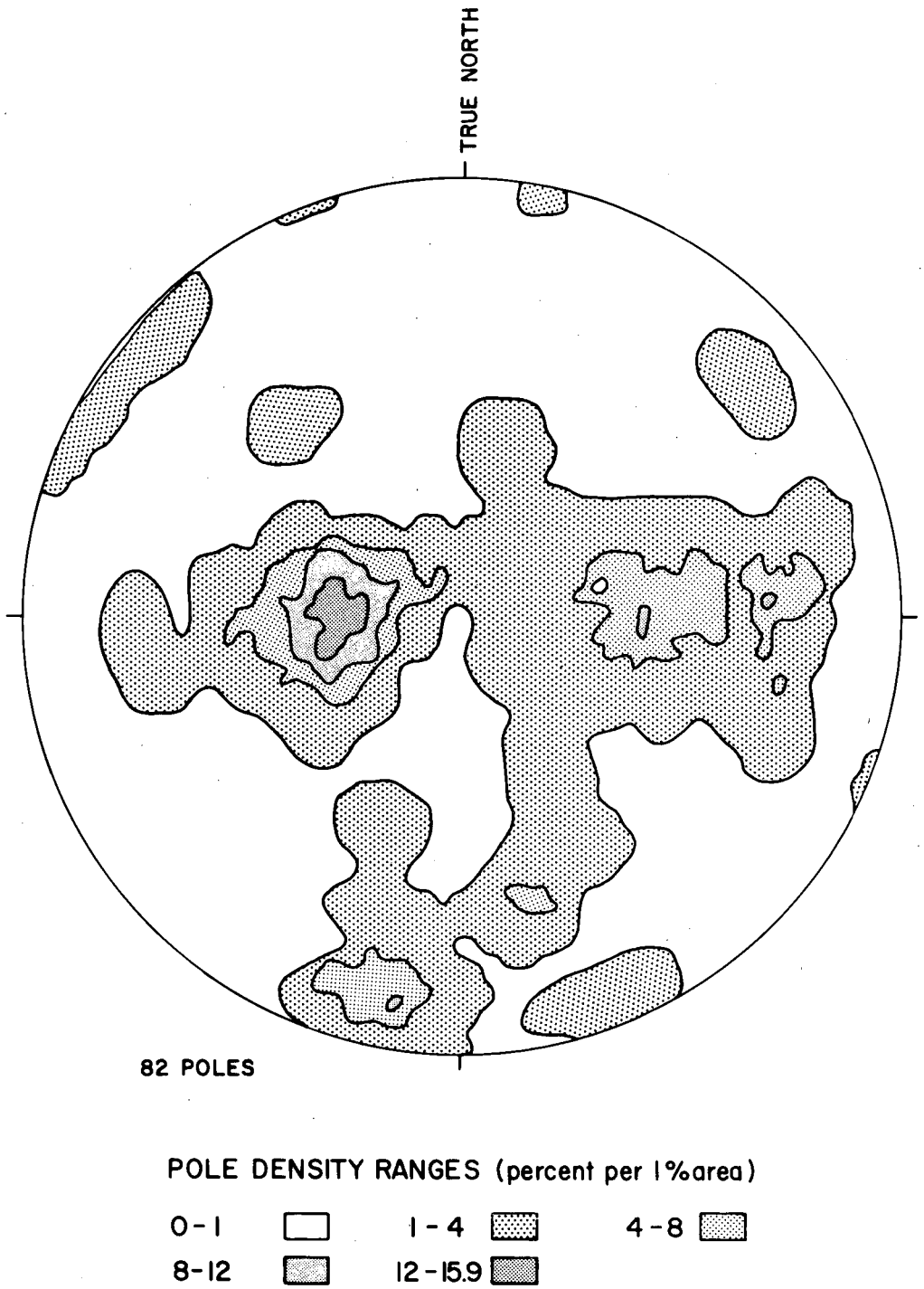

XBL 8411-5042

Fig. A.6. Pole diagram for the average plane of fracture zones measured on the faces of the ventilation drift.

APPENDIX B. LISTING OF SELECTED COMPUTER PROGRAMS USED IN TRACE LENGTH AND SPACING ANALYSIS.

This appendix contains the listing of the following programs:

CENS SAS - Program to compute the statistics and to make a histogram of a progressively censored trace length distribution.

SPAC1 SAS - Program to compute the spacing values for each fracture set in a borehole and to compute the basic statistics.

SPAC2 SAS - Program to combine the spacing data from many boreholes for a fracture set, to make a histogram and to compute the statistics.

WEIBULL FORTRAN - Program to compute the Maximum Likelihood estimates of the parameters of a sample from a Weibull distribution.

EXPON SAS, LNORM SAS and WEIBULL SAS - Programs to compute the Kolmogorov-Smirnov statistics, and to construct the cumulative frequency and quantile plots for the exponential, the lognormal and the Weibull distributions respectively.

```
*            CENS  SAS                          *
*                                               *
*************************************************;
*PROGRAM TO COMPUTE STATISTICS AND PLOT HISTOGRAM FOR
PROGRESSIVELY CENSORED TRACE LENGTHS ;
*************************************************;
OPTIONS  LS=100        ;
*************************************************;
MACRO A
* STATISTICS AND GRAPHS ;
PROC UNIVARIATE ; VAR SIZ ;
PROC CHART ;
  VBAR SIZ/NOSPACE MIDPOINTS=0.75 TO 6.25 BY 0.5 ;  %
*************************************************;
TITLE1 STRIPA  VENTILATION DRIFT  ALL WALLS AND FLOOR  SET 4;
DATA DRFTCENS.SET4 ;
  SET EWCENS.SET4 FLCENS.SET4 NWCENS.SET4 WWCENS.SET4 ;
  PROC PRINT ;
  TITLE2  FILE DRFTCENS.SET4;
DATA CENS0 ; SET DRFTCENS.SET4 ;
  IF CENS=0 ;
  PROC PRINT ;
  TITLE2        BOTH ENDS OBSERVABLE ;
  A ;
DATA CENS1 ; SET DRFTCENS.SET4 ;
  IF CENS=1 ;
  PROC PRINT ;
  TITLE2        ONE END OBSERVABLE ;
  A ;
DATA CENS2 ; SET DRFTCENS.SET4 ;
  IF CENS=2 ;
  PROC PRINT ;
  TITLE2        NO END OBSERVABLE ;
  A ;
```

```
*                    SPAC1  SAS                *
*                                              *
*************************************************
  PROGRAM TO CALCULATE THE SPACING FOR EACH FRACTURE SET
  FOR A BOREHOLE AND TO COMPUTE THE BASIC STATISTICS;
*************************************************;
CMS FILEDEF R10FR DISK R10FRAC ORIENT (LRECL 90 ;
OPTIONS  LS=100 ;
*************************************************;
MACRO C
* CALCULATE SPACING ;
COSPHI = LS*LBH + MS*MBH + NS*NBH ;
PHI = ARCOS(COSPHI) ;
RETAIN COSPHI;
SPAC1 = DIF1(DIST)*COSPHI;
SPAC = ABS(SPAC1);
DPHI = PHI*57.29578;
KEEP DIST DIPDIR DIP SPAC ; %
*************************************************;
MACRO DIRCOS
* COMPUTE DIRECTION COSINES ;
AVPLUNG = -(90-AVDIP) ;
AVAZ = AVDIPDIR ;
AZRAD = AVAZ/57.29578;
PLRAD = AVPLUNG/57.29578;
LS = COS(AXRAD)*COS(PLRAD);
MS = SIN(AZRAD)*COS(PLRAD);
NS = SIN(PLRAD); %
*************************************************;
MACRO JST1DEF
* DEFINITION OF JOINT SET 1 ;
IF   (342<=DIPDIR<=359 AND 56<=DIP<=88) OR
     (  0<=DIPDIR<= 46 AND 56<=DIP<=88) OR
     ( 16<=DIPDIR<= 46 AND 89<=DIP<=90) OR
     (196<=DIPDIR<=226 AND 60<=DIP<=90) ;
AVDIPDIR = 23 ;
AVDIP = 76 ;
DIRCOS;
RETAIN LS MS NS ; %
*************************************************;
MACRO JST2DEF
* DEFINITION OF JOINT SET 2 ;
IF   ( 47<=DIPDIR<=124 AND 56<=DIP<=90) OR
     (227<=DIPDIR<=304 AND 69<=DIP<=90) ;
AVDIPDIR = 83 ;
AVDIP = 95 ;
DIRCOS;
RETAIN LS MS NS ; %
*************************************************;
MACRO JST3DEF
* DEFINITION OF JOINT SET 3 ;
IF   (257<=DIPDIR<=304 AND 32<=DIP<=68) ;
AVDIPDIR = 278;
AVDIP = 53 ;
```

```
DIRCOS;
RETAIN LS MS NS ; %
*****************************************************;
MACRO JST4DEF
* DEFINITION OF JOINT SET 4 ;
IF   (212<=DIPDIR<=359 AND  0<=DIP<=25) OR
     (  0<=DIPDIR<= 40 AND  0<=DIP<=25) OR
     ( 41<=DIPDIR<=115 AND  0<=DIP<=53) OR
     (116<=DIPDIR<=146 AND  0<=DIP<=32) OR
     (147<=DIPDIR<=211 AND  0<=DIP<=52) ;
AVDIPDIR = 155;
AVDIP = 12 ;
DIRCOS;
RETAIN LS MS NS ; %
*************************************************************;
************                          ***************************;
************  DRIVER  PROGRAM          ***************************;
************                          ***************************;
*************************************************************;
* READ IN DATA ;
TITLE1 BOREHOLE R-10 ;
DATA R10.FRAC ;
  FILE PRINT ;
  INFILE R10FR;
  INPUT FLAG $ 1-4 @ ;
  IF FLAG='R10 ' THEN DO ;
     INPUT BEAR 65-69 PLUNG 73-77 ;
     BRAD = BEAR/57.29578 ; PLRAD = PLUNG/57.29578 ;
     LBH = COS(BRAD)*COS(PLRAD) ;
     MBH = SIN(BRAD)*COS(PLRAD) ;
     NBH = SIN(PLRAD) ;
     DROP BEAR PLUNG BRAD PLRAD ;
     RETAIN LBH MBH NBH ;
     PUT //'BOREHOLE ORIENTATION :' // @10 BEAR= PLUNG= LBH=
       MBH= NBH= ;
     END ;
  IF FLAG EQ '11  ' THEN DO ;
     INPUT DIST 5-12 TYPE 25-26 DIPDIR 80-85 DIP 86-90 ;
     IF TYPE NE 2 ;
     IF DIPDIR NE . AND DIP NE . ;
     END ;
  DROP FLAG ;
  IF DIST=. THEN DELETE ;
PROC SORT ; BY DIST ;
PROC PRINT ;
*****************************************************;
* SEPARATE FRACTURE SETS ;
DATA R10.SET1 ; SET R10.FRAC ;
   JST1DEF
     FILE PRINT ;
   C
   IF SPAC=. THEN PUT / 'AVERAGE ORIENTATION OF SET 1 '  ///
           @21 AVDIPDIR= AVDIP= AVPLUNG= LS=MS=NS= /
           @21 DPHI= COSPHI= ;
```

```
   TITLE2 JOINT SET 1 ;
   PROC PRINT ;
   PROC UNIVARIATE ; VAR SPAC ;
DATA R10.SET2 ; SET R10.FRAC ;
   JST2DEF
     FILE PRINT ;
   C
   IF SPAC=. THEN PUT / 'AVERAGE ORIENTATION OF SET 2 '  ///
           @21 AVDIPDIR= AVDIP= AVPLUNG= LS=MS=NS= /
           @21 DPHI= COSPHI= ;
   TITLE2 JOINT SET 2 ;
   PROC PRINT ;
   PROC UNIVARIATE ; VAR SPAC ;
DATA R10.SET3 ; SET R10.FRAC ;
   JST3DEF
     FILE PRINT ;
   C
   IF SPAC=. THEN PUT / 'AVERAGE ORIENTATION OF SET 3 '  ///
           @21 AVDIPDIR= AVDIP= AVPLUNG= LS=MS=NS= /
           @21 DPHI= COSPHI= ;
   TITLE2 JOINT SET 3 ;
   PROC PRINT ;
   PROC UNIVARIATE ; VAR SPAC ;
DATA R10.SET4 ; SET R10.FRAC ;
   JST4DEF
     FILE PRINT ;
   C
   IF SPAC=. THEN PUT / 'AVERAGE ORIENTATION OF SET 4 '  ///
           @21 AVDIPDIR= AVDIP= AVPLUNG= LS=MS=NS= /
           @21 DPHI= COSPHI= ;
   TITLE2 JOINT SET 4 ;
   PROC PRINT ;
   PROC UNIVARIATE ; VAR SPAC ;
DATA R10ALSET ;
   SET R10.SET1 R10.SET2 R10.SET3 R10.SET4 ;
   PROC SORT ; BY DIST ;
DATA R10.NOSET ;
   MERGE R10.FRAC (IN=INA) R10ALSET (IN=INB) ; BY DIST ;
   IF INB=0 ;
   KEEP TYPE DIST DIPDIR DIP ;
   PROC PRINT ;
   TITLE2 DATA NOT IN ANY SET ;
```

```
*                    SPAC2  SAS              *
*                                            *
**********************************************;
* PROGRAM TO COMBINE SPACING DATA FROM MANY BOREHOLES ,
* PLOT HISTOGRAM AND COMPUTE STATISTICS;
**********************************************;
CMS FILEDEF OUT DISK SET4 HGR ;
OPTIONS        LS=100 ;
DATA HGRALL.SET4 ;
  SET HG12345.SET4 R1235.SET4 R6780.SET4 ;
  PROC SORT ; BY SPAC ;
  PROC RANK TIES=MEAN ; VAR SPAC ; RANKS RKSPAC ;
DATA HGRALL.SET4  ;SET  ;
TITLE1 BOREHOLES R'S AND HG'S   SET 4 ;
  PROC PRINT ;
  PROC CHART ; VBAR SPAC /MIDPOINTS=0.25 TO 8.75 BY 0.5 ;
  PROC UNIVARIATE ; VAR SPAC LSPAC ;
DATA   ; SET;
  FILE OUT ;
  IF _N_=1 THEN
     PUT @2 'HOLE' @7 'DIST.'    @13 'SPACING' @23 'LOG SPAC.'
       @33 'RANK' ;
  PUT (HOLE DIST SPAC LSPAC RKSPAC)(@2 3. @6 6.2 @13 9.5 @23
   9.4 @33 5.1) ;
```

```
*                    WEIBULL  FORTRAN          *
*                                              *
C ***********************************************************
C
C
C  PROGRAM TO COMPUTE THE PARAMETERS OF THE WEIBULL
C  DISTRIBUTION FOR A SAMPLE OF SPACING DATA ,
C  USING THE MAXIMUM LIKELIHOOD METHOD.
C
C
C
C P.D.F. : (C/B)(X/B)**(C-1)*EXP(-(X/B)**C)
C  WHERE  C= SHAPE PARAMETER ,
C         B= SCALE PARAMETER ,
C         X= SPACING  , SPAC .
C
C ***********************************************************
C
      COMMON  SPAC(350),LSPAC(350),NOBS ,ITER ,SUM(3)
      REAL LSPAC
      EXTERNAL WEIB
      DOUBLE PRECISION WEIB ,C ,EPS ,XL ,XR
C
      ITER = -2
      READ(1,10) EPS, NSIG, XL, XR, ITMAX
   10 FORMAT(F10.0,I5 ,2F5.0,I5)
      I = 1
   18 READ(1,20 ,END=30) SPAC(I) , LSPAC(I)
   20 FORMAT(12X,F9.0,1X,F9.0)
      I = I+1
      GO TO 18
   30 NOBS = I-1
C
      CALL ZFALSE(WEIB,EPS,NSIG,XL,XR,C,ITMAX,IER)
C
      B = (SUM(1)/NOBS)**(1/C)
      WRITE(2,40) ITMAX, NSIG, XL, XR, IER, C, B
   40 FORMAT('1',10X,'OUTPUT  FROM  IMSL  ZFALSE',
     * //,1X,'NUMBER OF ITERATIONS REQUIRED : ',I4,
     * //,1X,'NUMBER OF SIGNIFICANT DIGITS FOR C : ',I4,
     * /,1X,'STARTING RANGE FOR C : BETWEEN ',F4.2,'  AND  ',
     *  F4.2,
     * /,1X,'ERROR CODE  (IER) = ',I4 ,
     * //,'   PARAMETERS  OF  WEIBULL  DISTRIBUTION  '
     * / ,5X,'SHAPE PARAMETER (C) = ',F6.4,
     * / ,5X,'SCALE PARAMETER (B) = ',F6.4 )
      STOP
      END
C
C
      FUNCTION WEIB(C)
C
C  SUBPROGRAM TO COMPUTE THE VALUE OF AN EXPRESSION (WEIB)
C  RESULTING FROM THE COMBINATION OF THE TWO DERIVATIVES
```

```
C   OF THE WEIBULL LIKELIHOOD FUNCTION (ONE W/R TO C
C   AND ONE W/R TO B ) . THAT EXPRESSION IS A FUNCTION OF THE
C   SHAPE PARAMETER (C) ONLY .
C
      COMMON SPAC(350),LSPAC(350) ,NOBS ,ITER ,SUM(3)
      REAL LSPAC
      DOUBLE PRECISION WEIB, C
      CALL SAMPLE(C)
      WEIB = SUM(3) / SUM(1) - 1/C - SUM(2)/NOBS
      WRITE(2,60) ITER, C, SUM, WEIB
   60 FORMAT(1X,'ITERATION  ',I4,5X,'C = ',F10.4,/
     *                ,21X,'SUM(SPAC(I)**C) =...........',F10.4,/
     *                ,21X,'SUM(LSPAC(I)) =.............',F10.4,/
     *                 21X,'SUM(SPAC(I)**C * LSPAC(I))= ',F10.4,/
     * '          WEIB = ',D10.3,//)
      ITER = ITER + 1
      RETURN
      END
C
C
      SUBROUTINE SAMPLE(C)
C
C    SUBROUTINE TO COMPUTE THREE TERMS INVOLVING THE SUM
C    OF THE SPACING (AND/OR ITS LOGARITHM ) OF ALL THE
C    ELEMENTS OF THE SAMPLE .
C
      COMMON SPAC(350),LSPAC(350) ,NOBS ,ITER ,SUM(3)
      REAL LSPAC
      DOUBLE PRECISION C
      IF (ITER .GT. -2) GO TO 90
      SUM(2) = 0.
      DO 85   I=1,NOBS
      SUM(2) = SUM(2) + LSPAC(I)
   85 CONTINUE
   90 SUM(1) = 0.
      SUM(3) = 0.
      DO 100 I = 1,NOBS
      SUM(1) = SUM(1) + SPAC(I)**C
      SUM(3) = SUM(3) + SPAC(I)**C * LSPAC(I)
  100 CONTINUE
      RETURN
      END
```

```
*                    EXPON  SAS          *
*                                        *
*****************************************************************;
*  PROGRAM TO COMPUTE KOLMOGOROV-SMIRNOV STATISTICS AND MAKE ;
*  C.D.F. AND QUANTILE PLOTS FOR  EXPONENTIAL DISTRIBUTION ;
*****************************************************************;
OPTIONS   LS=110 ;
TITLE1  ALL HG & R HOLES  SET 4 ;
DATA HGREXPO.SET4 ; SET HGRALL.SET4 ;
  N=319 ;
  MSPAC=0.506143 ;
  IF SPAC=. THEN DELETE ;
  STEP =(RKSPAC -0.5)/N ;
  FEXPON = 1-EXP(-(1/MSPAC)*SPAC) ;
  DI = STEP-FEXPON ;
  CONF = SQRT((1/(2*N))*LOG(2/0.05)) ;
  HIGH = FEXPON+CONF ;
      IF HIGH GT 1.  THEN HIGH=. ;
  LOW = FEXPON-CONF ;
      IF LOW LT  0. THEN LOW=. ;
  QUANT = -LOG(1-STEP)*MSPAC ;
PROC PRINT ;
PROC PLOT ;
  PLOT STEP*SPAC  FEXPON*SPAC='*' HIGH*SPAC='H'  LOW*SPAC='L' /
       OVERLAY  HAXIS=0.0 TO 9.5 BY 0.5 ;
  PLOT SPAC*QUANT  QUANT*QUANT='*' / OVERLAY ;
```

```
*              LNORM  SAS            *
*                                    *
*************************************************************;
*  PROGRAM TO COMPUTE KOLMOGOROV-SMIRNOV STATISTICS AND MAKE ;
*  C.D.F. AND QUANTILE PLOTS FOR LOGNORMAL DISTRIBUTION;
*************************************************************;
OPTIONS   LS=110 ;
TITLE1  ALL HG & R HOLES  SET 4 ;
DATA                ; SET HGRALL.SET4 ;
  N=318 ;
  IF SPAC=. THEN DELETE ;
  RKLSPAC = RKSPAC - 1 ;
  IF RKLSPAC<=0. THEN RKLSPAC=. ;
  STDLSPAC=LSPAC ;
  STEP =(RKLSPAC-0.5)/N ;
PROC STANDARD M=0. STD=1. ; VAR STDLSPAC ;
PROC RANK NORMAL=BLOM ; VAR STDLSPAC ; RANKS NSCORE ;
DATA HGRNORM.SET4 ; SET  ;
  FNORM = 0.5 + ERF(STDLSPAC/SQRT(2)) / 2 ;
  DI = STEP-FNORM ;
  CONF = SQRT((1/(2*N))*LOG(2/0.05)) ;
  HIGH = FNORM +CONF ;
      IF HIGH GT 1.  THEN HIGH=. ;
  LOW = FNORM -CONF ;
      IF LOW LT  0. THEN LOW=. ;
PROC PRINT ;
PROC UNIVARIATE NORMAL ; VAR LSPAC ;
PROC PLOT ;
  PLOT STEP*SPAC  FNORM*SPAC='*'  HIGH*SPAC='H'  LOW*SPAC='L' /
       OVERLAY  HAXIS=0.0 TO 9.5 BY 0.5 ;
  PLOT STDLSPAC*NSCORE  NSCORE*NSCORE='*' / OVERLAY ;
```

```
*                WEIBULL  SAS          *
*                                      *
*************************************************************;
*  PROGRAM TO COMPUTE KOLMOGOROV-SMIRNOV STATISTICS AND MAKE;
*  C.D.F. AND QUANTILE PLOTS FOR THE WEIBULL DISTRIBUTION;
*************************************************************;
OPTIONS   LS=105  ;
TITLE1  ALL HG & R HOLES  SET 4 ;
DATA HGRWEIB.SET4 ; SET HGRNORM.SET4;
  N = 318 ;
  C = 0.7981;
  B = 0.4075;
  IF SPAC=. THEN DELETE ;
  DROP RKSPAC STDLSPAC NSCORE FNORM HIGH LOW ;
  FWEIB = 1 - EXP(-(SPAC/B)**C) ;
  DI = STEP-FWEIB  ;
  QUANT = B * ( LOG(1/(1-STEP)) )**(1/C) ;
PROC PRINT ;
PROC PLOT ;
  PLOT STEP*SPAC       / HAXIS=0.0 TO 9.5 BY 0.5  VAXIS=0.0
   TO 1.0 BY 0.1;
  PLOT FWEIB*SPAC='*'  / HAXIS=0.0 TO 9.5 BY 0.5  VAXIS=0.0
   TO 1.0 BY 0.1 ;
  PLOT SPAC*QUANT  QUANT*QUANT='*' / OVERLAY ;
  PLOT DI*SPAC / HAXIS = 0.0 TO 9.5 BY 0.5  VREF=0.0 ;
```

APPENDIX C. MAXIMUM LIKELIHOOD ESTIMATION OF THE PARAMETERS FOR THE WEIBULL MODEL

A variable X follows a Weibull distribution when it is distributed according to the probability density function:

$$f_W\ (x;\Theta,\lambda) = \frac{\lambda}{\Theta}\ (\frac{x}{\Theta})^{\lambda-1}\ \text{EXP}\ [-(\frac{x}{\Theta})^{\lambda}], \qquad 0<x,\Theta,\lambda \tag{1}$$

where Θ and λ are called the scale and shape parameters respectively.

The Weibull cumulative distribution function is found directly by integration:

$$F_W(x;\Theta,\lambda) = \int_0^x f_W(t;\Theta,\lambda)\ dt = 1 - \text{EXP}\ [-(\frac{x}{\Theta})^{\lambda}] \tag{2}$$

The method of Maximum Likelihood (ML) is particularly suitable to estimate the parameters Θ and λ. (see for instance Bury, 1975). The likelihood function (LF) of a sample of n independent Weibull observations is

$$LF(x;\Theta,\lambda) = \prod_{i-1}^{n} f_W\ (x_i;\Theta,\lambda)$$

$$= \lambda^n\ \Theta^{-n\lambda} \prod_{i=1}^{n} x_i^{\lambda-1}\ \text{EXP}\ [-\Theta^{-\lambda} \sum_{i=1}^{n} x_i^{\lambda}] \tag{3}$$

The ML principle asserts that the estimates of Θ and λ should be chosen so that the LF is maximized. The ML estimate is thus defined by the conditions:

$$\frac{\partial LF}{\partial \Theta} (x;\Theta,\lambda) = 0 \tag{4}$$

and

$$\frac{\partial LF}{\partial \lambda} (x;\Theta,\lambda) = 0 \tag{5}$$

The log-likelihood function (LLF) is simply expressed as:

$$LLF(x;\Theta,\lambda) = \ell n\ LF(x;\Theta,\lambda) \tag{6}$$

Since the LF and the LLF maximize simultaneously, we use the latter because it is simpler to evaluate.

The ML equations are thus

$$\hat{\Theta} = [\frac{1}{n}] \sum_{i=1}^{n} x_i^{\hat{\lambda}}]^{1/\hat{\lambda}} \tag{7}$$

and

$$\frac{n}{\hat{\lambda}} - n\ \ell n\ \Theta + \sum_{i=1}^{n} \ell n\ x_i - \sum_{i=1}^{n} (\frac{x_i}{\hat{\Theta}})^{\lambda}\ \ell n(\frac{x_i}{\hat{\Theta}}) = 0 \tag{8}$$

These two equations must be solved simultaneously. Substituting (7) into (8) yields an expression in λ only:

$$\left[\sum_{i=1}^{n} x_i^{\hat{\lambda}}\ \ell n\ x_i\right] \left[\sum_{i=1}^{n} x_i^{\hat{\lambda}}\right]^{-1} - \frac{1}{\hat{\lambda}} - \frac{1}{n} \sum_{i=1}^{n} \ell n\ x_i = 0 \tag{9}$$

The ML estimate $\hat{\lambda}$ can be obtained from (9) by an iterative procedure. The ML estimate Θ then follows by substitution into (7).

The FORTRAN program used to compute the ML estimates of the Weibull distribution is listed in Appendix B. This program solves equation (9) by calling the ZFALSE subroutine of IMSL, which uses the Regula Falsi method to find the zero of a function given an interval containing the zero.

This report is part of a cooperative Swedish-American project supported by the U.S. Department of Energy and/or the Swedish Nuclear Fuel Supply Company. Any conclusions or opinions expressed in this report represent solely those of the author(s) and not necessarily those of The Regents of the University of California, the Lawrence Berkeley Laboratory, the Department of Energy, or the Swedish Nuclear Fuel Supply Company.

Reference to a company or product name does not imply approval or recommendation of the product by the University of California or the U.S. Department of Energy to the exclusion of others that may be suitable.

LAWRENCE BERKELEY LABORATORY
TECHNICAL INFORMATION DEPARTMENT
UNIVERSITY OF CALIFORNIA
BERKELEY, CALIFORNIA 94720